PERFORMANCE OF A NITROGEN HEAT PIPE WITH VARIOUS CAPILLARY STRUCTURES

A THESIS

Presented to

The Faculty of the Division

of Graduate Studies

By

James D. Hare

In Partial Fulfillment

of the Requirements for the Degree

Master of Science in Mechanical Engineering

Georgia Institute of Technology

June, 1975

PERFORMANCE OF A NITROGEN HEAT PIPE
WITH VARIOUS CAPILLARY STRUCTURES

Approved:

Gene T. Colwell, Chairman

James H. Rust

William Z. Black

Date approved by Chairman: 5/27/75

ACKNOWLEDGMENTS

The author wishes to express his sincere appreciation to Dr. G. T. Colwell, his thesis advisor, for his patience, interest, and guidance during this study.

The author also extends his appreciation to Dr. James Rust and Dr. William Z. Black, members of the reading committee, for their careful review of this thesis.

Additionally, the author wishes to express his gratitude to Mr. William Ryszytiwskyj for his aid in computer programming techniques.

Finally, the author expresses his gratitude for financial assistance provided by the Environmental Protection Agency (grant number U-910320-01) and the National Aeronautics and Space Administration (contract number NSG 2054).

TABLE OF CONTENTS

Page

ACKNOWLEDGMENTS ii

LIST OF TABLES vi

LIST OF ILLUSTRATIONS vii

NOMENCLATURE x

SUMMARY xv

Chapter

I. INTRODUCTION 1

A. Definition of Heat Pipe
B. Statement of the Problem
C. General Description of the Heat Pipe and its Operation
D. Literature Survey

II. ANALYTICAL PROCEDURE 10

A. Objective
B. Pipe Geometry and Physical Parameters
C. Thermodynamic Property Equations
D. Wire Screen Properties and Geometry
E. Computer Programs

III. THEORY 28

A. Objective
B. Thermal Resistances
   1. Thermal Resistance of the Pipe Wall
   2. Thermal Resistance of the Circumferential Wick-Liquid Combination
   3. Thermal Resistance of the Circumferential Wick-Vapor Interface
   4. Thermal Resistance of the Vapor
   5. Total Thermal Resistance
C. Heat Pipe Performance Limitations
   1. Capillary Structure Limitation
   2. Sonic Limitation

Chapter Page

IV. PARAMETRIC DISCUSSION AND RESULTS. 48

A. Objective
B. Discussion of Performance Parameters--This Study
C. Comparison with Published Data
D. Results of Study

V. CONCLUSIONS AND RECOMMENDATIONS. 78

A. Conclusions
B. Recommendations for Future Study

REFERENCES. 80

Appendix

A. DISCUSSION OF SCREEN PROPERTIES. 85

B. THERMODYNAMIC PROPERTY EQUATIONS 93

1. Nitrogen
2. Thermal Conductivity of Pipe Material

C. COMPUTER PROGRAM USED TO CALCULATE THERMAL RESISTANCES. 95

D. COMPUTER PROGRAM USED TO CALCULATE THE CAPILLARY-LIMITED HEAT TRANSFER RATE AND HEAT PIPE NUMBER. 107

E. COMPUTER PROGRAM USED TO CALCULATE THE SONIC-LIMITED HEAT TRANSFER RATE 115

F. SAMPLE CALCULATION OF THE EFFECTIVE THERMAL CONDUCTIVITY OF THE CIRCUMFERENTIAL WICK/LIQUID COMBINATION 120

G. SAMPLE CALCULATION OF THERMAL RESISTANCES. . . . 123

H. SAMPLE CALCULATION OF HYDRAULIC RADIUS 130

I. DERIVATION OF EQUATION (3.19). 131

J. ESTIMATION OF THE EFFECTIVE THERMAL CONDUCTIVITY OF THE HEAT PIPE. 138

K. ESTIMATION OF HEAT TRANSFER CAPABILITY 140

Appendix Page

L. SAMPLE CALCULATION OF WICK THICKNESS. 141

M. SAMPLE CALCULATION OF EFFECTIVE INVERSE PERMEABILITY. 143

N. SAMPLE CALCULATION OF NON-RESTRICTED HEAT TRANSFER RATE 144

O. SAMPLE CALCULATION OF CAPILLARY-LIMITED HEAT TRANSFER RATE 145

P. SAMPLE CALCULATION OF THE SONIC-LIMITED HEAT TRANSFER RATE 147

LIST OF TABLES

Table		Page
1.	Geometry and Physical Data of Heat Pipe Considered in this Study.	11
2.	Description of the Composite Wick Systems Considered in this Study.	26
3.	Physical Description of Heat Pipes Compared . . .	69
4.	Summary of Heat Pipe Performance Using Different Wick Compositions	76
5.	Screen Data Used in this Study.	88
6.	Screen Properties from Reference [21]	89
7.	Screen Properties from Reference [22]	89
8.	Screen Properties from Reference [24]	89
9.	Screen Properties from Reference [23]	90
10.	Screen Properties from Reference [25]	90
11.	Screen Properties from Reference [38]	90
12.	Cross-Sectional Area of Vapor Space for Various Wick Compositions	148

LIST OF ILLUSTRATIONS

Figure		Page
1.	General Layout of Heat Pipe.	12
2.	Close-up of Composite Slab and Circumferential Wick at Heat Transfer Section.	13
3.	Cross Section of Heat Transfer Section	14
4.	Nitrogen Vapor Pressure Versus Temperature . . .	16
5.	Nitrogen Viscosity Versus Temperature.	17
6.	Nitrogen Density Versus Temperature.	18
7.	Thermal Conductivity of Liquid Nitrogen Versus Temperature.	19
8.	Heat of Vaporization of Nitrogen Versus Temperature.	20
9.	Surface Tension of Liquid Nitrogen Versus Temperature.	21
10.	Ratio of Specific Heat of Nitrogen Versus Temperature.	22
11.	Heat Pipe Number Versus Vapor Temperature. . . .	24
12.	Thermal Conductivity of 304 Stainless Steel Versus Temperature	25
13.	Schematic Representation of Heat Pipe Thermal Resistances.	30
14.	Cut Away Views of Composite Wick System.	32
15.	Circumferential Wicks Showing Existing Conditions for Maximum Capillary-Limited Heat Transfer Rate.	41
16.	Thermal Resistances Versus Vapor Temperature-- Wick Composition 1	49

Figure Page

17. Thermal Resistances Versus Vapor Temperature--Wick Composition 6. 50

18. Capillary-Limited Heat Transfer Rate Versus Vapor Temperature 52

19. Constant Driving Potential Performance Chart--Wick Composition 5. 53

20. Constant Driving Potential Performance Chart--Wick Composition 6. 54

21. Constant Vapor Temperature Performance Chart--Wick Composition 5. 56

22. Constant Vapor Temperature Performance Chart--Wick Composition 6. 57

23. Fluid Vapor Pressure Versus Capillary-Limited Heat Transfer Rate. 58

24. Effective Thermal Conductivity Versus Vapor Temperature--Wick Composition 1 59

25. Effective Thermal Conductivity Versus Vapor Temperature--Wick Composition 3 60

26. Effective Thermal Conductivity Versus Vapor Temperature--Wick Composition 5 61

27. Effective Thermal Conductivity Versus Vapor Temperature--Wick Composition 6 62

28. Heat Transfer Capability Versus Vapor Temperature 64

29. Sonic-Limited Heat Transfer Rate Versus Vapor Temperature 65

30. Performance Envelope Chart--Wick Composition 4. . 66

31. Performance Envelope Chart--Wick Composition 6. . 67

32. Comparison of Capillary-Limited Heat Transfer Rate. 70

33. Comparison of Effective Thermal Conductivity--Wick Composition 1 with Data from [3] 71

Figure Page

34. Comparison of Heat Transfer Rate. 73

35. Comparison of Heat Transfer Rate Versus ΔT for Various Studies 74

36. Inverse Permeability and Porosity Versus Screen Mesh Size Used in this Study. 91

37. Inverse Permeability and Porosity Versus Screen Mesh Size from Reference [21] 92

38. Flow Diagram of the Computer Program Used for Calculating the Thermal Resistance of each Heat Pipe Component 96

39. Flow Diagram of the Computer Program Used for Calculating the Heat Pipe Number and Capillary-Limited Heat Transfer Rate. 108

40. Flow Diagram of the Computer Program Used for Calculating the Sonic-Limited Heat Transfer Rate. 116

41. Close-up of Porous Media Showing the Average Distance Traveled by a Liquid Mass Element in the Circumferential Wick. 135

NOMENCLATURE

Latin Symbol Used in:

Text	Computer Program	Meaning	Units
A_{w_t}		total cross sectional area of wick	ft^2
A_x	XAVS	cross sectional area of vapor space	ft^2
A		cross sectional area of pipe	ft^2
b	B	width of slab wick	ft
c		velocity of sound in vapor	ft/sec
g_c		conversion factor	$\frac{lb_m}{lb_f}\frac{ft}{sec^2}$
h_{fg}	XLAM	heat of vaporization of nitrogen	Btu/lb
K_A		inverse permeability--"A" portion of slab wick	ft^{-2}
K_B		inverse permeability--"B" portion of slab wick	ft^{-2}
K_C	XKC	inverse permeability of circumferential wick	ft^{-2}
$\overline{K}$	XKBAR	effective inverse permeability of composite slab	ft^{-2}
k	XKSHR	ratio of specific heats of nitrogen	
k_L	XKAY	thermal conductivity of liquid nitrogen	$\frac{Btu}{hr\text{-}ft°R}$
k_p	XKP	thermal conductivity of pipe wall and metal screen material	$\frac{Btu}{hr\text{-}ft°R}$
k_w	XKW	effective thermal conductivity of the circumferential wick and liquid	$\frac{Btu}{hr\text{-}ft°R}$
k'		effective thermal conductivity of heat pipe	$\frac{Btu}{hr\text{-}ft°R}$

Latin Symbol Used in:

Text	Computer Program	Meaning	Units
L	CEL	average arc distance traveled by element of mass in circumferential wick	ft
ℓ_a		length of adiabatic section of pipe	ft
ℓ_c	CL	length of the condenser section of pipe	ft
ℓ_e	EL	length of the evaporator section of pipe	ft
ℓ_{eff}	EFFL	effective length of pipe	ft
M		molecular weight of nitrogen	$\frac{lb_m}{lb_m\text{-mole}}$
$\dot{m}$		mass flow rate	$\frac{lb_m}{hr}$
$\dot{m}_L$		liquid mass flow rate	lb_m/hr
$\dot{m}_V$		vapor mass flow rate	lb_m/hr
N	HPN	heat pipe number	$\frac{Btu}{ft^2 hr}$
n_A		number of screen layers composing "A" component of composite wick	
n_B		number of screen layers composing "B" component of composite wick	
n_C		number of screen layers in the circumferential wick	
P_V	VPRE or VPRES	vapor pressure of nitrogen	lb_f/ft^2
ΔP_{cap}		pressure drop in capillary structure	lb_f/ft^2
ΔP_V		pressure drop in vapor due to viscosity	lb_f/ft^2
ΔP_L		pressure drop in liquid due to viscosity	lb_f/ft^2
$\dot{Q}_{max}$	Q2	theoretical maximum heat transfer rate disregarding all limitations	Btu/hr

Latin Symbol Used in:

Text	Computer Program	Meaning	Units
$\dot{Q}_{CL}$	Q1	capillary limited heat transfer rate	Btu/hr
$\dot{Q}_{SL}$	QMSL	sonic limited heat transfer rate	Btu/hr
R_{pe}	RPE	thermal resistance of pipe wall at evaporator end	$\frac{hr°R}{Btu}$
R_{we}	RWE	thermal resistance of circumferential wick at evaporator	$\frac{hr°R}{Btu}$
R_{ie}	RIE	thermal resistance of the wick-vapor interface at the evaporator end	$\frac{hr°R}{Btu}$
R_V	RV	thermal resistance of vapor	$\frac{hr°R}{Btu}$
R_{ic}	RIC	thermal resistance of the wick-vapor interface at condenser end	$\frac{hr°R}{Btu}$
R_{wc}	RWC	thermal resistance of circumferential wick at the condenser end	$\frac{hr°R}{Btu}$
R_{pc}	RPC	thermal resistance of the pipe wall at the condenser end	$\frac{hr°R}{Btu}$
R_T	SUMR	sum of the thermal resistances of the components of the heat pipe	$\frac{hr°R}{Btu}$
R_u		universal gas constant	$\frac{ft\text{-}lb_f}{lb_m\text{-}mole°R}$
R		gas constant for nitrogen	$\frac{ft\text{-}lb_f}{lb_m°R}$
r_A	RA	outside radius of pipe	ft
r_B	RB	inside radius of pipe	ft
r_C	RC	inside radius of the circumferential wick-radius of "C" layer	ft
r_{cd}		menisus radius at the condenser end	ft
r_{ev}		menisus radius at the evaporator end	ft

Latin Symbol Used in:

Text	Computer Program	Meaning	Units
r_p	RPORE	pore radius of the screen	ft
r_v	R	hydraulic radius of vapor space	ft
r_{ws}	DWIRE/2	radius of screen element	ft
T_e	TE	temperature of the pipe outer wall surface at evaporator end	°R
T_1	T1	interfacial temperature between the pipe inner surface and the circumferential wick at the evaporator end	°R
T_2	T2	interfacial temperature between the circumferential wick inner surface and the vapor space at the evaporator end	°R
T_3	T3	temperature of the vapor at the evaporator end	°R
T_4	T4	temperature of the vapor at the condenser end	°R
T_V		average vapor temperature	°R
T_5	T5	interfacial temperature between the circumferential wick inner surface and the vapor space at the condenser end	°R
T_6	T6	interfacial temperature between the pipe inner surface and the circumferential wick at the condenser end	°R
T_c	TC	temperature of the pipe outer wall surface at the condenser end	°R
ΔT	TEMTC	temperature difference between the evaporator and condenser ends, driving potential	°R
u		velocity of vapor	ft/sec

Greek Symbol Used in:

Text	Computer Program	Meaning	Units
β		heat transport capability	$\frac{\text{Btu-ft}}{\text{hr}}$
δ_A		thickness of screen used in "A" portion of composite slab (surface)	ft
δ_B		thickness of screen used in "B" portion of composite slab (interior)	ft
δ_C	DELC	thickness of screen used in the circumferential wick	ft
δ_T	DELT	total thickness of the slab	ft
ε		porosity of the screens	
μ_L	XMUL	viscosity of the liquid	$(lb_f\text{-sec})/ft^2$
μ_V	XMUV	viscosity of the vapor	$(lb_f\text{-sec})/ft^2$
π	PI	constant 3.141592654	
ρ_L	RHOL	density of liquid	lb_m/ft^3
ρ_V	RHOV	density of vapor	lb_m/ft^3
σ	SIG	surface tension of liquid	lb_f/ft

SUMMARY

The heat pipe is a self-contained device which has the capability of transporting large quantities of heat through a small temperature gradient. By operating on a closed liquid-vapor cycle similar to that of a heat engine, this device has exhibited an effective thermal conductivity many times that of a pure copper rod of similar dimensions.

This thesis is a theoretical study of the performance of a cryogenic heat pipe using nitrogen as the working fluid. Polynomial equations are developed to describe the thermodynamic properties of nitrogen as functions of temperature. These equations are combined with the governing mass- and heat-transport equations herein given and coded into three computer programs. These programs, taken together, give capillary and sonic limitations on the performance of the pipe and the thermal resistances of each heat pipe component. The data obtained is converted into several performance graphs and charts which are helpful in the design of composite slab wicks used in heat pipes of this type.

CHAPTER I

INTRODUCTION

A. Definition of the Heat Pipe

The heat pipe is best defined as a self-contained device capable of transferring large quantities of heat from a heat source to a heat sink through a relatively small temperature gradient. The operational concept of the heat pipe is based on a combination of the phenomena of liquid vaporization, mass transport in the vapor phase, vapor condensation, heat transfer through solids by conduction, heat transfer through fluids by convection, heat transfer from surfaces by convection and radiation, and mass transport in the liquid phase by capillary pumping through a porous media. The heat pipe is unique in that it brings these several phenomena of mass and heat transport together into what is actually a simple and useful device.

B. Statement of the Problem

This analytical study focuses on the computer modeling of a composite wick system to be used in a cryogenic heat pipe intended for a special and limited application. That is, to transfer heat from the temperature-sensitive electronic components of a space vehicle operating in an environment of zero gravity and extremely low temperature to a heat sink

which radiates to space.

The physical size and material of the heat pipe and the temperature range were specified by the sponsoring agency.* Thus the problem, which this study attempts to solve by theoretical analysis, is to design a composite wick system capable of supporting a liquid flow rate sufficient for maintaining a rate of heat transfer of approximately thirty-five Btu's per hour. In addition, this wick system must meet the geometric specifications for use in a .420 inch inside diameter pipe three feet long. The remaining sections of this study give the theoretical considerations and outline the procedure used to accomplish this goal.

C. General Description of the Heat Pipe and Its Operation

Generally, the heat pipe consists of a sealed container inside of which a working fluid undergoes a vaporization-condensation cyclic process which transports the latent heat of vaporization of the fluid through the effective length of the pipe. Although the shape of the vessel may vary with application, it is usually a metal circular cylinder or parallelepiped. An internal wick or capillary structure provides a porous medium for the transport of the working fluid in its liquid phase by capillary pumping. The design of this wick may vary greatly. Although circumferential

*National Aeronautics and Space Administration

wicks made of metal screens of various mesh sizes are common, the literature offers many studies, both theoretical and experimental, of heat pipe performance using axial grooves [1], annular-wicks [2], cloth [3,4], and beds of packed beads as wicks [5].

Before being put into service, the heat pipe must be charged. This is accomplished by evacuating the container and introducing the proper amount of working fluid to completely saturate the internal capillary structure. The pipe is then sealed. The working fluid is now in a state of two-phase thermodynamic equilibrium. Under most operating conditions, the internal pressure of the pipe is equal to the vapor pressure of the fluid at the temperature of the surroundings.

As heat is added to the evaporator section of the pipe, the equilibrium is disturbed. A mass element of liquid in the evaporator wick absorbs its heat of vaporization and passes into the vapor space. It is assumed, in this study, that the total energy input to the pipe is taken up in this phase change process [6,7]. The introduction of this additional mass into the vapor space creates a slight pressure gradient causing a movement of vapor toward the condenser. At the condenser, the temperature of the pipe wall and wick is somewhat less than that of the vapor. Thus the vapor condenses on the capillary structure, giving up its latent heat of vaporization. This heat is then conducted

through the pipe wall to be dissipated to the environment.

As the liquid is vaporized at the evaporator end, its surface recedes slightly into the pores of the capillary structure, forming small radii of curvature at the liquid/vapor interface. On the other hand, the condensing vapor at the opposite end tends to fill the pores of the wick, forming greater radii of curvature. It is this difference in the radii of curvature at the vapor/liquid interface between the two ends of the pipe which creates a slight pressure differential in the liquid. The net result of this pressure gradient is the phenomenon known as capillary pumping.

In selecting the proper working fluid, much consideration must be given to the thermodynamic properties of the candidate fluid in the temperature range of operation. The well-known thermodynamic properties of liquid nitrogen and liquid oxygen make them good working fluids for use in the cryogenic temperature range. This work investigates the heat pipe performance using liquid nitrogen as a working fluid.

Although the heat pipe is a very efficient heat transfer device, it is not free from performance limitations. Four such limiting conditions are discussed in Section C of Chapter III.

D. Literature Survey

Although it has not always been known by the name

heat pipe, this closed cycle, high heat transfer device has been in existence for many years. An early device which operated on the principle of the present day heat pipe was patented by R. S. Gaugler [8] in 1944. Grover, et al. [9] rediscovered the device in 1964 and were first to use the descriptive name heat pipe. Since these early works, there have been many theoretical and experimental investigations in the field of heat pipe operation and performance.

While the number of heat pipe investigations is too great to give a complete listing, among the better known was performed by Cotter [10], who first presented a quantitative engineering theory for predicting heat pipe performance. It was Cotter's conclusion that the phenomenon of mass transport in the porous media governs the heat pipe performance. Cotter also pointed out the performance limiting condition of boiling in the evaporator section (see Section C of Chapter III).

Cosgrove [11] is another well-known heat pipe investigator who in 1965 made an important analytical study of its performance. By balancing the governing equations of mass, heat, and momentum transport, and assuming that the performance was restricted by the capillary limitations, Cosgrove reached the conclusion that the maximum heat transfer rate depended on the thermodynamic properties of the working fluid and the liquid-transport characteristics of the porous wick structure. His experimental work provided good

agreement with the predictions obtained by using the analytical model.

The Heat Pipe Design Handbook has been published by Skrabek and Bienert [12]. Among the data given in this impressive work are the thermodynamic properties of several heat pipe working fluids and experimental values of wick properties.

Using dimensional analysis, Williams [6] identified twenty-four dimensionless heat pipe parameter groups. These dimensionless groups enabled Williams to correlate data from his experimental work with data found in the literature.

A correlation model was developed by Williams and Colwell [13] for study of steady-state performance of a horizontal heat pipe with internally self adjusting evaporator and condenser lengths. The conclusions drawn from this study were as follows: (1) the axial vapor Reynolds number influences the length along which condensation occurs, and (2) the wick geometry and meniscus radius at the evaporator determine the length along which evaporation occurs.

Experimental and theoretical investigations in the field of cryogenic heat pipe performance are somewhat more limited in number. From his experimental study of a nitrogen filled pipe, Haskin [14] concluded that the major temperature drops were due to conduction through the pipe walls and the liquid-filled porous structure adjacent to the walls. The experimental data presented by Haskin has been extremely

valuable to heat pipe designers.

In a qualitative investigation, Chi and Cygnarowicz [15] developed design and performance charts for cryogenic heat pipes using different working fluids. This work takes into account the variation of fluid properties on the heat pipe performance. For their study, Chi and Cygnarowica used a heat pipe with a circumferential capillary structure resulting in relative low computed values of heat transfer rates.

From a study of cryogenic and low temperature heat pipes for spacecraft application, Sherman and Brennan [16] concluded that nitrogen and oxygen are the best fluids for operation in the cryogenic temperature range. In addition, this study points out the composite slab wick as a reliable "state-of-the-art" porous media adequate for present day and projected NASA applications.

Joy [17] has studied the capillary and boiling limitations on the performance of cryogenic heat pipes using nitrogen and oxygen as working fluids. In this study, Joy took into consideration the gravitational effects for application on a spin-stabilized spacecraft.

In an experimental investigation using a nitrogen filled heat pipe, Armaly and Dodheker [3] observed the effect of heat pipe performance of varying the angle of inclination of the pipe. From the results of this investigation, the conclusion was drawn that the radial thermal resistance at

the evaporator is the major factor limiting the power load of this low temperature heat pipe.

Kroliczek and Brennan [1] studied the performance of an axially grooved heat pipe. Data relating to the heat transport capability for working fluids of ammonia, methane, and nitrogen were obtained.

A theoretical study was performed by Paulius and Lang [2] analyzing the capillary pressure drops for both homogeneous-wick and annular-wick heat pipes operating in the cryogenic temperature range. Comparisons were made of the heat transfer capacity of pipes employing these two wick configurations and working fluids of hydrogen, nitrogen, and oxygen. The result of their theoretical study indicates that superior performance may be realized with the annular-wick design.

Using the Applications Technology Satellite (ATS-F), Kirkpatrick and Brennan [18] conducted controlled experiments to evaluate the performance of a heat pipe in a space environment. They concluded that heat pipes are useful temperature control devices for space applications.

In his presentation at the 1973 National Science Foundation Heat Pipe Conference, Olindorf [19] outlined the state-of-the-art of cryogenic coolers for spacecraft application. Included in his presentation was a discussion of the performance of cryogenic heat pipes using various working fluids and different wick configurations.

Several authors (Refs. [20,21,22,23,24,25,26 and 27]) have studied the capillary properties of wire mesh screens which may be used for heat pipe applications. Appendix A summarizes the findings of these studies.

CHAPTER II

ANALYTICAL PROCEDURE

A. Objective

The objective of this chapter is to outline and clarify the analytical procedures used in this study. The following sections discuss the pipe geometry and general wick design, the equations used for determining the thermodynamic properties of the materials used, wire screen properties and geometry, and the computer programs used in optimizing the composite wick.

B. Geometry and Physical Data of Heat Pipes Considered in this Study

Given in Table 1 is a listing of the heat pipe geometry and physical characteristics suggested by the sponsoring agency. Drawings showing the general configuration of the heat pipe and composite wick system are given by Figs. 1, 2, and 3.

C. Thermodynamic Property Equations

The thermodynamic properties of nitrogen, the working fluid, in the cryogenic temperature range are well known. Reference [28] gives plots of vapor pressure, liquid and vapor viscosity and density, liquid thermal conductivity,

Table 1. Geometry and Physical Data of Heat Pipe Considered by this Study

Total length	3 feet
Length of adiabatic section	1.5 feet
Length of evaporator section	.5 feet
Length of condenser section	1.0 feet
Outside diameter of pipe	.041667 feet
Wall thickness of pipe	.003333 feet
Inside diameter of pipe	.035000 feet
Material of pipe and capillary structure	304 stainless steel
Working fluid	Nitrogen
General wick configuration	Composite central slab, circumferential at heat transfer sections

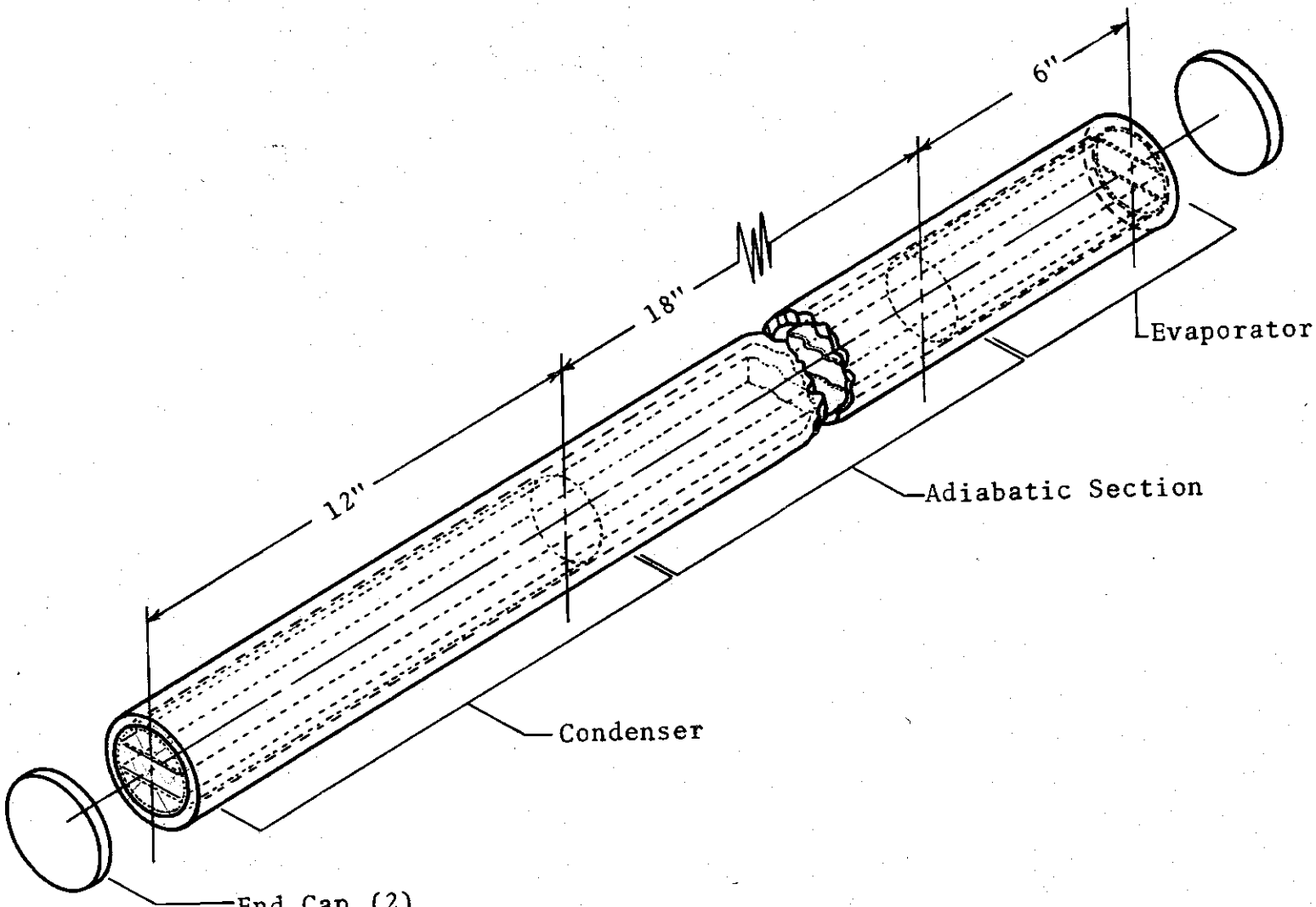

Figure 1. General Layout of Heat Pipe

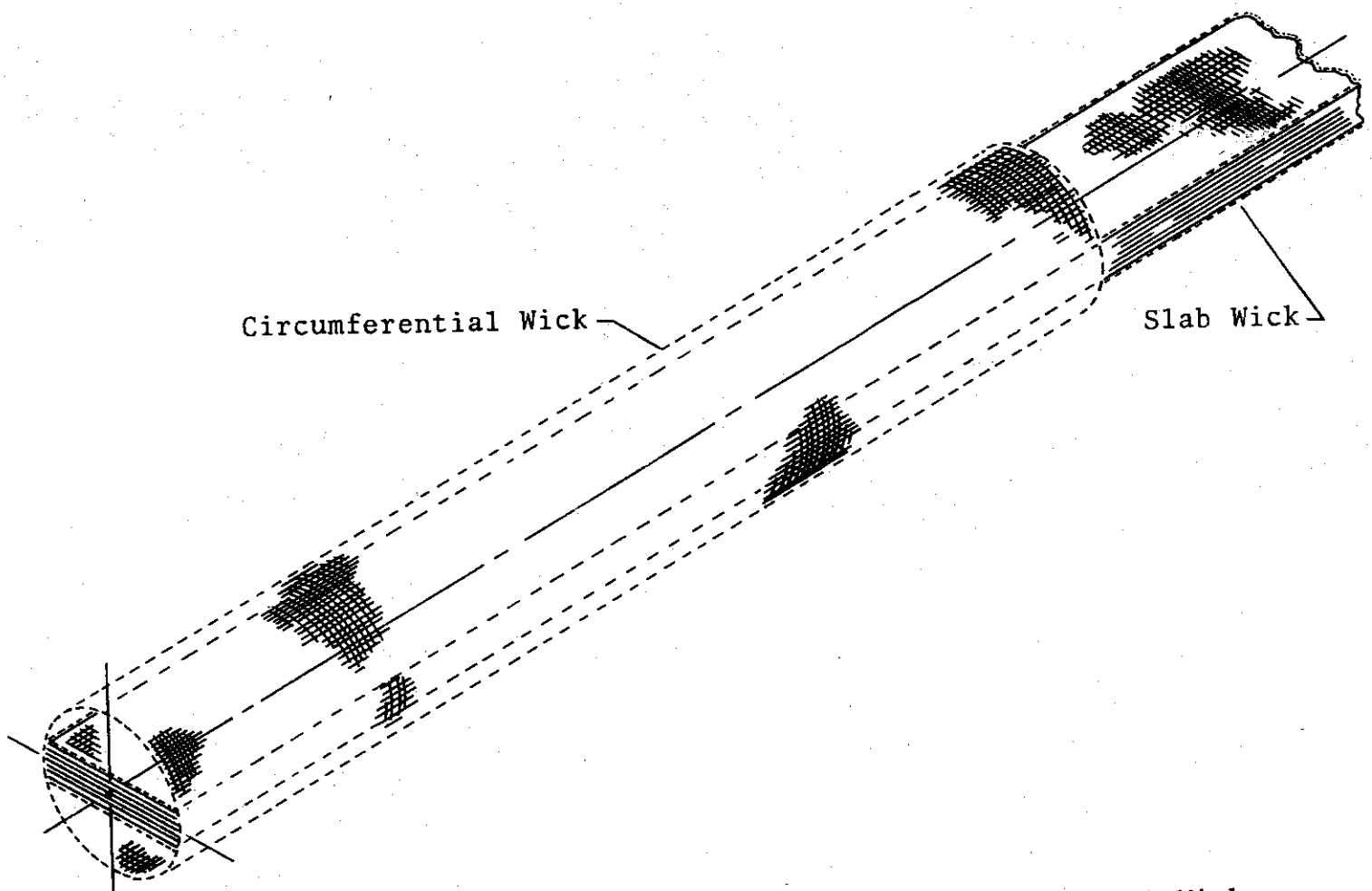

Figure 2. Close-Up of Composite Slab and Circumferential Wick at Heat Transfer Section

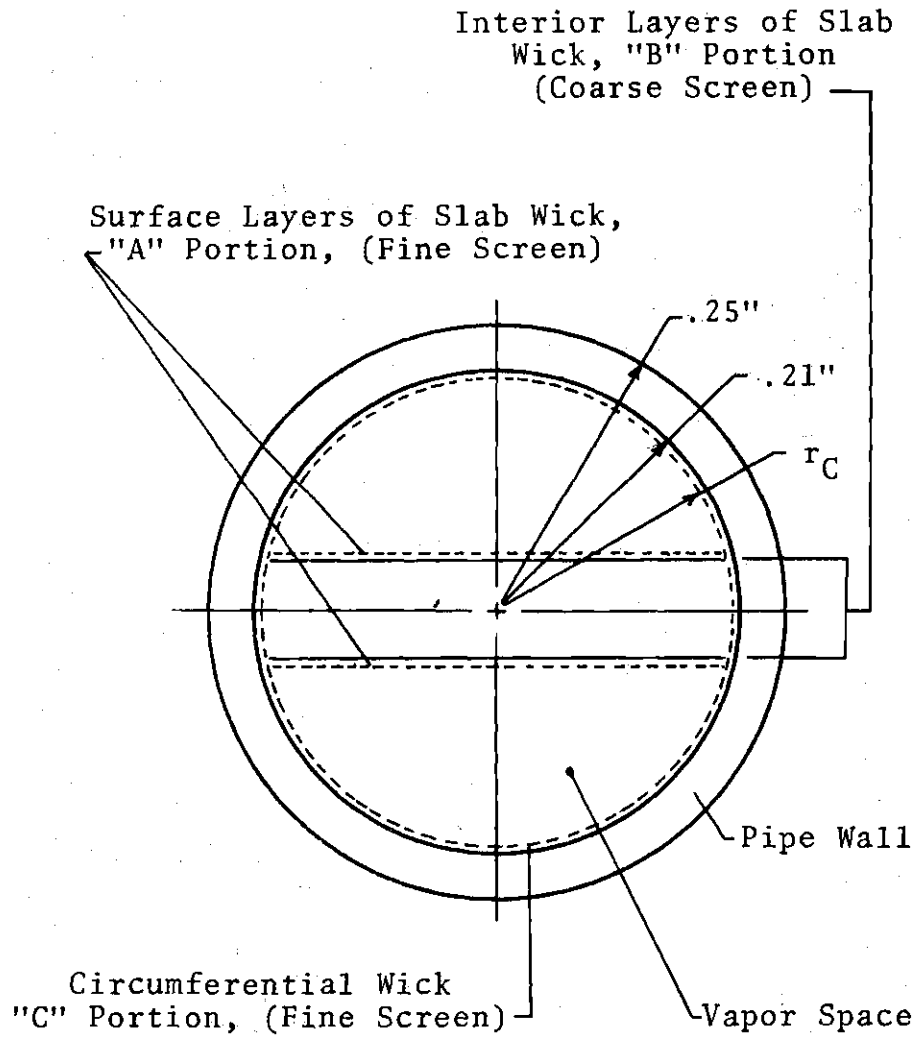

Figure 3. Cross-Section of Heat Transfer Section

heat of vaporization, and surface tension as functions of temperature over the range $65°K \leq T \leq 125°K$. However, the computer programs used to model the composite wick system require mathematical equations describing each property as a function of temperature. Such equations were generated by using the data given in Ref. [28] in a least-squares regression analysis program on the Wang 720 calculating machine. The property equations thus generated are of the form:

$$X = b_n T^n + b_{n-1} T^{n-1} + \cdots + b_o \qquad (2.1)$$

$$1 \leq n \leq 7$$

where

X = thermodynamic property

b_n = polynomial coefficient

T_n = temperature, °R

Data taken from Refs. [29] and [30] were used in the curve fit procedure to generate polynomial equations, describing the ratio of specific heats of nitrogen and the thermal conductivity of 304 stainless steel as functions of temperature. A complete listing of these property equations is given in Appendix B.

Figures 4 through 10 illustrate various thermodynamic

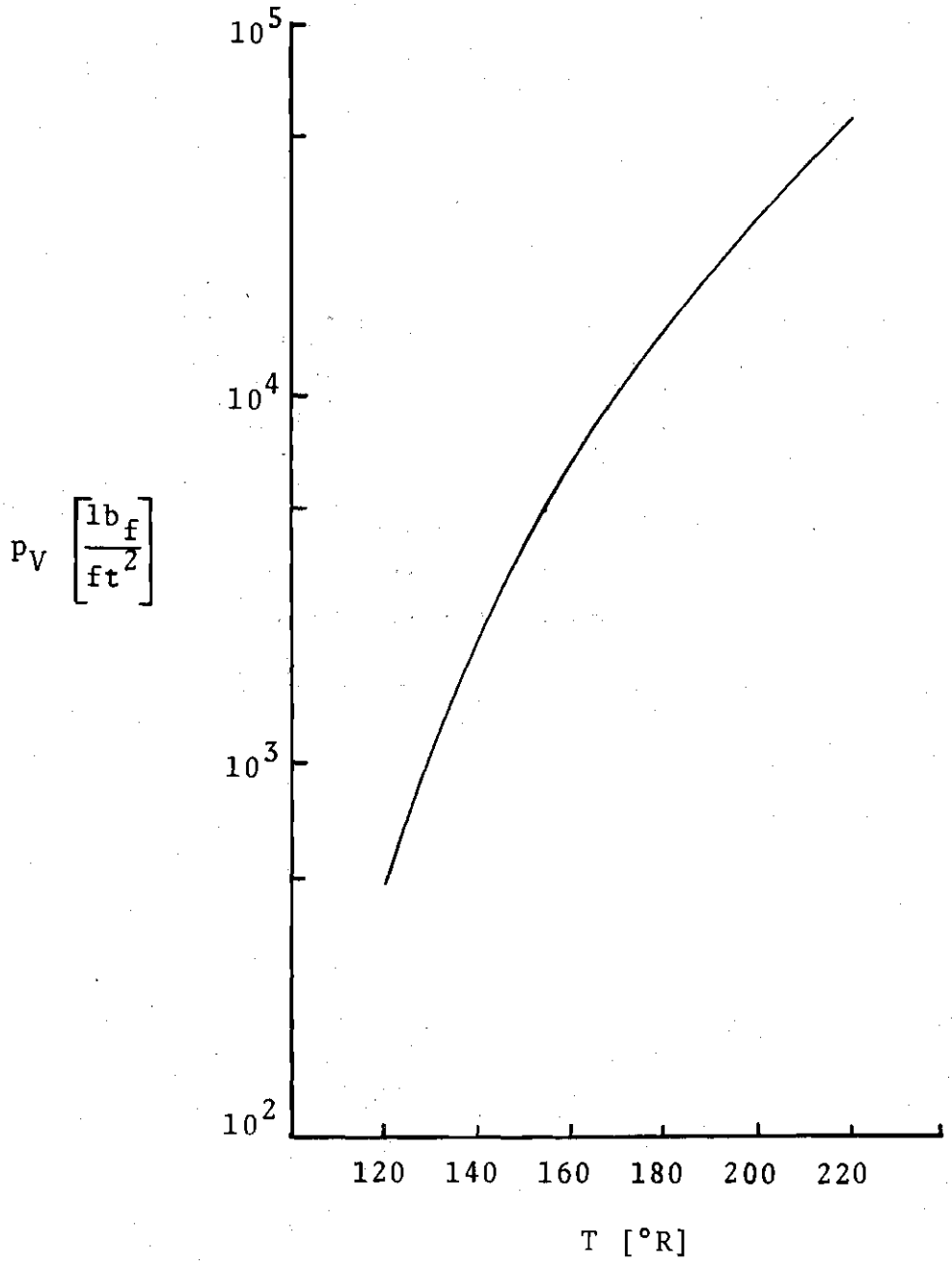

Figure 4. Nitrogen Vapor Pressure Versus Temperature [28]

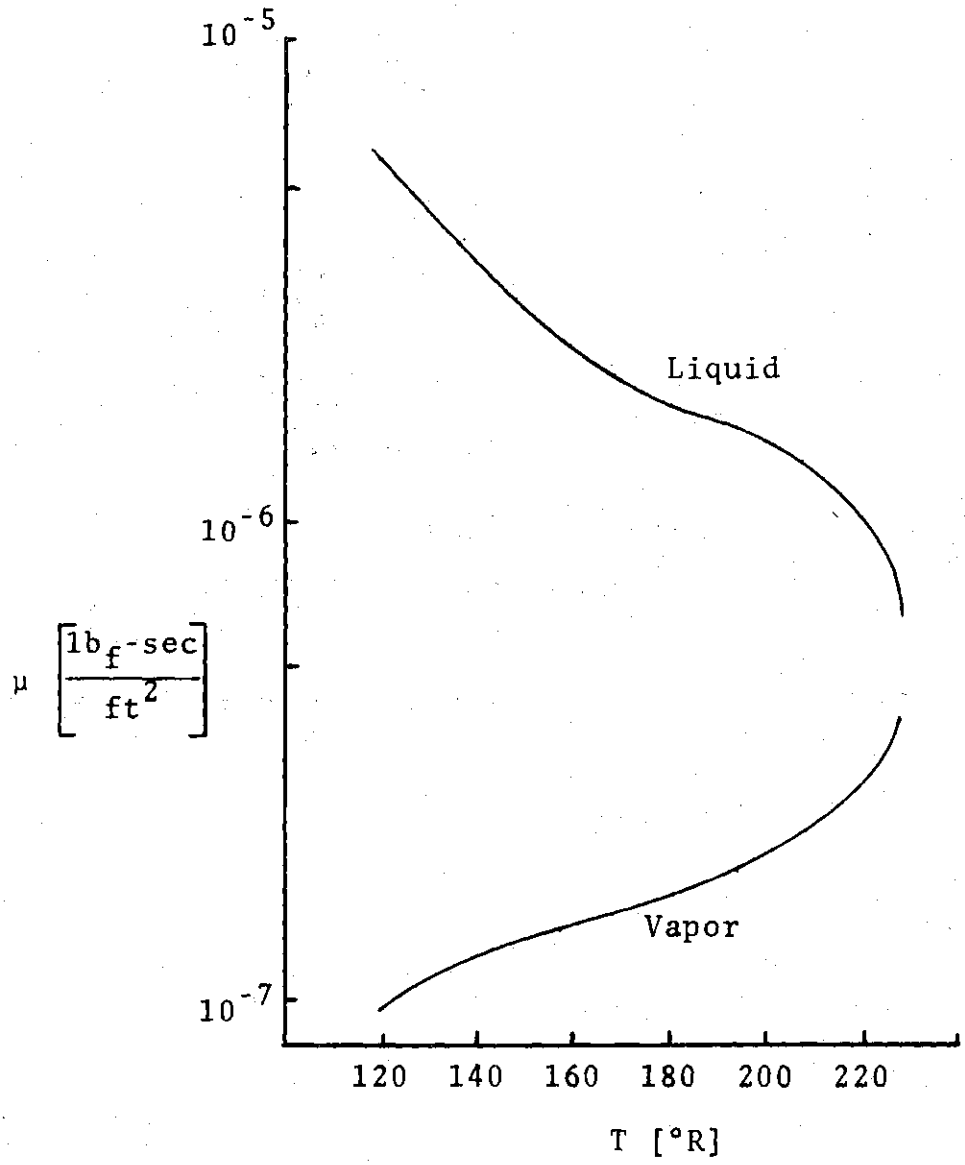

Figure 5. Nitrogen Viscosity Versus Temperature [28]

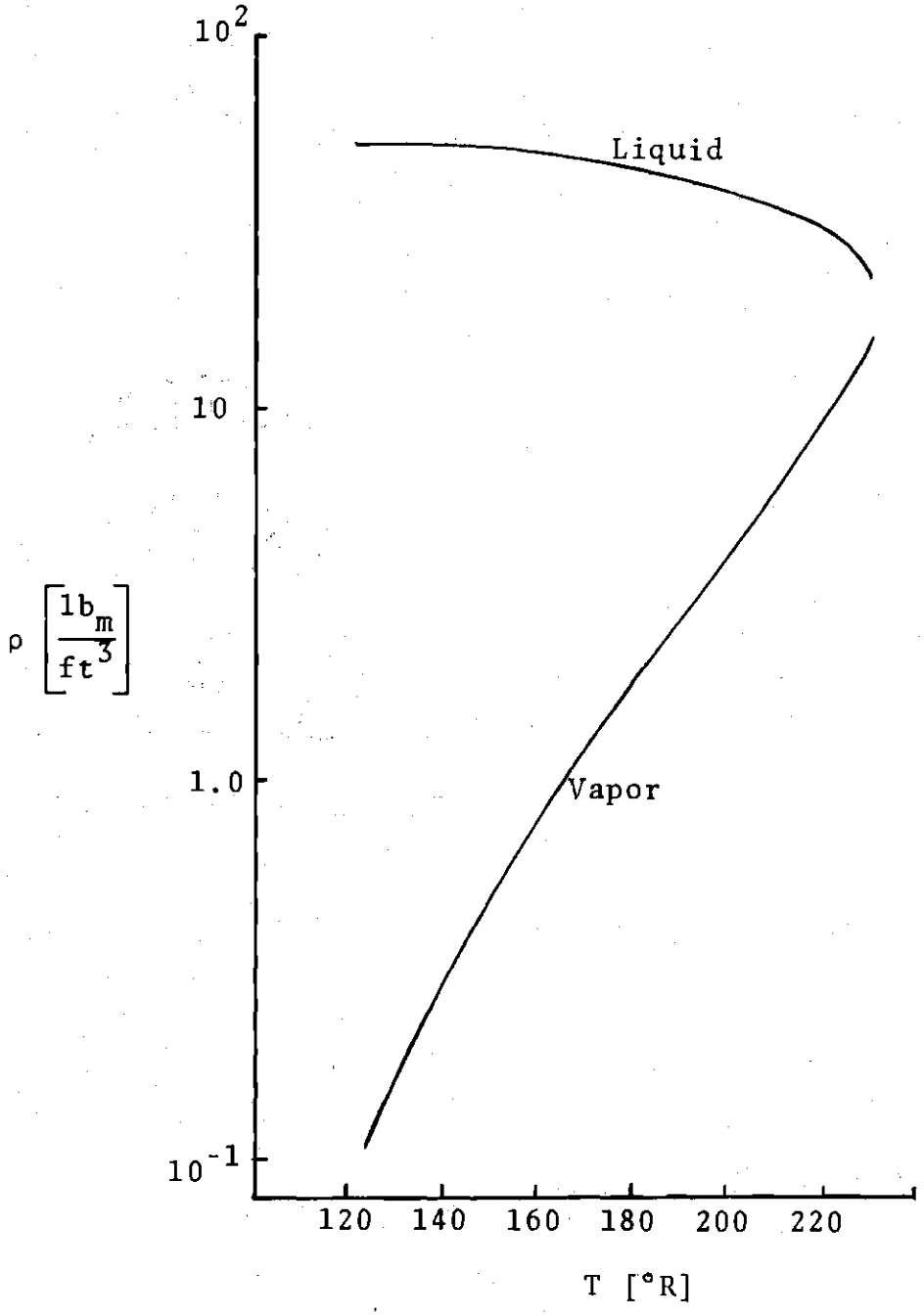

Figure 6. Nitrogen Density Versus Temperature [28]

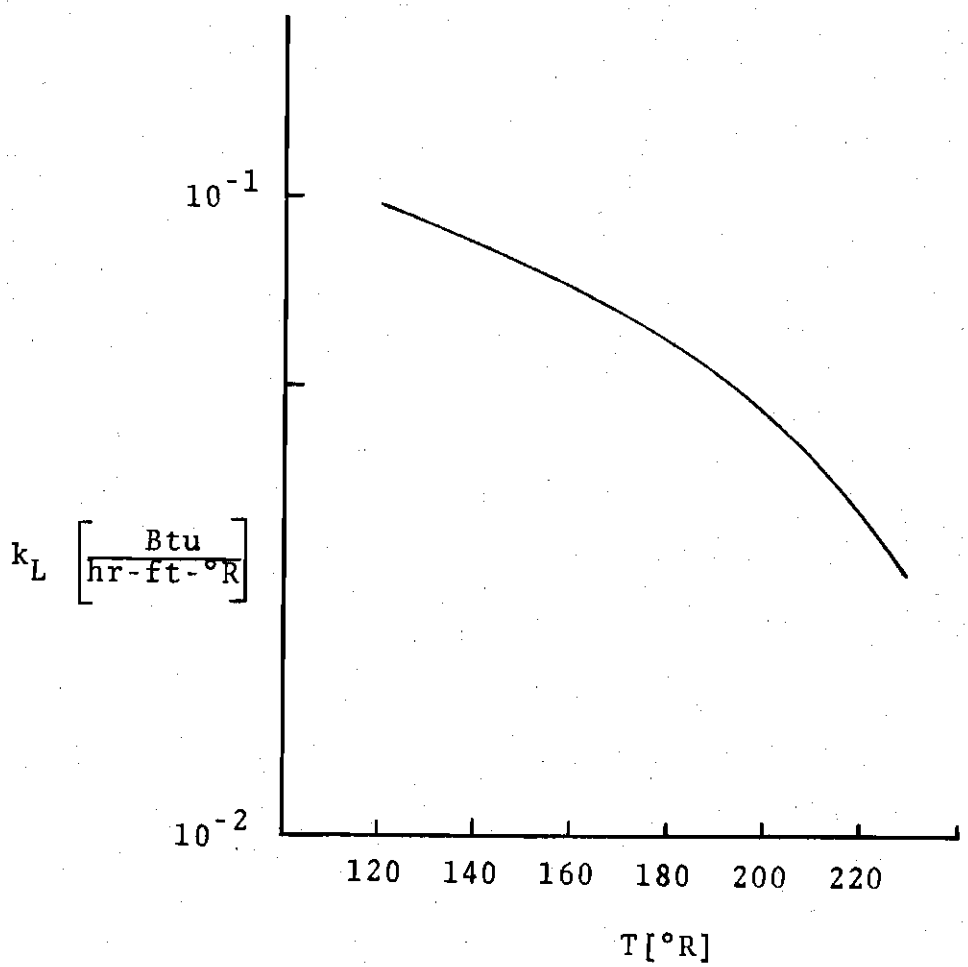

Figure 7. Thermal Conductivity of Liquid Nitrogen Versus Temperature [28]

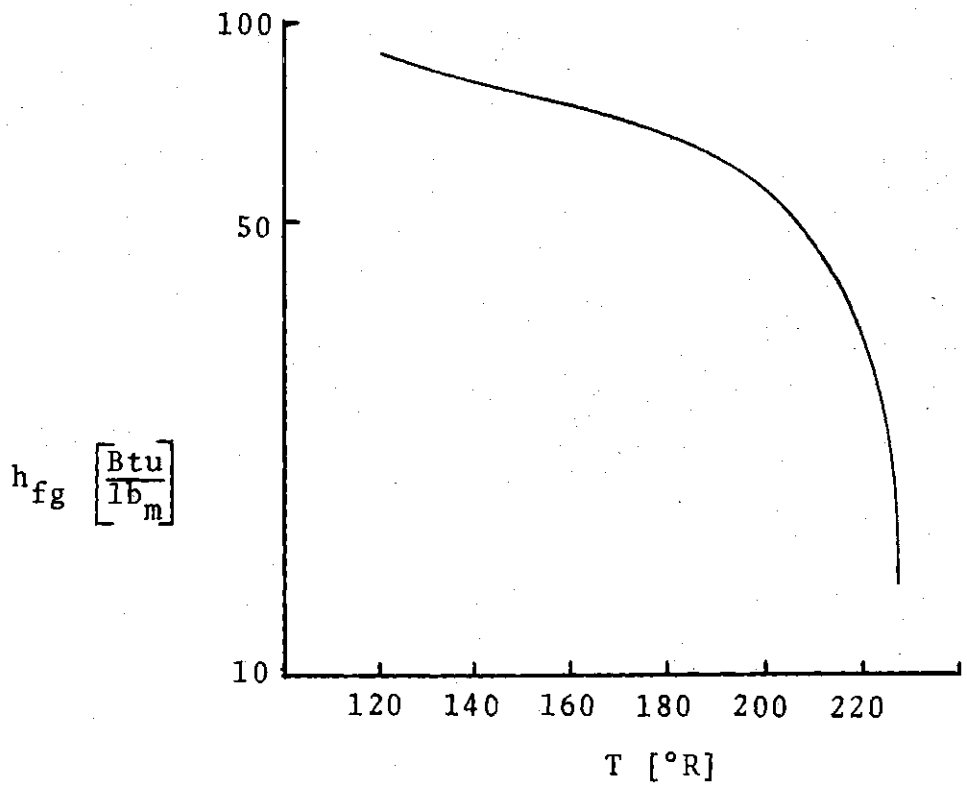

Figure 8. Heat of Vaporization of Nitrogen Versus Temperature [28]

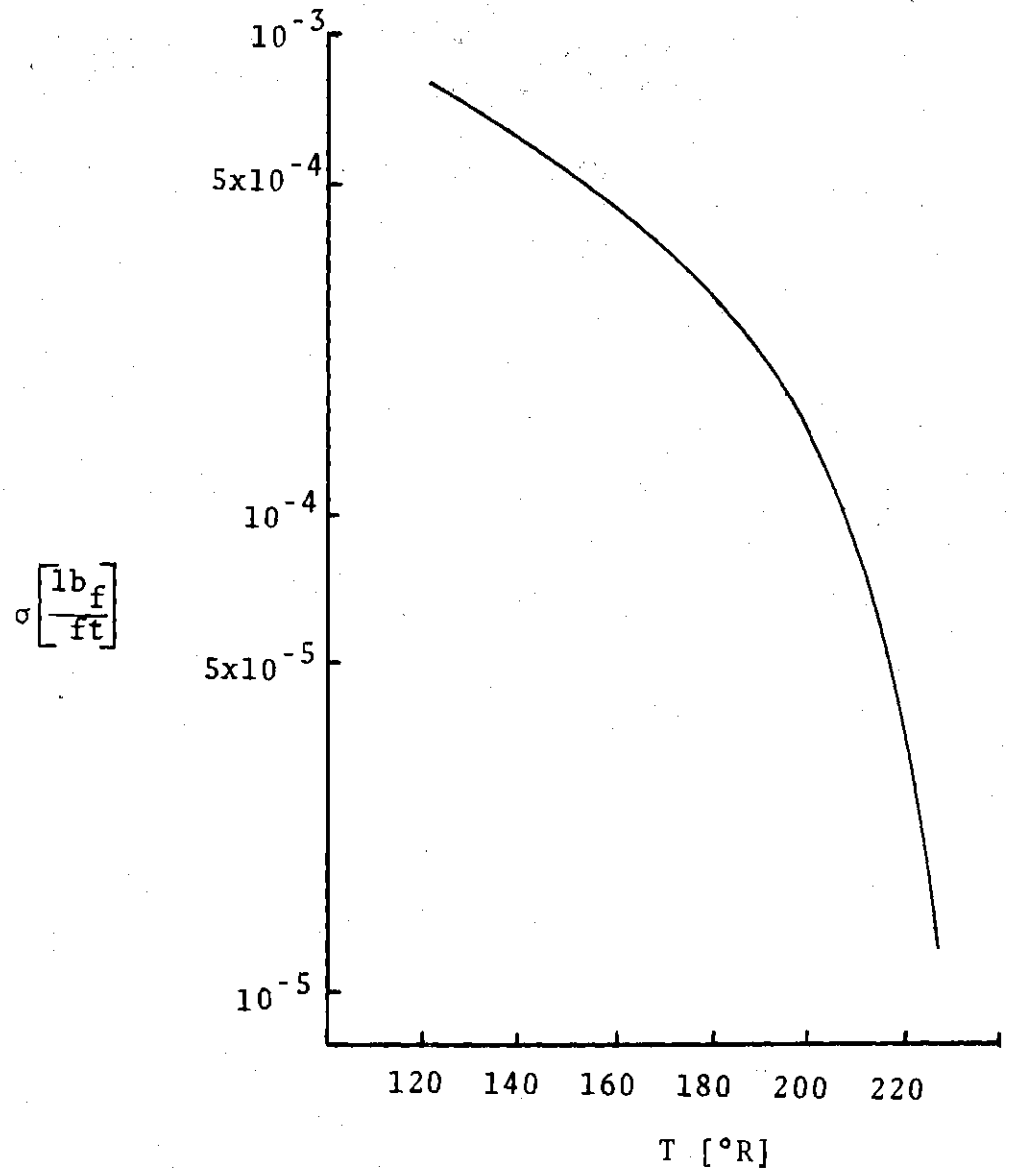

Figure 9. Surface Tension of Liquid Nitrogen Versus Temperature [28]

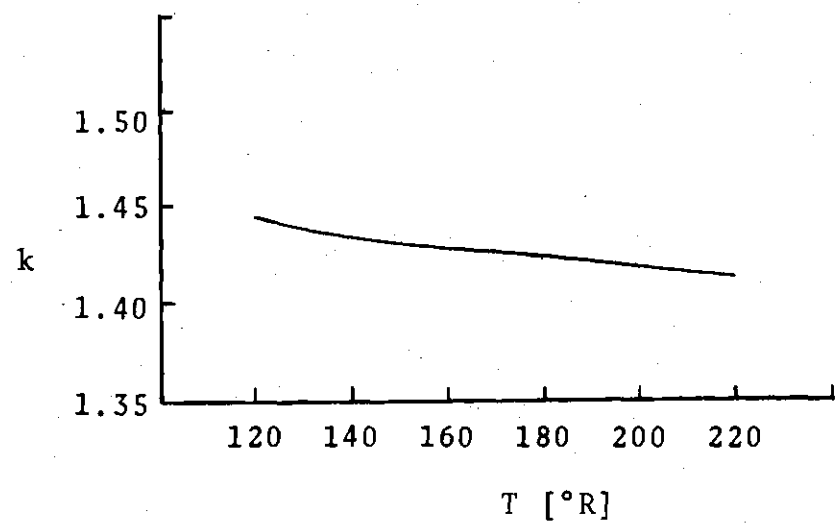

Figure 10. Ratio of Specific Heat of Nitrogen Versus Temperature [28]

properties used in this study. Figure 11 gives a plot of the heat pipe number. A function of several fluid properties, this useful design parameter is calculated using Eq. (3.23). Figure 12 shows a plot of thermal conductivity of 304 stainless steel versus temperature.

D. Wire Screen Properties and Wick Geometry

Since it is the screen properties that govern the liquid transport characteristics of the wick, they are the major factors to be considered in selecting screen to make up the internal porous media. Considerable variation in published screen property data dictated the use of conservation values of screen porosity and permeability resulting in relatively low heat fluxes. By modeling various combinations of screens, the relationship between the liquid transport ability of the porous media and the performance of the heat pipe is numerically illustrated. Table 2 gives a description of the six composite wick systems modeled in this theoretical study.

E. Computer Programs

The previously discussed pipe geometry, thermodynamic properties of the materials and working fluid, and the wick screen properties are used in conjunction with the mass- and heat-transport equations given in Chapter III to predict the heat pipe performance. For machine computation, the three computer programs shown in Appendices C, D and E were

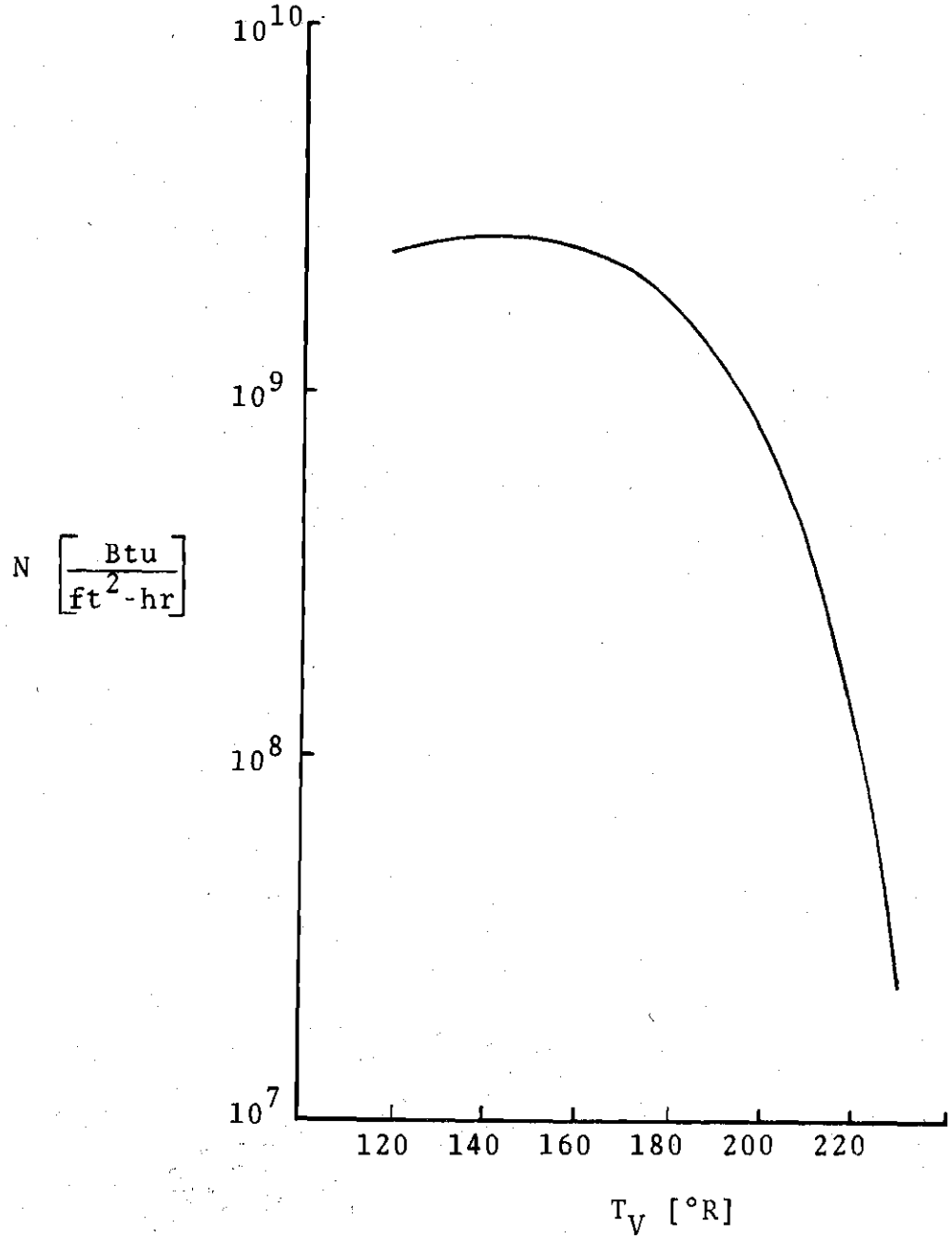

Figure 11. Heat Pipe Number Versus Vapor Temperature

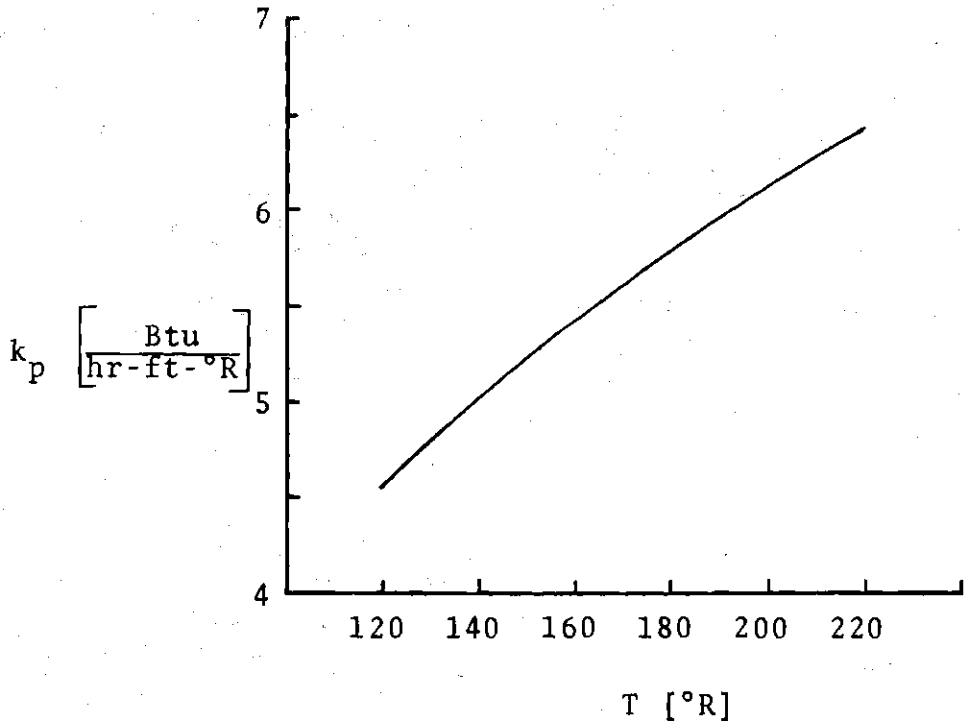

Figure 12. Thermal Conductivity of 304 Stainless Steel Versus Temperature [30]

Table 2. Description of Composite Wick Systems Considered in this Study

Wick Composition Number	Screen Mesh Size			Number of Layers			Screen Thickness-Ft			Total Thickness of Slab-Ftx10^3
	A	B	C	n_A	n_B	n_C	$\delta_A x10^4$	$\delta_B x10^3$	$\delta_C x10^4$	$\delta_T=n_A\delta_A+n_B\delta_B$
1	250	100	250	2	8	1	2.84	1.03	2.84	8.808
2	325	70	325	2	6	1	2.67	1.37	2.67	8.754
3	400	50	400	2	5	1	2.44	1.47	2.44	7.838
4	400	30	400	2	4	1	2.44	2.04	2.44	8.648
5	400	30	400	2	6	1	2.44	2.04	2.44	12.728
6	400	30	400	4	5	2	2.44	2.04	2.44	11.176

Wick Composition Number	Wire Diameter "C" Layer Ft x 10^4	Pore Radius "C" Layer Ft x 10^4	Inverse Permeability-Ft^{-2}			Effective Permeability-Ft^{-2}
			$K_A x10^{-9}$	$K_B x10^{-7}$	$K_C x10^{-9}$	$\bar{K}=\delta_T/(\frac{n_A\delta_A}{K_A}+\frac{n_B\delta_B}{K_B})x10^{-7}$
1	1.58	1.176	5.43	243	5.43	252.6
2	1.30	1.00	10.99	117.2	10.99	123.95
3	1.02	.625	15.168	18.1	15.168	19.286
4	1.02	.625	15.168	5.908	15.168	6.2598
5	1.02	.625	15.168	5.908	15.168	6.1426
6	1.02	.625	15.168	5.908	15.168	6.4709

written. These computer programs calculate the following parameters over the temperature range $120°R \leq T \leq 225°R$:

(1) Thermal resistances of each pipe and wick component as well as theoretical heat transfer, disregarding all performance restrictions.

(2) Capillary-limited heat transfer rates and heat pipe numbers.

(3) Sonic-limited heat transfer rates.

In each of these computer programs it is a simple matter to alter the properties of the internal capillary structure. Therefore, values of the parameters listed above may be obtained for each of the six wick compositions described in Table 2. By doing so, a composite wick system corresponding to the optimum heat pipe performance may be computer modeled. A sample output of each program is given for wick composition 6 in Appendices C, D and E, respectively.

CHAPTER III

THEORY

A. Objective

The objective of this chapter is to list and discuss the several mass- and heat-transport equations which govern the performance of cryogenic heat pipes.

B. Thermal Resistances

The total thermal resistance of the heat pipe, given by Eq. (3.1), is the sum of the thermal resistances of each heat pipe component.

$$R_T = R_{pe} + R_{we} + R_{ie} + R_V + R_{ic} + R_{wc} + R_{pc} \quad \left[\frac{hr\ °R}{Btu}\right] \quad (3.1)$$

where

R_{pe}, R_{pc} = thermal resistance of the pipe wall at the evaporator and condenser, respectively.

R_{we}, R_{wc} = thermal resistance of circumferential wick/liquid combination at the evaporator and condenser, respectively.

R_{ie}, R_{ic} = thermal resistance of the circumferential wick-vapor interface at evaporator and condenser, respectively.

R_V = thermal resistance of the vapor.

These individual component resistances may be more clearly envisioned from the schematic representation shown in Fig. 13.

1. Thermal Resistance of the Pipe Wall

The terms R_{pe} and R_{pc} appearing in Eq. (3.1) are given by the equation for the thermal resistance of concentric cylindrical bodies [31]:

$$R_{pe} = \frac{\ln (r_A/r_B)}{2\pi k_{p_e} \ell_e} \qquad \left[\frac{hr\ ^\circ R}{Btu}\right] \tag{3.2.a}$$

and

$$R_{pc} = \frac{\ln (r_A/r_B)}{2\pi k_{p_c} \ell_c} \qquad \left[\frac{hr\ ^\circ R}{Btu}\right] \tag{3.2.b}$$

where k_{p_e} and k_{p_c} are values of the pipe wall thermal conductivity evaluated at Te and Tc, respectively.

2. Thermal Resistance of the Circumferential Wick-Liquid Combination

The equation giving the thermal resistance of concentric cylindrical bodies is again used to determine the thermal resistance of the circumferential wick-liquid combination at both the evaporator and condenser ends. These equations are given as follows:

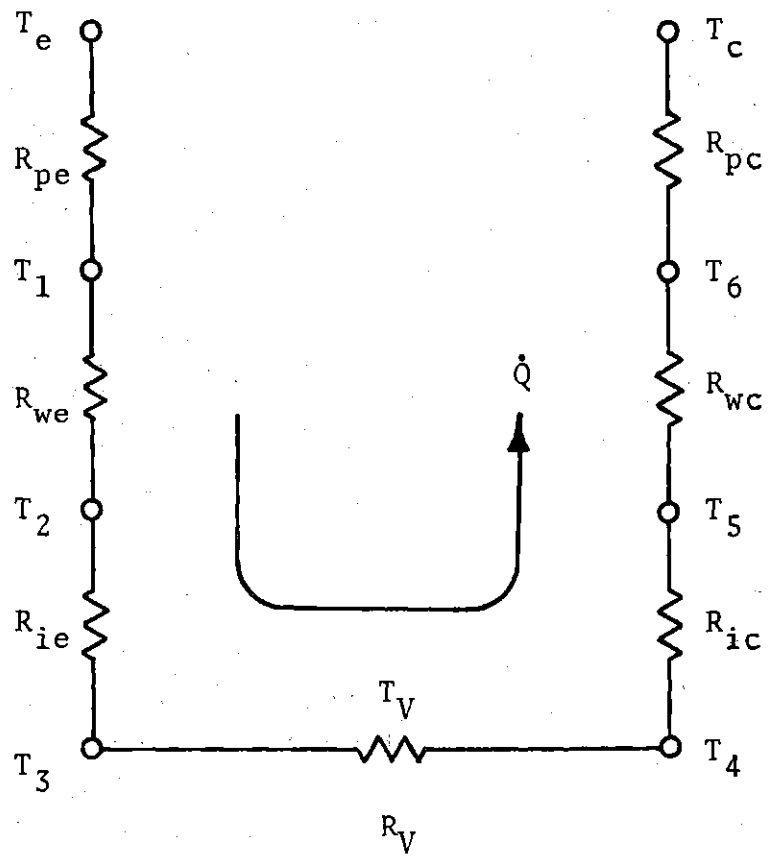

Figure 13. Schematic Representation of Heat Pipe Thermal Resistances

$$R_{we} = \frac{\ln (r_B/r_C)}{2\pi\, k_{w_2}\, \ell_e} \qquad \left[\frac{hr\ ^\circ R}{Btu}\right] \tag{3.3.a}$$

and

$$R_{wc} = \frac{\ln (r_B/r_C)}{2\pi\, k_{w_5}\, \ell_c} \qquad \left[\frac{hr\ ^\circ R}{Btu}\right] \tag{3.3.b}$$

The terms r_A, r_B, and r_C seen in the equations above are the radii of the pipe outer wall, inner wall/wick interface, and inner circumferential wick/vapor interface, respectively. These terms are shown graphically in Fig. 14.

The terms k_{w_2} and k_{w_5} appearing in Eqs. (3.3.a) and (3.3.b) represent the effective thermal conductivity of the circumferential wick/liquid combination evaluated at the temperature of the wick/vapor interface for the evaporator and condenser ends, respectively. Numerical values of these parameters are found by using the following expression developed by Williams [6] (see Appendix F for a sample calculation using Eq. (3.4):

$$\frac{k_w(t)}{k_L(t)}^{*} = \frac{1}{[A][2D+C]} + \frac{2.0}{[A][D][B]} + \frac{1}{[B]^2} \tag{3.4}$$

where

---

*Note: (t) indicates function of temperature.

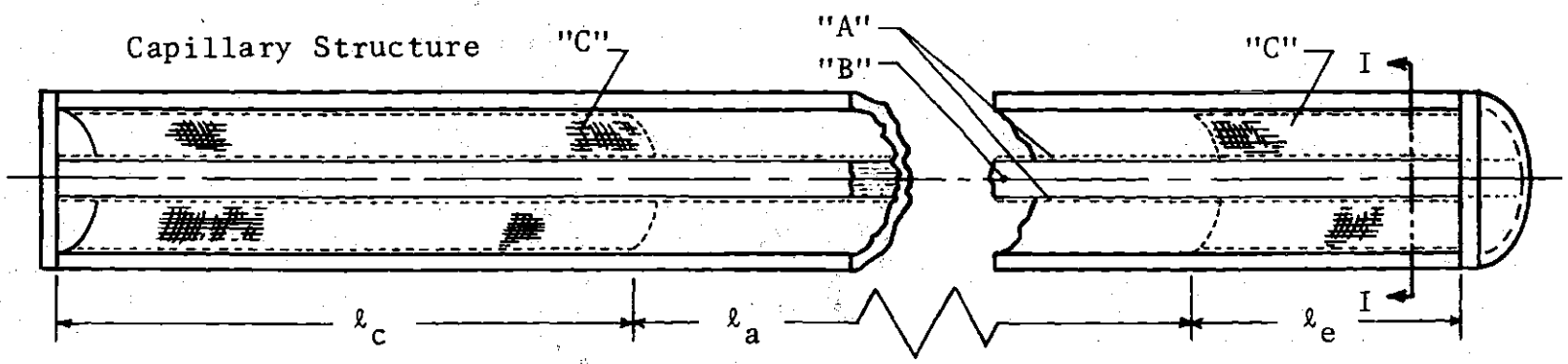

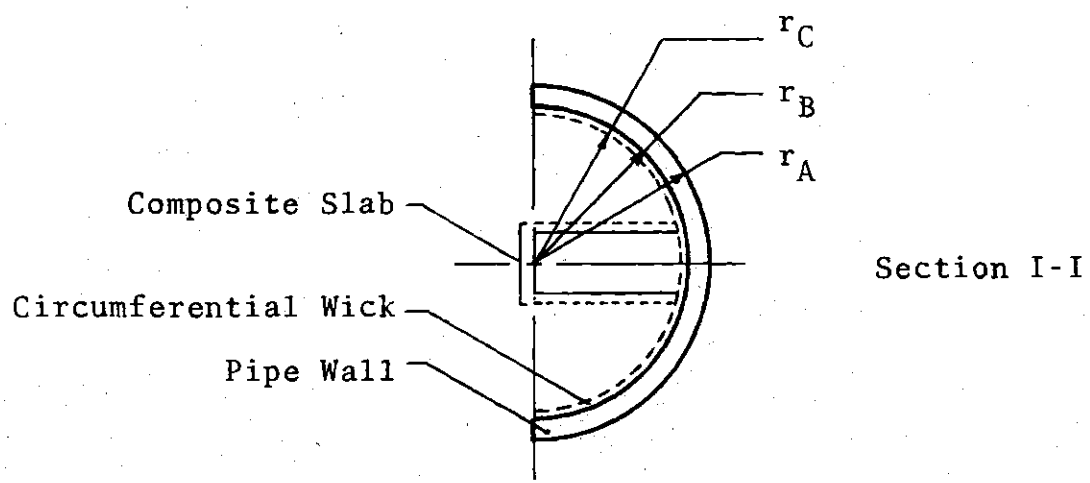

Figure 14. Cut-Away Views of Composite Wick System

$$[A] = \frac{r_p}{r_{ws}} + 1.0 \qquad (3.4.a)$$

$$[B] = \frac{r_{ws}}{r_p} + 1.0 \qquad (3.4.b)$$

$$[C] = \frac{r_p}{r_{ws}} - 1.0 \qquad (3.4.c)$$

$$[D] = \frac{k_L(t)}{k_p(t)} \qquad (3.4.d)$$

r_{ws} = radius of screen element

r_p = screen pore radius

3. Thermal Resistance of the Circumferential Wick/Vapor Interface

The following expressions, derived from kinetic theory [6,7], may be used to determine the interfacial thermal resistance between the circumferential wick and the vapor at the evaporator and condenser, respectively:

$$R_{ie} = \frac{(2\pi)^{1/2}\ R^{3/2}\ T_2^{5/2}}{4\pi\ r_C\ \ell_e\ P_{V_2}\ h_{fg_2}^2\ g_c^{1/2}} \quad \left[\frac{hr\ ^\circ R}{Btu}\right] \qquad (3.5.a)$$

and

$$R_{ic} = \frac{(2\pi)^{1/2}\ R^{3/2}\ T_5^{5/2}}{4\pi\ r_C\ \ell_c\ P_{V_5}\ h_{fg_5}^2\ g_c^{1/2}} \quad \left[\frac{hr\ ^\circ R}{Btu}\right] \qquad (3.5.b)$$

4. Thermal Resistance of the Vapor

By assuming relatively small pressure gradients in the vapor space [4,7], an expression for the thermal resistance of the vapor may be obtained from the Clausius-Clapeyron equation [6].

$$T_3 - T_4 = \frac{\Delta P_V \; T_3 \; (\frac{1}{\rho_V} - \frac{1}{\rho_V})}{h_{fg}} \qquad [°R] \qquad (3.6)$$

where

$T_3 - T_4$ = temperature gradient in the vapor space.

In addition, the assumption is made that fully-developed, laminar flow conditions exist in the vapor space. Therefore, the Poiseuille flow equation may be used to give the vapor pressure drop due to viscous effects [32]. Thus:

$$^{*}\ \Delta P_V = \frac{8\mu_V \dot{m}_V \ell_{eff}}{\pi \rho_V r_v^4} \qquad \left[\frac{lb_f}{ft^2}\right] \qquad (3.7)$$

where:

ℓ_{eff} = effective length of the heat pipe

$= \ell_a + 1/2\ (\ell_e + \ell_c)$

r_v = hydraulic radius of the vapor space (see Appendix H).

*The Poiseuille flow equation is given further consideration in Section C.1 of Chapter III.

The heat transfer rate in the vapor space is given by:

$$\dot{Q} = \frac{T_3 - T_4}{R_V} \qquad \left[\frac{Btu}{hr}\right] \tag{3.8}$$

or, rearranging,

$$R_V = \frac{T_3 - T_4}{\dot{Q}} \qquad \left[\frac{°R\ hr}{Btu}\right] \tag{3.8.a}$$

For the purposes of this theoretical study, it is assumed that the heat transferred axially by the pipe wall is negligible. In addition, the assumption is made that the total energy input to the pipe is taken up in the phase change of the working fluid [6]. With these assumptions the heat transfer rate is given by

$$\dot{Q} = \dot{m}_V\, h_{fg} \qquad \left[\frac{Btu}{hr}\right] \tag{3.9}$$

Equations (3.8.a) and (3.9) are combined to give:

$$R_V = \frac{T_3 - T_4}{\dot{m}_V\, h_{fg_3}} \qquad \left[\frac{°R\ hr}{Btu}\right] \tag{3.10}$$

However $T_3 - T_4$, the driving potential in the vapor space, is

given by Eq. (3.6). Substitution of Eq. (3.6) into Eq. (3.10) gives

$$R_V = \frac{\Delta P_V \; T_3}{\dot{m}_V \; h_{fg}^2} \left(\frac{1}{\rho_V} - \frac{1}{\rho_L}\right) \qquad \left[\frac{^\circ R \; hr}{Btu}\right] \tag{3.11}$$

A substitution of Eq. (3.7) into Eq. (3.11) gives:

$$R_V = \frac{8\mu_V \; \ell_{eff} \; T_3 \left(\frac{1}{\rho_V} - \frac{1}{\rho_L}\right)}{\pi \; \rho_V \; h_{fg}^2 \; r_v^4} \qquad \left[\frac{hr \; ^\circ R}{Btu}\right] \tag{3.12}$$

The thermodynamic property terms in Eq. (3.12) are evaluated at the vapor temperature, T_3.

5. The Total Thermal Resistance

By substituting the equations giving the thermal resistance of each component, Eq. (3.1) may be written as

$$R_T = \frac{\ln (r_A/r_B)}{2\pi \; k_{p_e} \; \ell_e} + \frac{\ln (r_B/r_C)}{2\pi \; k_{w_2} \; \ell_e} +$$

$$+ \frac{(2\pi)^{1/2} \; R^{3/2} \; T_2^{5/2}}{4\pi \; r_C \; \ell_e \; P_{V_2} \; h_{fg}^2 \; g_c^{1/2}} + \frac{8\mu_v \; \ell_{eff} \; T_3 \left(\frac{1}{\rho_V} - \frac{1}{\rho_L}\right)}{\pi \; \rho_V \; h_{fg_3}^2 \; r_v^4} +$$

$$+ \frac{(2\pi)^{1/2} \; R^{3/2} \; T_5^{5/2}}{4\pi \; r_C \; \ell_c \; P_{V_5} \; h_{fg_5}^2 \; g_c^{1/2}} + \frac{\ln (r_B/r_C)}{2\pi \; k_{w_5} \; \ell_c} + \frac{\ln (r_A/r_B)}{2\pi \; k_{p_c} \; \ell_c} \qquad \left[\frac{hr \; ^\circ R}{Btu}\right]$$

where k_{w_2} and k_{w_5} are given by Eq. (3.4) evaluated at T_2 and T_5, respectively.

The theoretical heat transfer rate of the pipe, disregarding performance limitations, is given by

$$\dot{Q}_{max} = \frac{\Delta T}{R_T} = \frac{T_e - T_c}{R_T} \qquad \left[\frac{Btu}{hr}\right] \tag{3.13}$$

Sample hand calculations showing thermal resistances of each heat pipe and wick component are presented in Appendix G. Additionally, Appendix C gives a computer listing of the thermal resistances for wick composition.

C. Heat Pipe Performance Limitations

Equation (3.13) gives the unrestricted heat transfer rate of the heat pipe. However, as stated in Chapter I, there are several factors which limit heat pipe performance [4]. Heat transfer rates which can be realized under these limitations form the upper bounds of heat pipe performance. The limiting conditions are defined as follows:

1. Capillary pumping limitations: A restriction occurring when the pumping mechanism of the capillary structure cannot maintain a sufficient flow rate of liquid to the evaporator. Thus the evaporator wick is starved causing it to dry out. This upsets the continuity of the liquid flow.

2. "Choking" or sonic limitation: A performance

limiting condition characterized by the vapor velocity approaching sonic velocity. This results in "choked flow" or shock conditions in the vapor space. Thus, no increase in mass flow rate can be realized for an increase in energy input.

3. Entrainment limitation: A condition also characterized by vapor velocities of large magnitude, occurring when liquid droplets are sheared from the wick surface by the rapidly passing vapor. This hinders the liquid flow, enhancing the possibility of failure due to dry-out.

4. Boiling in the evaporator: A condition which occurs when the heat input to the evaporator is so great that the vaporization mechanism is changed from evaporation to nucleate boiling or localized film boiling.

The performance of any heat pipe may safely be assumed to be governed by at least one of the above limitations [33]. For the purposes of this study, it was assumed that the restrictions imposed by entrainment and boiling in the evaporator have no influence on the heat pipe performance in the cryogenic temperature range. Therefore, only the capillary pumping and the sonic limitations were investigated in this work.

1. Capillary Structure Limitation

The purpose of this section is to apply the governing concepts of mass transport in the liquid phase to the composite wick system. By doing so, an expression will be

derived giving the heat transfer rate corresponding to the capillary pumping limitation. This rate of heat transfer shall be referred to as the capillary-limited heat transfer rate, and given the symbol $\dot{Q}_{CL}$.

Momentum Considerations. From conservation of momentum considerations, the following equation may be written for an element of mass in the heat pipe:

$$\Sigma \text{ external forces} = \frac{\partial}{\partial t}(mv) \tag{3.14}$$

A major simplifying assumption made in this study is that of steady-state operation in a zero gravitational field.* Under this assumption, the change of momentum with respect to time is taken to be zero. The problem is thus reduced to one of balancing the pressure gradients in the capillary structure with those due to viscosity. Equation (3.14) then becomes

$$\Delta P_{cap} = \Delta P_V + \Delta P_L \tag{3.15}$$

where

ΔP_{cap} = capillary pumping pressure

ΔP_L = pressure gradient in the liquid due to viscosity

*The consequences of this assumption are discussed by Williams [6].

ΔP_V = pressure gradient in the vapor due to viscosity. The interfacial pressure differentials have been neglected due to their extremely small magnitude [6,32].

Capillary Pumping Pressure. Scheidegger [34] gives the capillary pumping pressure as:

$$\Delta P_{cap} = \frac{2\sigma}{r_{ev}} - \frac{2\sigma}{r_{cd}} \qquad \left[\frac{lb_f}{ft^2}\right] \tag{3.16}$$

As the maximum capillary limited heat transfer is approached, the wick conditions shown graphically in Fig. 15 are realized. The wick at the condenser section tends to fill with liquid causing r_{cd}, the meniscus radius at the condenser, to approach infinity. Conversely, at the evaporator end, the liquid is evaporated more rapidly, causing the liquid surface to sink into the capillary structure. Ideally, as the heat transfer rate approaches that limited by the capillary structure, the meniscus radius at the evaporator, r_{ev}, approaches the pore radius of the wick screen, r_p. Therefore, in the limit, the following conditions exist:

$$\lim_{\dot{Q}\to\dot{Q}_{CL}} r_{cd} \to \infty \therefore \frac{2\sigma}{r_{cd}} \to 0 \tag{3.17.a}$$

and,

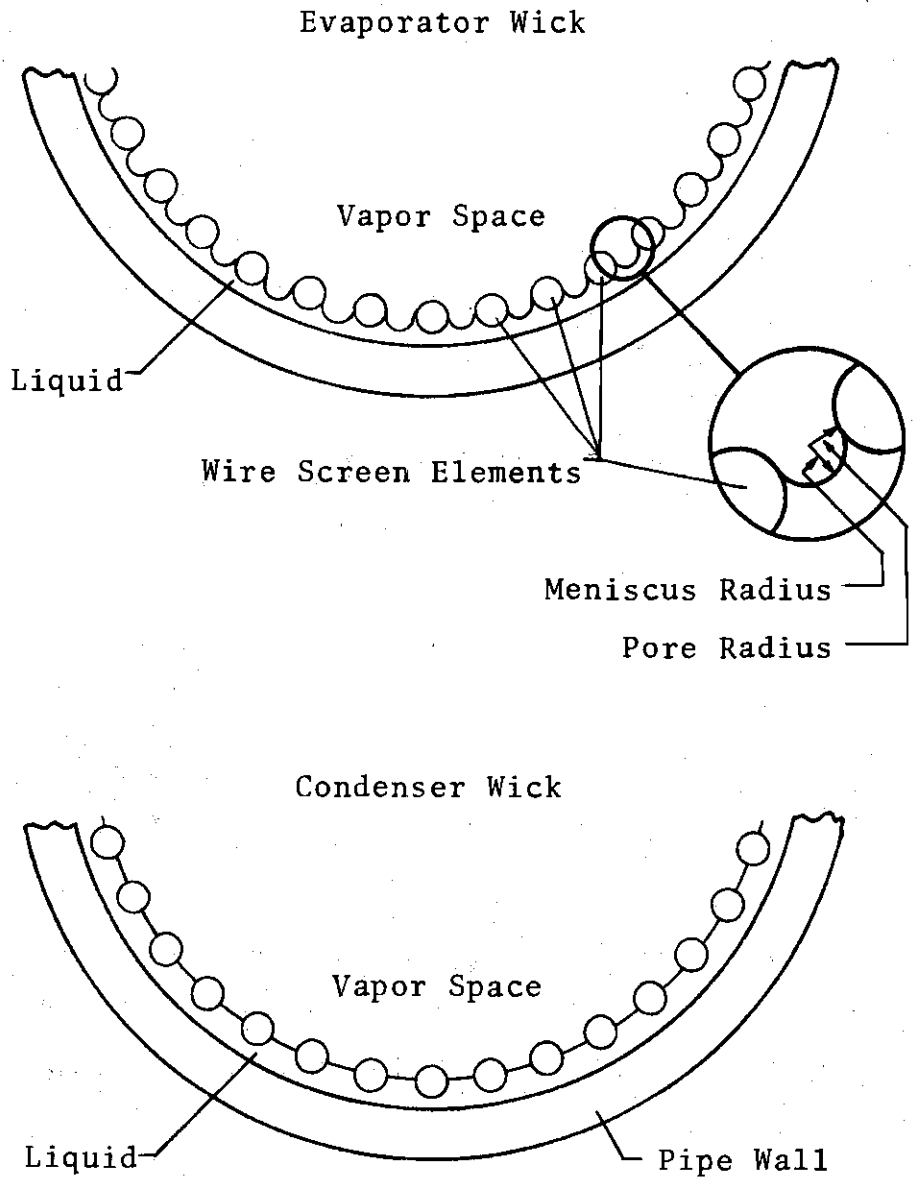

Figure 15. Circumferential Wicks Showing Existing Conditions for Maximum Capillary-Limited Heat Transfer Rate

$$\lim_{\dot{Q}\to\dot{Q}_{CL}} r_{ev} \to r_p \quad \therefore \quad \frac{2\sigma}{r_{ev}} \to \frac{2\sigma}{r_p} \tag{3.17.b}$$

Equation (3.16) may now be rewritten as:

$$\Delta P_{cap} = \frac{2\sigma}{r_p} \qquad \left[\frac{lb_f}{ft^2}\right] \tag{3.18}$$

where:

σ = liquid surface tension $\left[\frac{lb_f}{ft}\right]$.

Viscous Pressure Drop in the Vapor Space. By assuming fully-developed laminar flow in the vapor space, the vapor pressure drop due to viscous effects is given by the previously seen Poiseuille flow [35,36,37].

$$\Delta P_V = \frac{8\mu_V \dot{m}_V \ell_{eff}}{\pi \rho_V r_v^4} \qquad \left[\frac{lb_f}{ft^2}\right] \tag{3.7}$$

where:

r_v = hydraulic radius of the vapor space.

Viscous Pressure Drop in the Liquid. ΔP_L, the pressure drop in the liquid due to viscosity, is given by the following expression:

$$\Delta P_L = \frac{\dot{m}_L \mu_L}{\rho_L} \left[\frac{\overline{K}\,\ell_{eff}}{b\delta_T} + \frac{K_C L}{4n_C \delta_C}\left(\frac{1}{\ell_e} + \frac{1}{\ell_c}\right)\right] \qquad \left[\frac{lb_f}{ft^2}\right] \tag{3.19}$$

The derivation of Eq. (3.19) is given in Appendix I.

A substitution of the expressions giving the pressure differentials into Eq. (3.15), yields the following:

$$\frac{2\sigma}{r_p} = \frac{\dot{m}_L \mu_L}{\rho_L}\left[\frac{\overline{K}\,\ell_{eff}}{b\delta_T} + \frac{K_C L}{4n_C\delta_C}\left(\frac{1}{\ell_e} + \frac{1}{\ell_c}\right)\right] + \frac{8\mu_V \dot{m}_V \ell_{eff}}{\pi\,\rho_V\, r_v^4} \qquad (3.20)$$

Conservation of mass considerations require the vapor transport rate in the vapor space and the liquid transport rate in the composite wick to be equal. This is expressed as:

$$\dot{m}_L = \dot{m}_V = \dot{m} \qquad (3.21)$$

By substituting Eqs. (3.9) and (3.21), Eq. (3.20) may be rewritten as

$$\frac{2\sigma}{r_p} = \frac{\dot{Q}}{h_{fg}}\frac{\mu_L}{\rho_L}\left[\frac{\overline{K}\,\ell_{eff}}{b\delta_T} + \frac{K_C L}{4n_C\delta_C}\left(\frac{1}{\ell_e} + \frac{1}{\ell_c}\right)\right] + \frac{8\mu_V\,\dot{Q}\,\ell_{eff}}{\pi\,\rho_V\,h_{fg}\,r_v^4} \qquad (3.22)$$

Equation (3.22) may be rearranged to give the following expression for the capillary-limited heat transfer rate:

$$\dot{Q}_{CL} = \frac{(2h_{fg}\,\rho_L)/\mu_L}{r_p\left[\frac{\overline{K}\ell_{eff}}{b\delta_T} + \frac{K_C L}{4n_C\delta_C}\left(\frac{1}{\ell_e} + \frac{1}{\ell_c}\right) + \frac{8\mu_V\rho_L\ell_{eff}}{\pi\,\mu_L\rho_V\,r_v^4}\right]} \quad \left[\frac{Btu}{hr}\right] \qquad (3.22)$$

Being less than the nonrestricted heat transfer rate given by Eq. (3.13), the capillary limitation forms the upper boundary of the heat pipe performance. Increasing the power load beyond this upper boundary results in failure due to the inability of the wick to maintain a sufficient liquid flow rate.

The group of thermodynamic properties given in the numerator of Eq. (3.22) is known as the "heat pipe number, N."

$$N = \frac{\sigma\, h_{fg}\, \rho_L}{\mu_L} \qquad \left[\frac{Btu}{ft^2\ hr}\right] \tag{3.23}$$

Making the substitution, the capillary limitation heat transfer equation becomes:

$$\dot{Q}_{CL} = \frac{2N/r_p}{\frac{\overline{K}\,\ell_{eff}}{b\delta_T} + \frac{K_C L}{4n_C\delta_C}\left(\frac{1}{\ell_e} + \frac{1}{\ell_c}\right) + \frac{8\mu_V\rho_L\ell_{eff}}{\pi\,\mu_L\rho_V\,r_v^4}} \qquad \left[\frac{Btu}{hr}\right] \tag{3.24}$$

It is obviously desirable to maximize the capillary-limited heat transfer rate for optimum heat pipe performance. This may be accomplished by constructing a porous media having the characteristics of small pore radii and small values of inverse permeability. As indicated by Eq. (3.18), screens with small pore radii provide greater capillary

pumping pressure. For this reason, it appears that the larger mesh number screens would offer superior performance characteristics. Unfortunately, the large mesh screens have larger values of inverse permeability or friction factor (see Appendix A). Thus the liquid transport capability of the larger mesh screens is less than that of the smaller mesh screens. This conflict in the desired screen properties has led to the development of composite wick systems [12] such as that studied in this investigation.

The composite wick system is made up of three components: the central composite slab running the length of the heat pipe and the circumferential wicks lining the wall at the two heat transfer sections. The composite slab is composed of several layers of small mesh number screen "sandwiched" between layers of large mesh number screens. The coarse interior layers of the slab provide good liquid transport capability while the surface layers provide greater capillary pumping pressure. The two circumferential wicks are homogenous in that they are composed of one or more layers of a single mesh screen. The larger mesh number screens are used in these areas to provide sufficient capillary pumping. The concept of the composite wick system is shown graphically in Fig. 3.

2. Sonic Limitation

In any attempt to optimize the performance of a cryogenic heat pipe, consideration must be given to the sonic

limitation on the heat transfer rate of the pipe. As the heat input to evaporator end of the pipe increases, the mass flow in the vapor space likewise increases. The sonic-limited heat transfer rate is that rate of heat input at which the vapor velocity reaches sonic velocity.

Hansen [35] gives the speed of sound in a vapor for an ideal gas as

$$c = (g_c k R T)^{1/2} \tag{3.25}$$

where:

c = speed of sound in the vapor

k = ratio of vapor specific heat

R = vapor gas constant

T = vapor temperature

Although it is realized that nitrogen does not behave as an ideal gas, this assumption may be made in an approximation of the sonic-limitation. The continuity equation gives:

$$\dot{m}_V = A_x \rho_V U_V \tag{3.26}$$

where:

$\dot{m}_V$ = vapor mass flow rate

ρ_V = vapor density

U_V = vapor velocity

A_x = vapor space cross sectional area.

As stated earlier, the assumption is made that the total energy input to the pipe is taken up by phase change of the working fluid. Recalling Eq. (3.9)

$$\dot{m}_V = \frac{\dot{Q}}{h_{fg}} \qquad \left[\frac{lb_m}{hr}\right] \tag{3.9}$$

Obviously, the maximum mass flow rate in the vapor space gives the maximum value of heat transfer. This maximum heat transfer rate under these conditions shall be referred to as the sonic-limited heat flux, $\dot{Q}_{SL}$.

$$\dot{Q}_{SL} = \dot{m}_{V_{max}} h_{fg} \qquad \left[\frac{Btu}{hr}\right] \tag{3.27}$$

The maximum mass flow rate is given by Eq. (3.26) when $U_V = c = U_{max}$, the vapor velocity at which sonic conditions are reached. Therefore, combining these equations yields:

$$\dot{Q}_{SL} = h_{fg} A_x \rho_V [g_c KRT]^{1/2} \qquad \left[\frac{Btu}{hr}\right] \tag{3.28}$$

The computer program used to calculate $\dot{Q}_{SL}$ and the resulting computer output is given in Appendix E.

CHAPTER IV

PARAMETRIC DISCUSSION AND RESULTS

A. Objective

The purpose of this chapter is to discuss the influence of wick composition on heat pipe performance. In addition, the values of several performance parameters obtained from this study will be compared with published results of investigations involving heat pipes of similar design.

B. Discussion of Performance Parameters

There are several design parameters which may be varied in an attempt to optimize the heat pipe performance. These parameters include geometry, working fluid, material, and wick composition. However, as was stated in Chapter II, these parameters were fixed by the sponsoring agency, with the exception of wick composition. Therefore, this study focuses on the performance of a heat pipe of a single design employing several different wick compositions. Table 2, in describing these compositions, gives the properties and important physical dimensions of the screen composing each component of the composite wick system.

Figures 16 and 17 show, for wick compositions 1 and 6, respectively, thermal resistances of each heat pipe

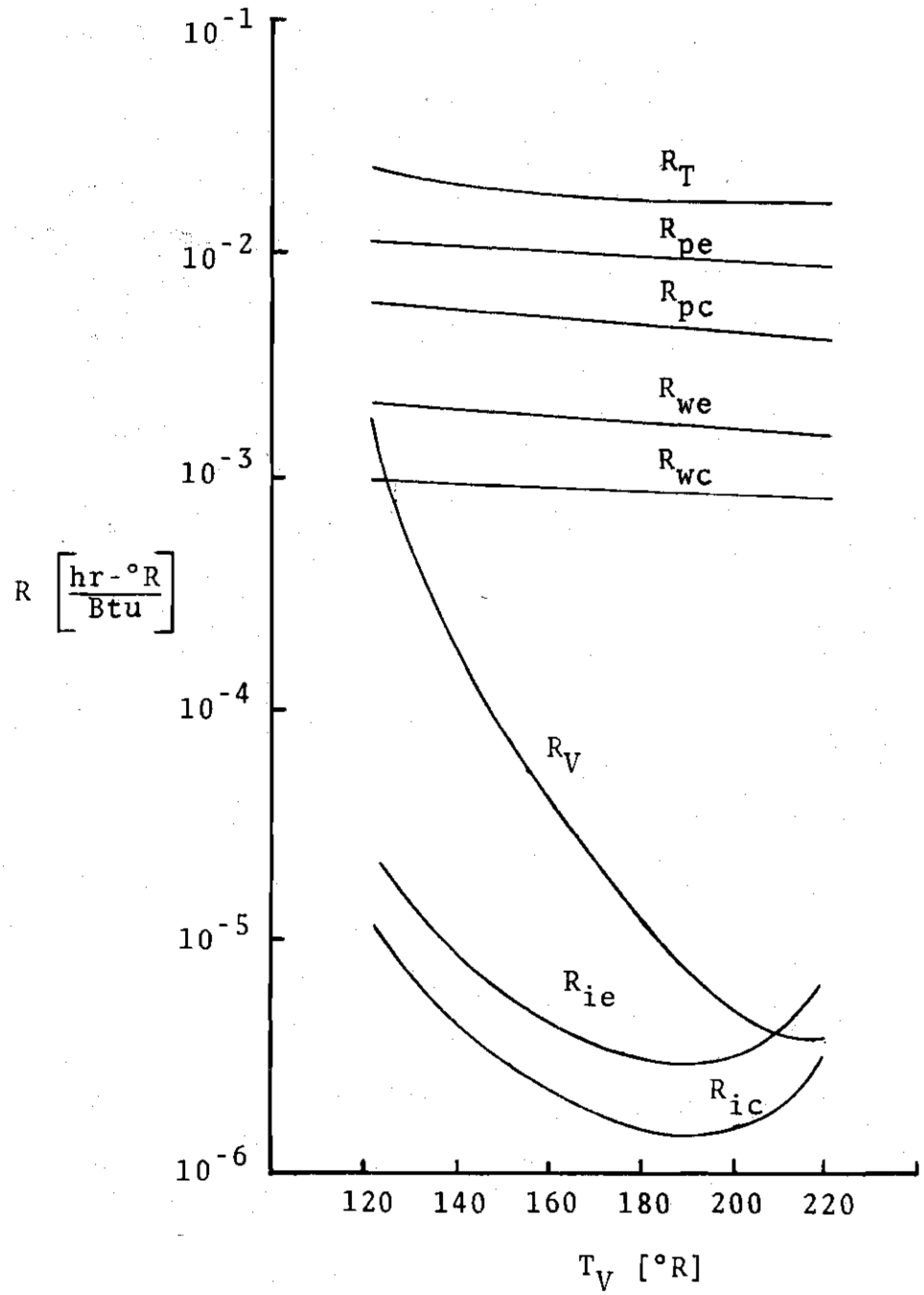

Figure 16. Thermal Resistances Versus Vapor Temperature Wick Composition 1

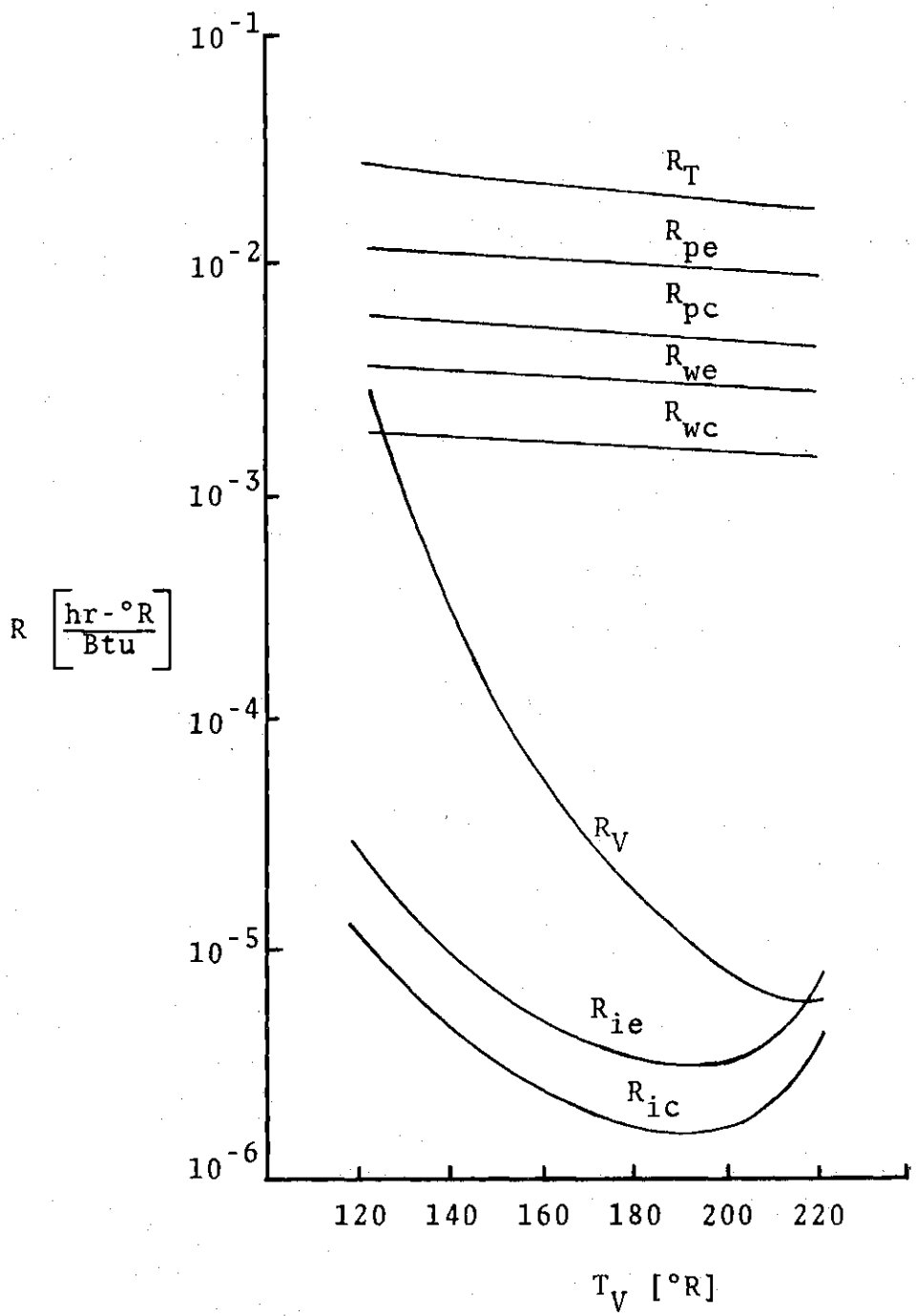

Figure 17. Thermal Resistances Versus Vapor Temperature Wick Composition 6

component and total thermal resistances over the temperature range $120°R \leq T \leq 225°R$. It is seen that the largest component of the total thermal resistance is that of the pipe wall at the heat transfer sections. The interfacial resistances and vapor resistance at the higher vapor temperatures, on the other hand, add little to this total. Therefore, it appears that the heat pipe is a high heat transfer device of almost negligible internal thermal resistance. A comparison of these two figures also points out the finding of this study that the thermal resistance of the heat pipe has little dependence on wick composition. The total thermal resistance of the heat pipe is an important parameter in calculating the theoretical nonrestricted heat transfer rate.

Figure 18 is a plot of capillary-limited heat transfer rate, $\dot{Q}_{CL}$, versus vapor temperature for wick compositions 1, 3, 4, and 6. By recognizing that the capillary limitation forms the upper boundary of the heat transport capability of the pipe, one realizes the substantial influence which the wick composition has on the overall heat pipe performance. This influence is governed by the liquid transport capability of the composite wick. The heat transfer rate versus vapor temperature plots depicted by Figs. 19 and 20 show several lines of constant driving potential as a parameter. The capillary limitation on the performance of the heat pipe is indicated on each figure. For wick composition 6, a maximum heat transfer rate of approximately 100 Btu's per hour is

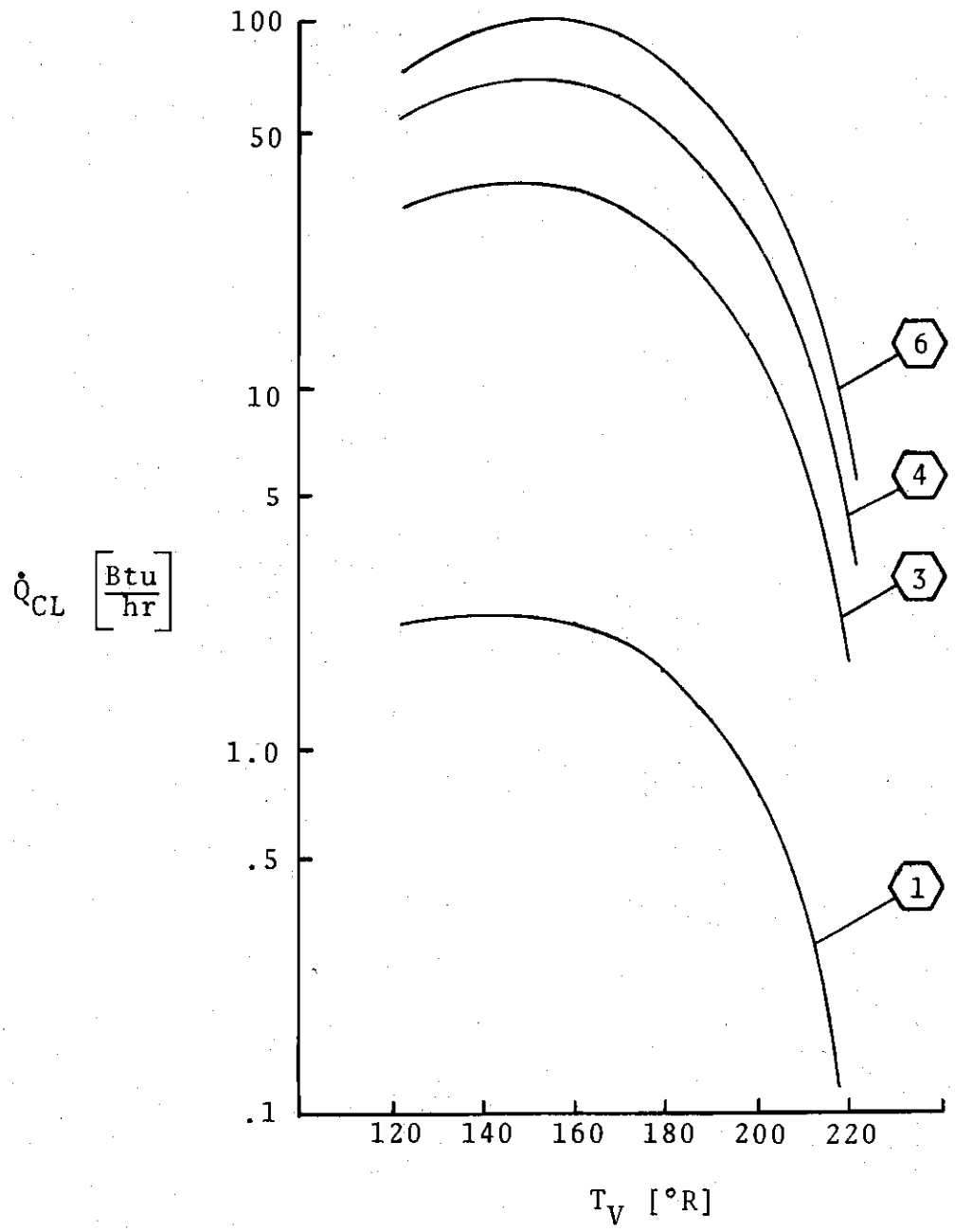

⬡ Indicates wick composition, see Table 1

Figure 18. Capillary-Limited Heat Transfer Rate Versus Vapor Temperature

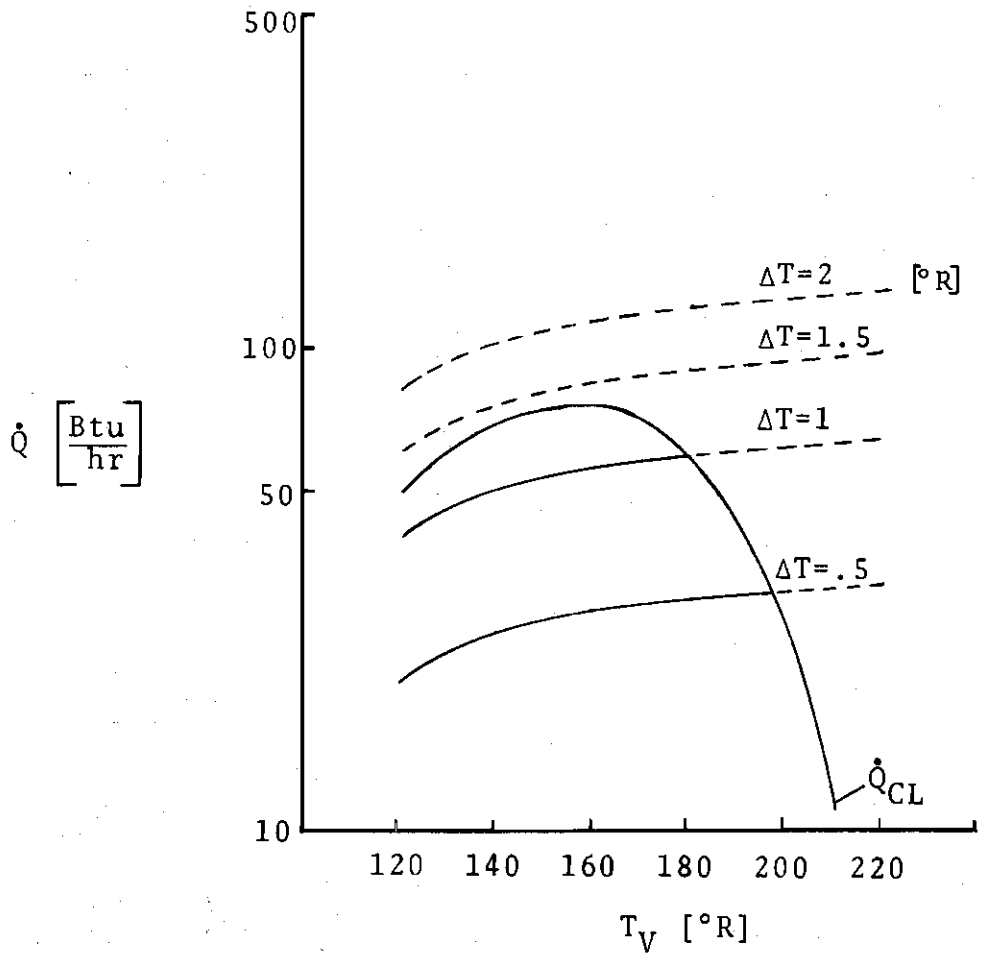

Figure 19. Constant Driving Potential Performance Chart
Wick Composition 5

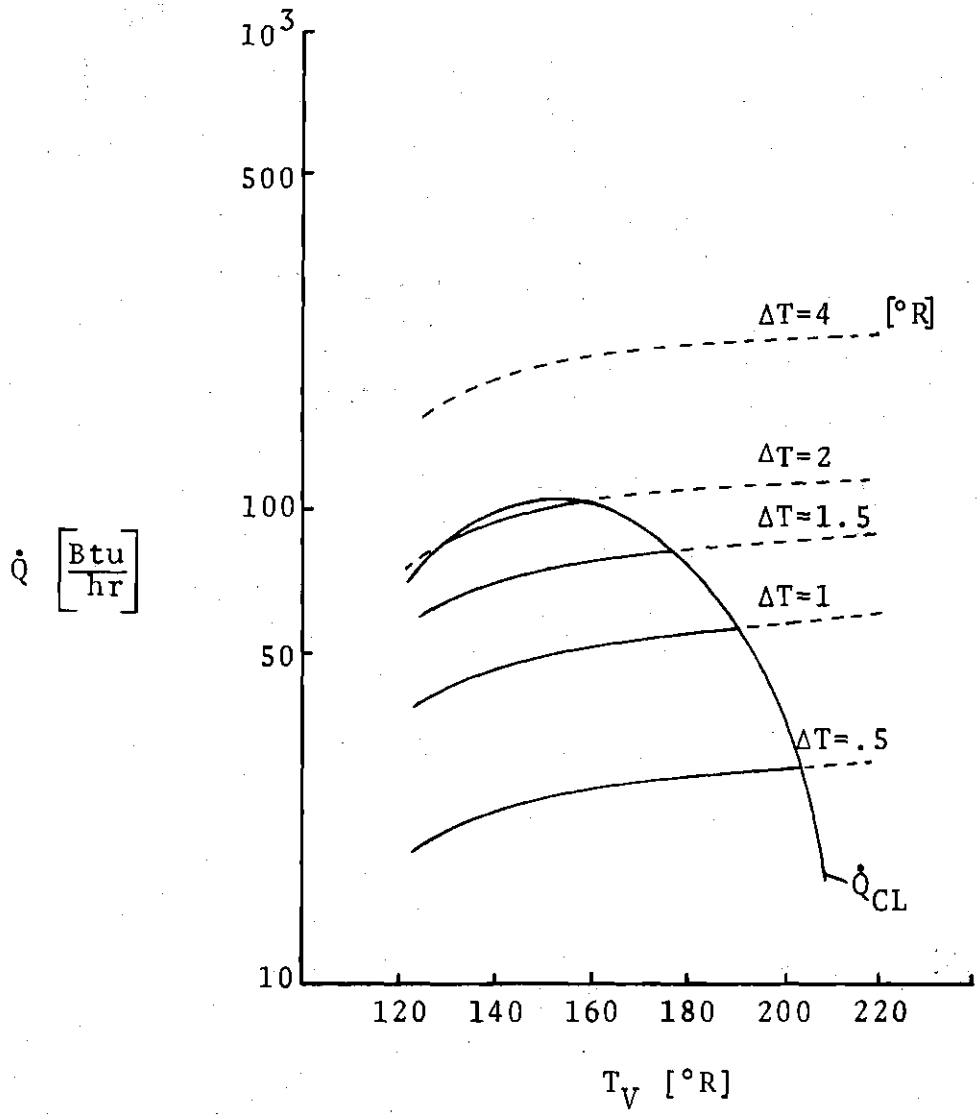

Figure 20. Constant Driving Potential Performance Chart
Wick Composition 6

obtained with a driving potential of two degrees Rankine and a vapor temperature of approximately 160 degrees Rankine. This is the maximum rate of heat transfer obtained in this study.

Figures 21 and 22 show plots of heat transfer rate versus temperature difference with lines of constant vapor temperature plotted as the parameter. The capillary-limited heat transfer rate is indicated on each line of constant vapor temperature. The plots shown in Figs. 19 through 22 are useful tools for predicting the performance of cryogenic heat pipes of this design.

Figure 23 shows as a function of working fluid vapor pressure for several wick compositions capillary-limited heat transfer rates. This plot is helpful in designing the heat pipe container to withstand high internal pressures at various heat transfer loads.

Figures 24 through 27 illustrate the effective thermal conductivity of the pipe versus vapor temperature for wick compositions 1, 3, 5 and 6, respectively. In these figures, the heat transfer driving potential is plotted as a parameter. The maximum effective thermal conductivity is obtained with wick composition 6. For comparison, the thermal conductivity of copper [30] is also shown in Fig. 26. A sample calculation illustrating the method used in determining the effective thermal conductivity of the pipe is given in Appendix J.

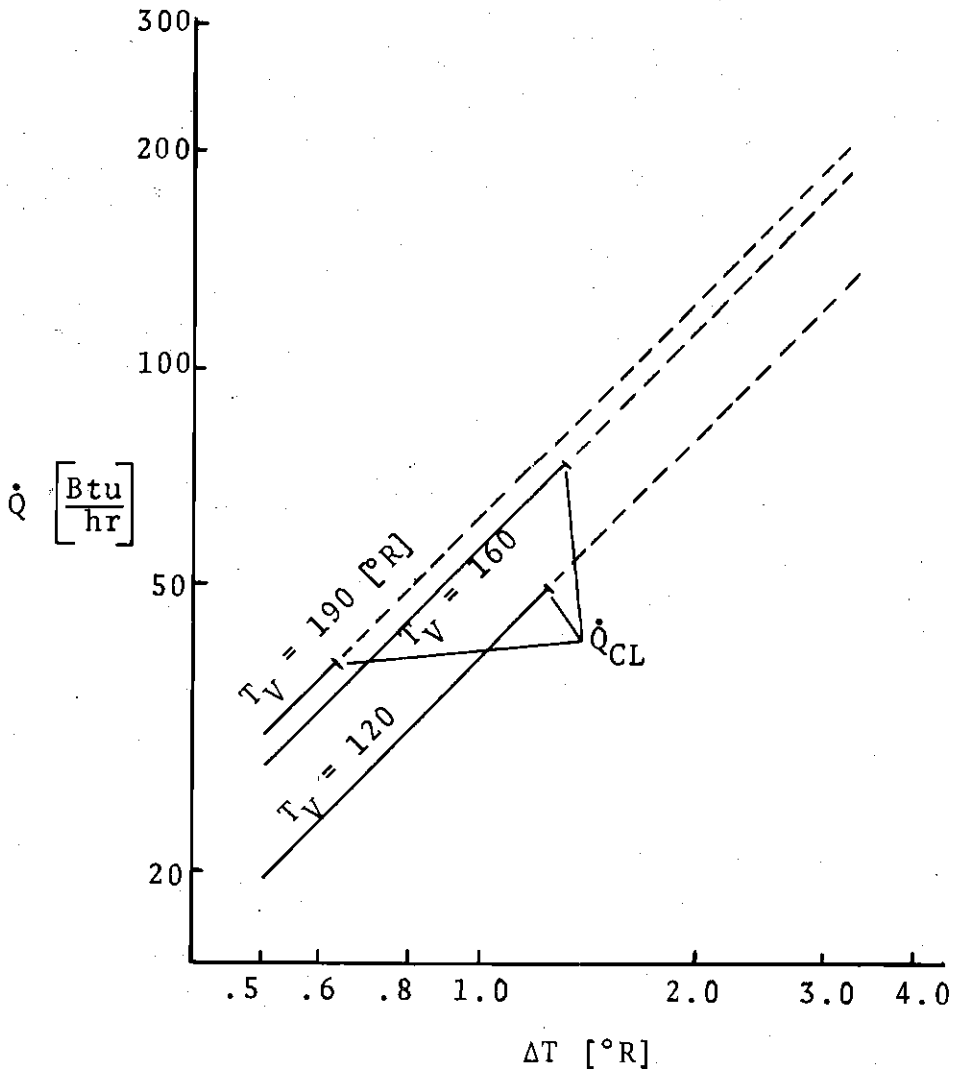

Figure 21. Constant Vapor Temperature Performance Chart
Wick Composition 5

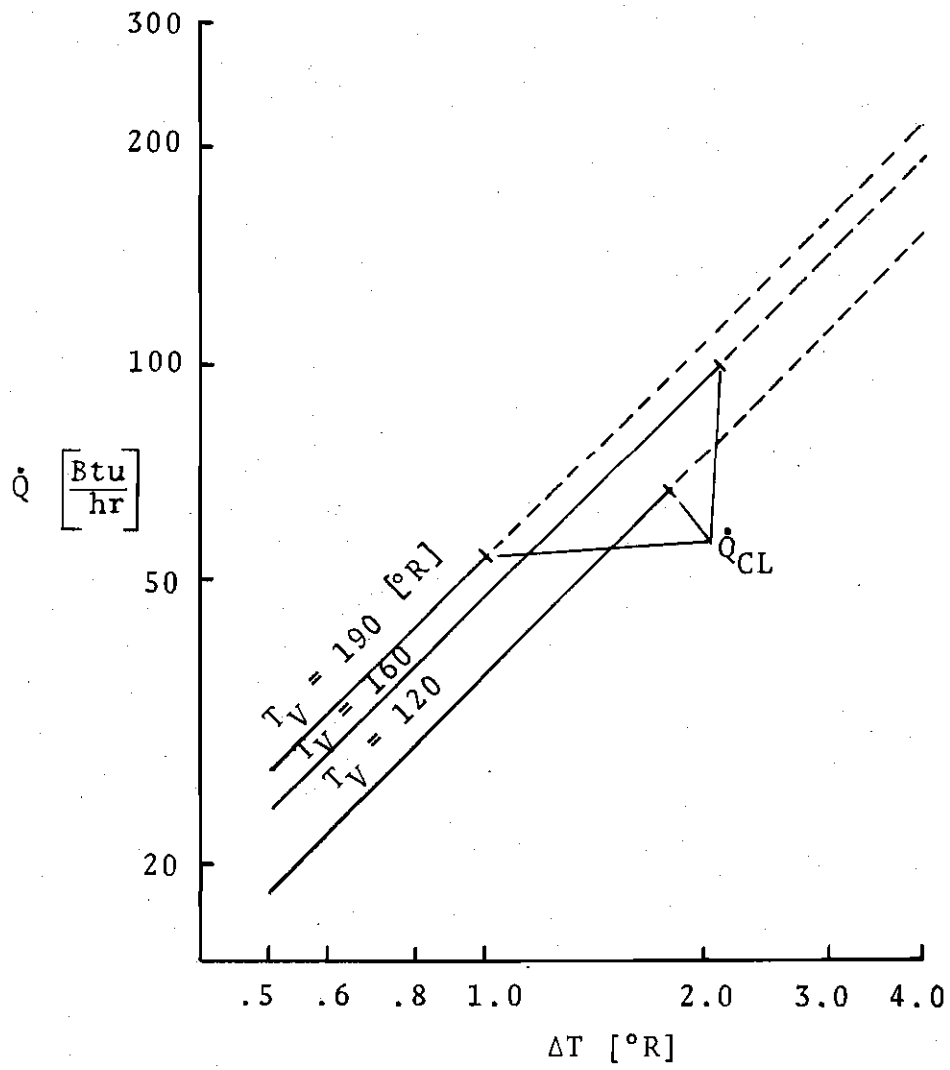

Figure 22. Constant Vapor Temperature Performance Chart, Wick Composition 6

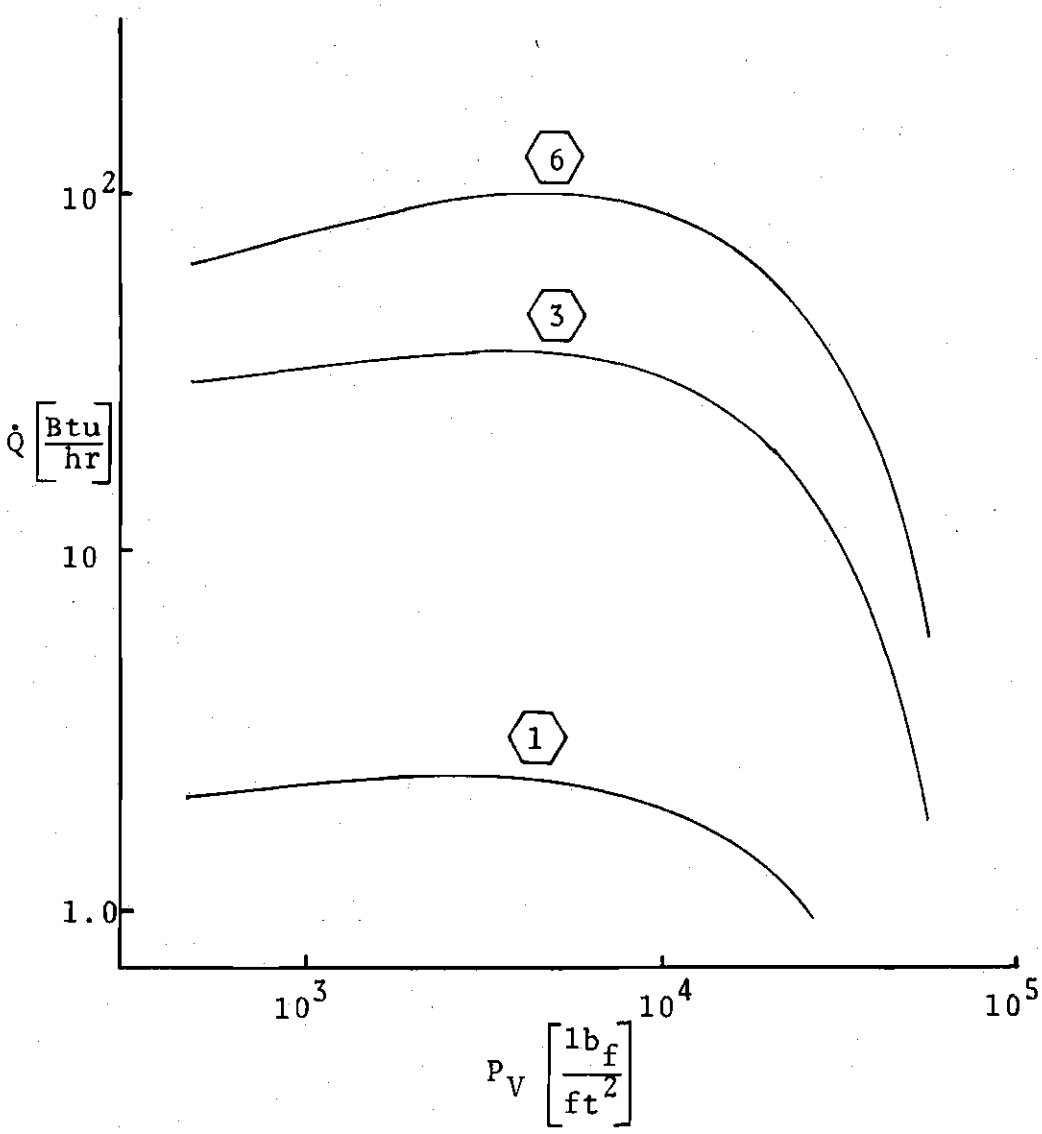

⬡ Indicates Wick Composition, see Table 1

Figure 23. Fluid Vapor Pressure Versus Capillary-Limited Heat Transfer Rate

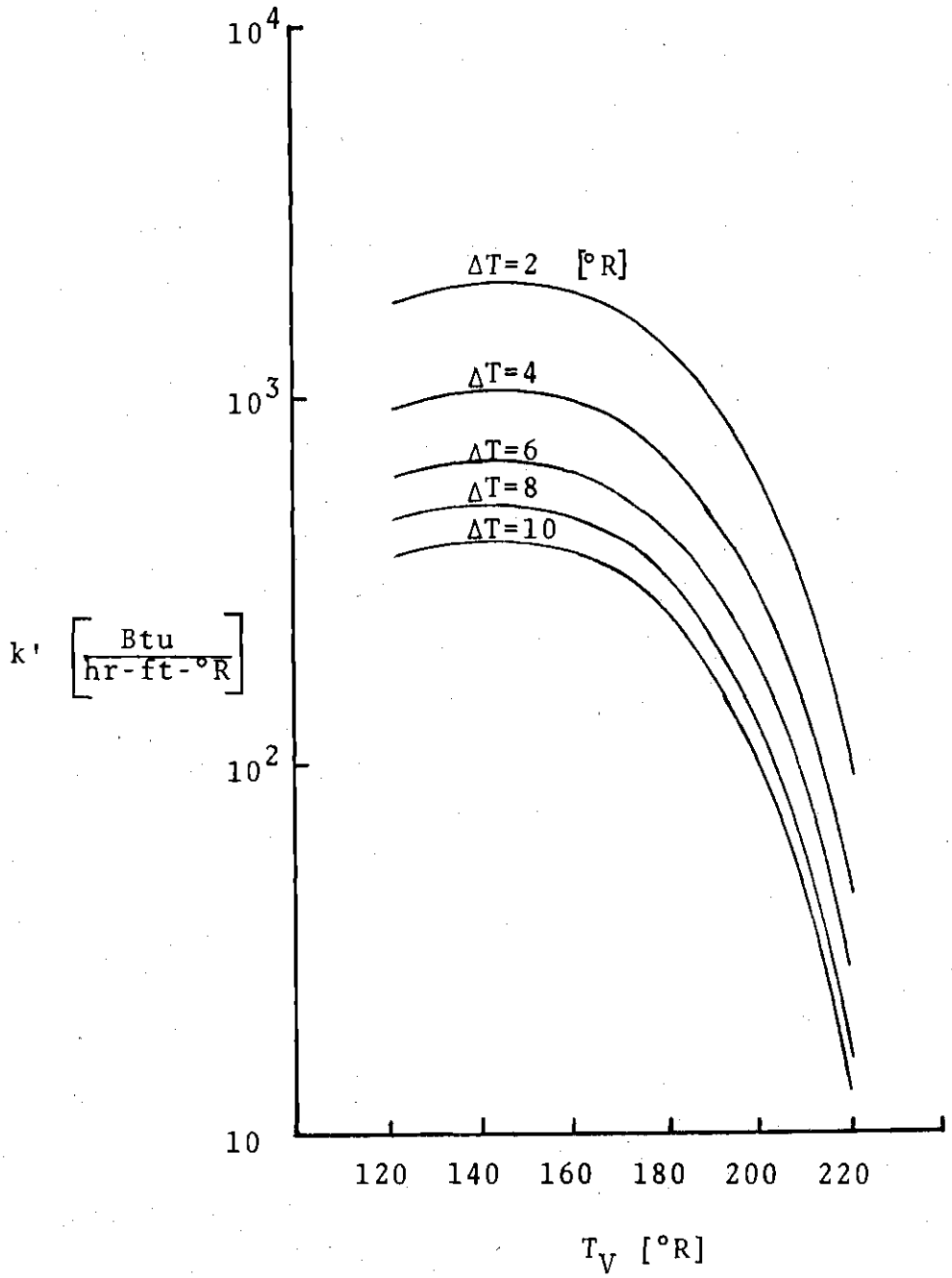

Figure 24. Effective Thermal Conductivity Versus Vapor Temperature, Wick Composition 1

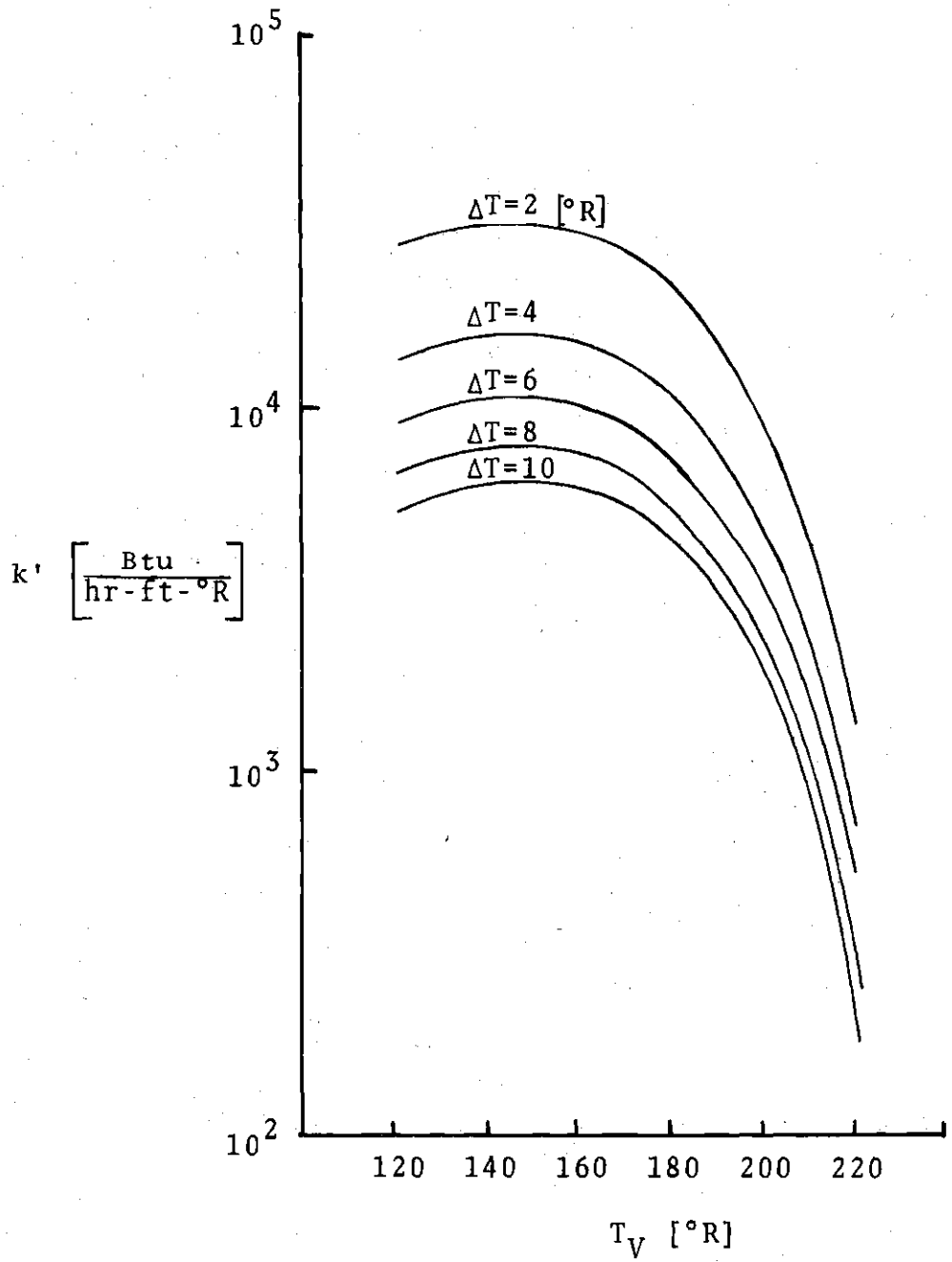

Figure 25. Effective Thermal Conductivity Versus Vapor Temperature, Wick Composition 3

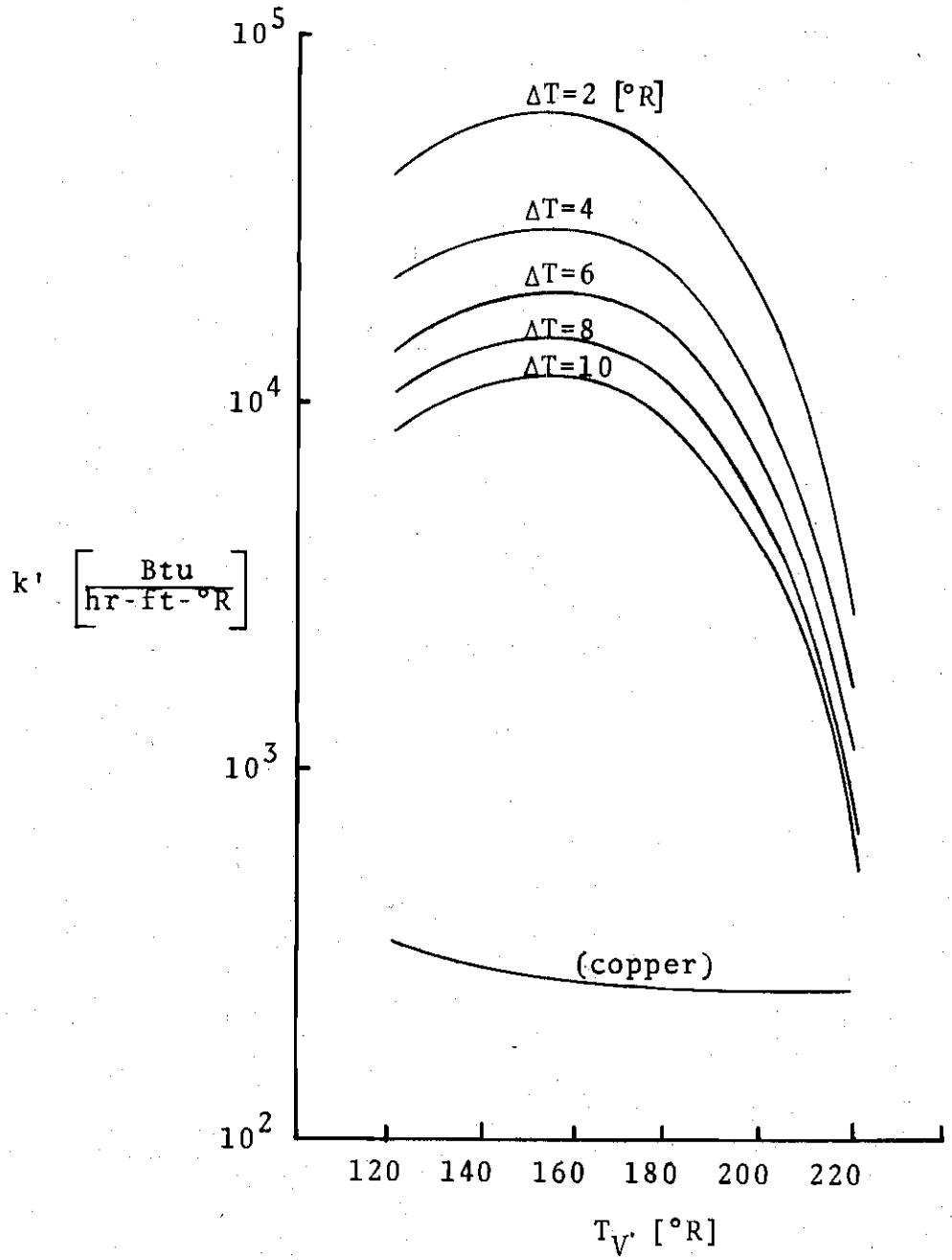

Figure 26. Effective Thermal Conductivity Versus Vapor Temperature Wick Composition 5

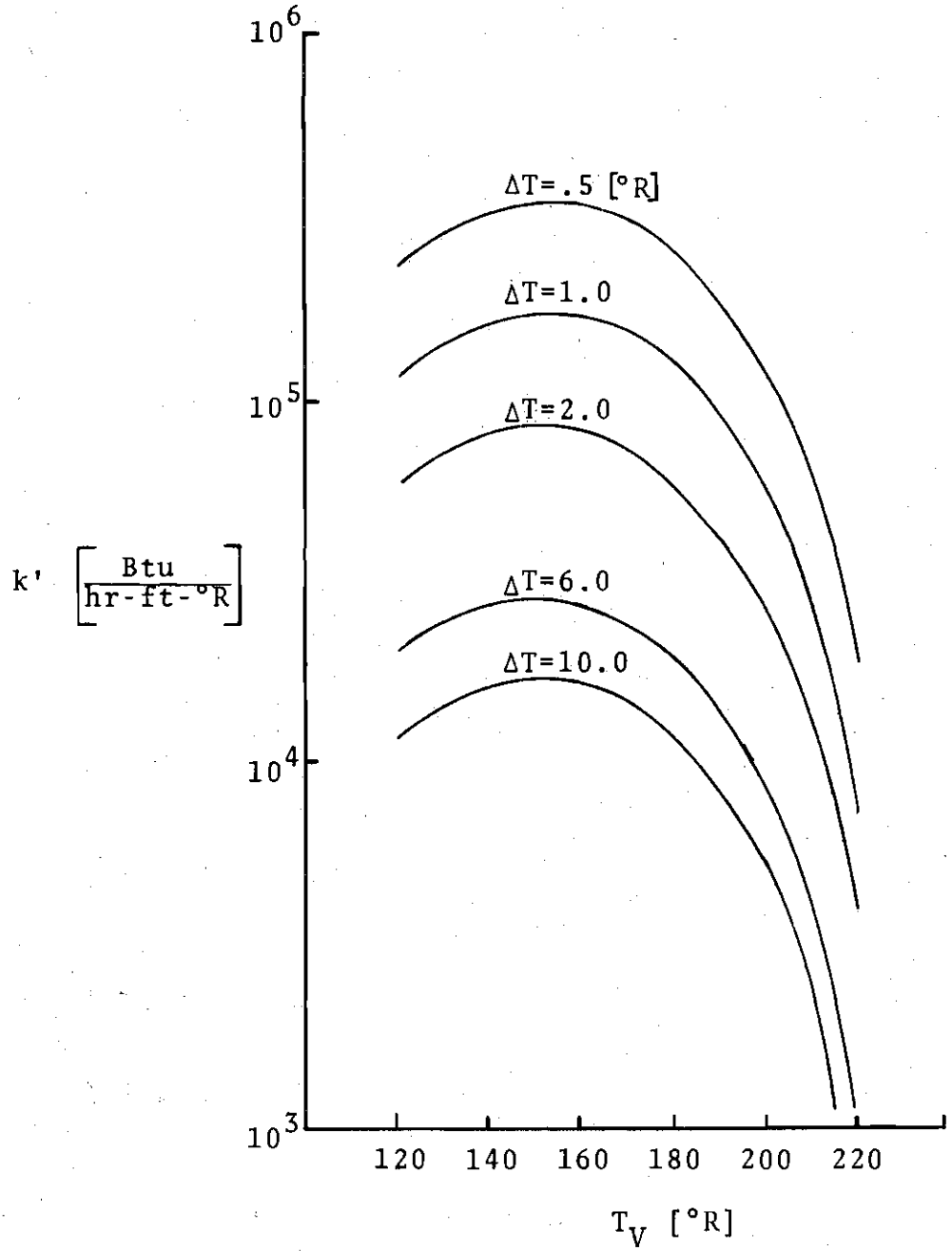

Figure 27. Effective Thermal Conductivity Versus Vapor Temperature, Wick Composition 6

A useful parameter for heat pipe comparison--and one often found in the literature--is that given by multiplying the capillary-limited heat transfer rate by the effective length of the pipe (see Appendix K). This parameter, referred to as the heat transfer capability, is plotted versus vapor temperature in Fig. 28. The maximum heat transfer capability is obtained with wick composition 6, at a vapor temperature of 160 degrees Rankine.

A plot of the sonic-limited heat transfer rate versus vapor pressure is shown by Fig. 29 for wick compositions 1 and 5. This figure shows that the sonic limitation on the heat transfer capability of the pipe is much greater than that imposed by the capillary structure at all values of vapor temperature. Therefore, no influence on the performance of the pipe due to the sonic limitation is expected.

The design charts shown in Figs. 30 and 31 were constructed from the data obtained by using wick compositions 4 and 6, respectively, in the wick model programs. In these figures, the temperature difference between the evaporator and condenser is plotted versus condenser temperature, with lines of constant heat transfer rate plotted as a parameter. The broken line shown in each figure is the performance limitation imposed by the capillary structure for the corresponding wick composition. Thus, these charts graphically illustrate the capillary limitation envelope which forms the boundaries of the region of operation of the

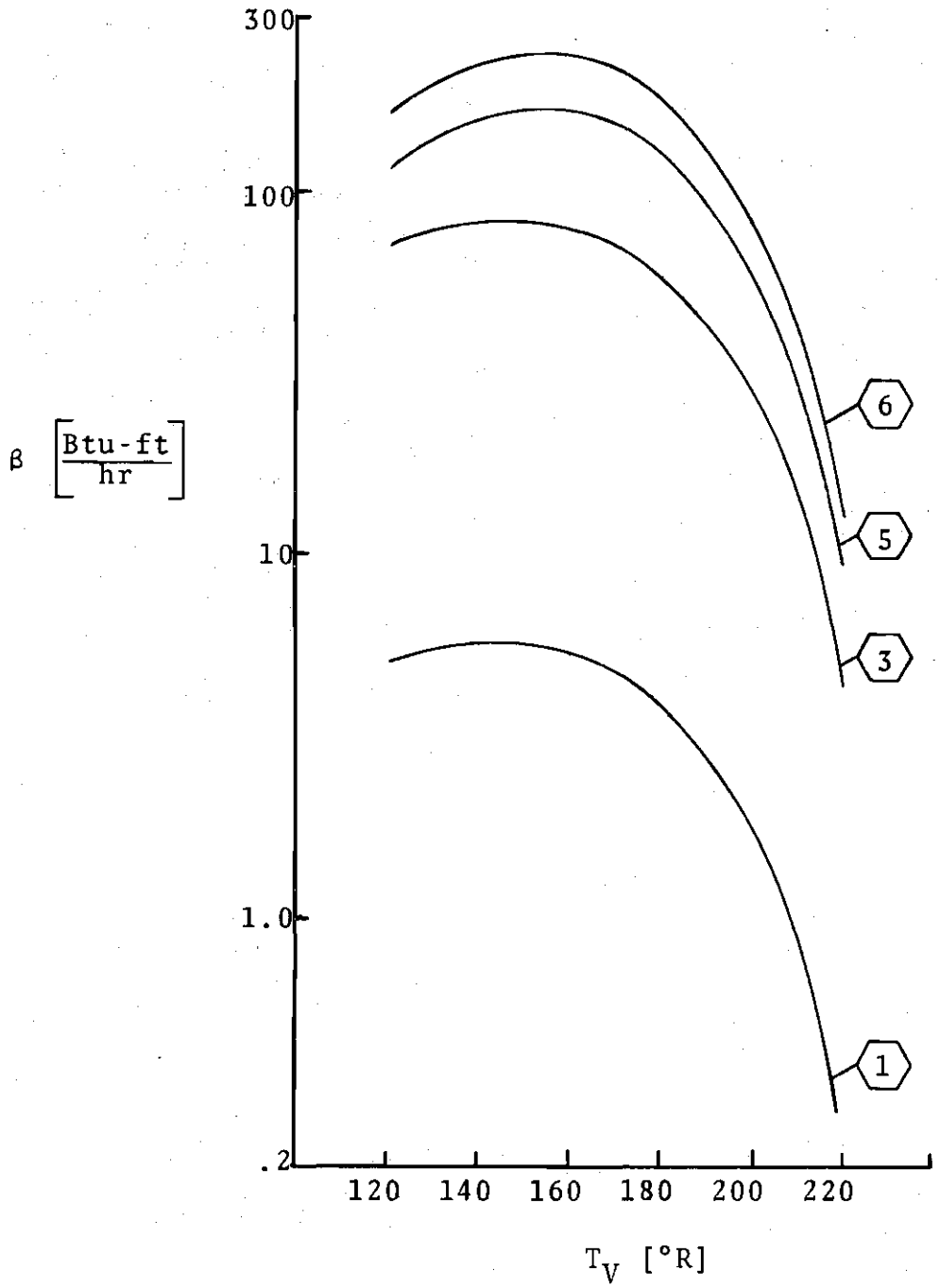

⬡ Indicates Wick Composition, see Table 1

Figure 28. Heat Transfer Capability Versus Vapor Temperature

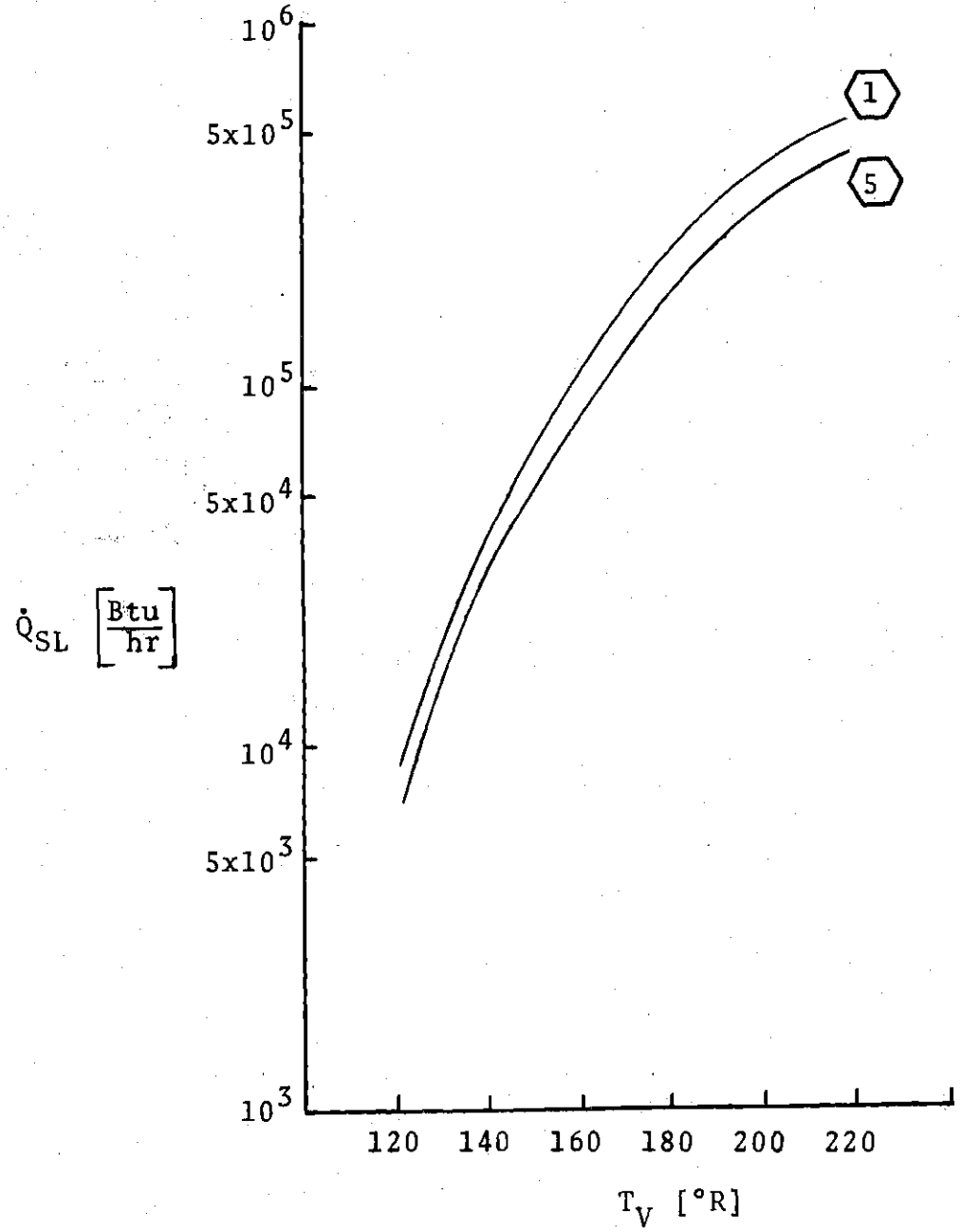

⬡ Indicates wick composition, see Table 1

Figure 29. Sonic-Limited Heat Transfer Rate Versus Vapor Temperature

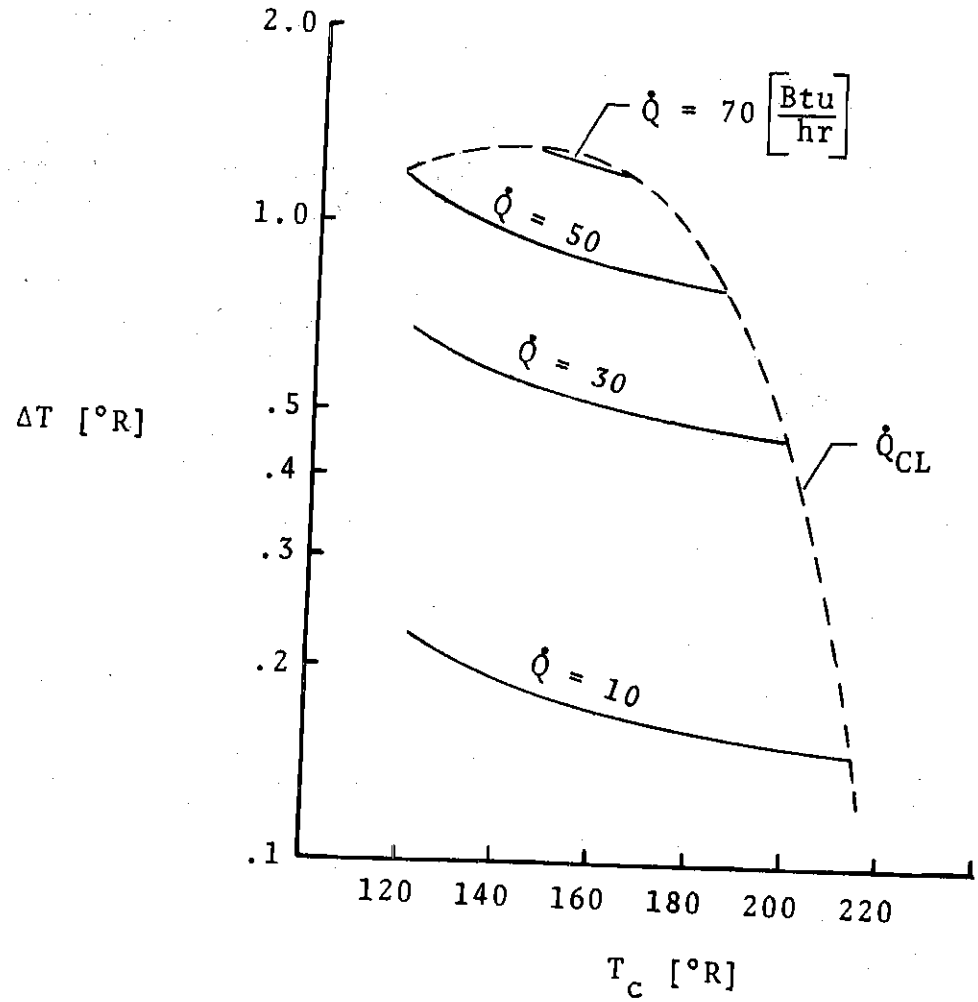

Figure 30. Performance Envelope Chart
Wick Composition 4

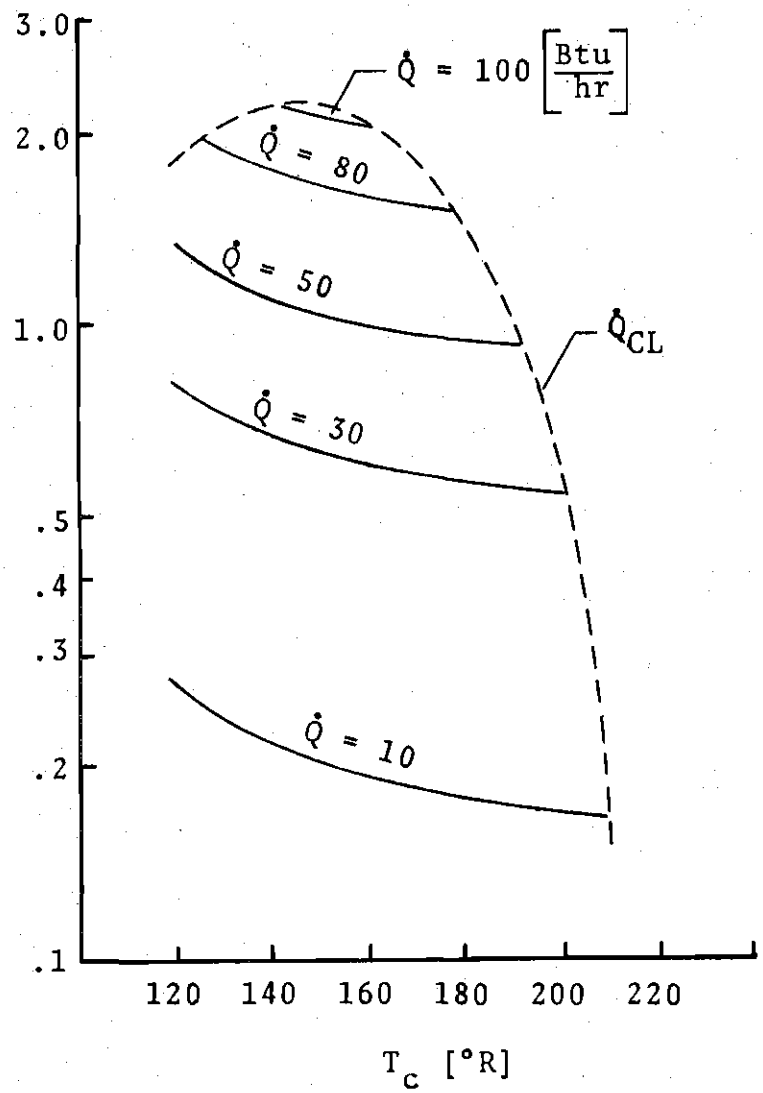

Figure 31. Performance Envelope Chart
Wick Composition 6

heat pipe.

C. Comparison with Published Data

Since the range of application of the cryogenic heat pipe is narrow, the extent of investigation of this device is somewhat restricted. Therefore, the amount of published data on its performance is less abundant than that for heat pipes intended for use in the higher temperature ranges. However, the literature does offer several excellent theoretical [1,2,15,17] and experimental studies [3,13,14] on cryogenic heat pipes. Table 3 compares the physical characteristics of heat pipes investigated by several authorities with those of the heat pipe considered in this study. This table is offered for convenient comparison of the heat pipe physical characteristics.

Figure 32 is a comparison of the capillary-limited heat transfer rate for three wick compositions investigated in this study with values of the same parameter taken from [2] and [15].

As indicated by Fig. 32, the capillary-limited heat transfer rate predicted in this study is within the bounds set by the data taken from the literature. It is also interesting to note the similarity in the shape of the data curves compared in Fig. 32.

Figure 33 shows the effective thermal conductivity obtained in this study corresponding to wick composition 1

Table 3. Physical Description of Heat Pipes Compared

Ref. No.	Inner Radius of Pipe-Ft	Thickness of Pipe Wall-Ft	Condenser Length Ft	Adiabatic Length Ft	Evaporator Length Ft	Pipe Material
1						6063 AL
2	.0158		1.58	.20	.20	
3	.0297	.0018	.833	1.104	.833	304 SS
12		.0029	.328	2.947	.328	AL
15	.0159	.00065	.20	1.57	.2	304 SS
17	varied					
14	.0292	.00233	.83	.83	1.0	304 SS
This Study	.0175	.0033	1.0	1.5	.5	304 SS

Ref. No.	Working Fluid	Wick Configuration	Wick Material	Wick Thickness Ft	Wick Mesh Size
1	nitrogen	Axial Grooves		Varied	
2	nitrogen	Annular			
3	nitrogen	Circum.	Modacrylic fiber cloth	.0033	100
12	nitrogen	Circum. & Slab	304 SS	Varied	Varied
15	nitrogen	Circum.	304 SS		
17	nitrogen	Grooves Homo.		Varied	
14	nitrogen	Circum.	Rayon cloth	.00292	100
This Study	nitrogen	Comp. slab circum.	304 SS	Varied	Varied

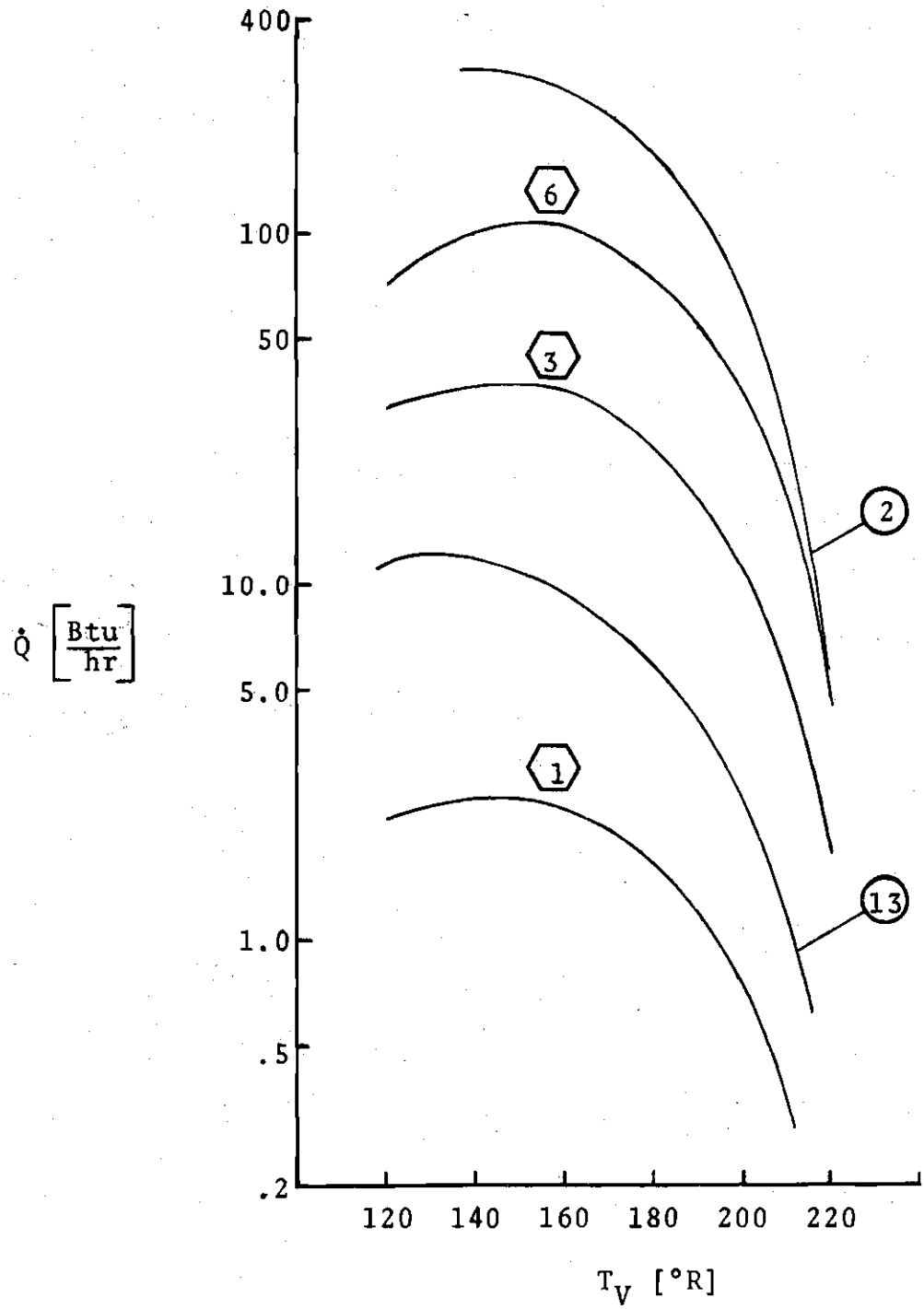

⬡ Indicates wick composition, see Table 1

◯ Indicates reference, see Table 2

Figure 32. Comparison of Capillary-Limited Heat Transfer Rate

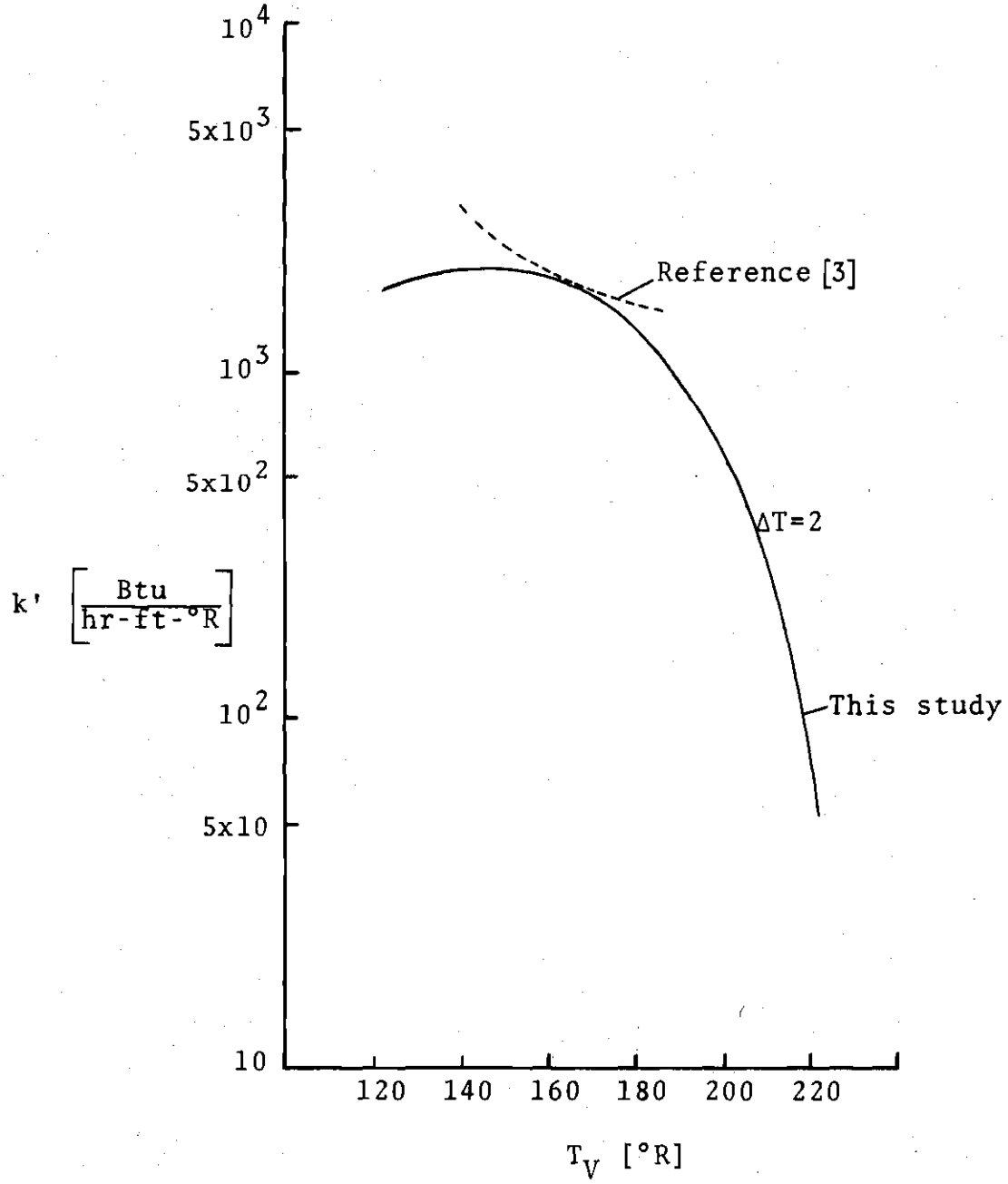

Figure 33. Comparison of Effective Thermal Conductivity: Wick Composition 1 with Data from Reference [3]

and to a temperature difference of two degrees Rankine, compared to data taken from Ref. [3]. This comparison is not highly favorable and indicates an area where additional experimental data would be beneficial.

Somewhat more favorable results are indicated by Fig. 34. Here the values of the heat transport capability, obtained for two wick compositions considered in this work, are compared with data taken from Refs. [1, 12, and 17]. As shown by the figure, good agreement with the data taken from Ref. [1] was obtained.

Figure 35 is a plot of the heat transfer rate versus temperature difference, comparing data from Refs. [3, 14, and 15] with that obtained in this study for wick composition 6 and a vapor temperature of 160 degrees Rankine. As indicated by the figure, similar but considerably more optimistic predictions are made by this work as to the driving potential required for an equivalent heat transport rate.

The discrepancy between the findings of this study and the data found in the literature is, in some comparisons, considerable. This discrepancy is attributable to the wide differences in the design of the heat pipes compared. In particular, some of the published data comes from studies using heat pipes with relatively thick circumferential wicks [3]. This added thickness in the capillary structure plus partial dry-out results in an increase in the thermal resistance at the heat transfer sections. Non-uniform

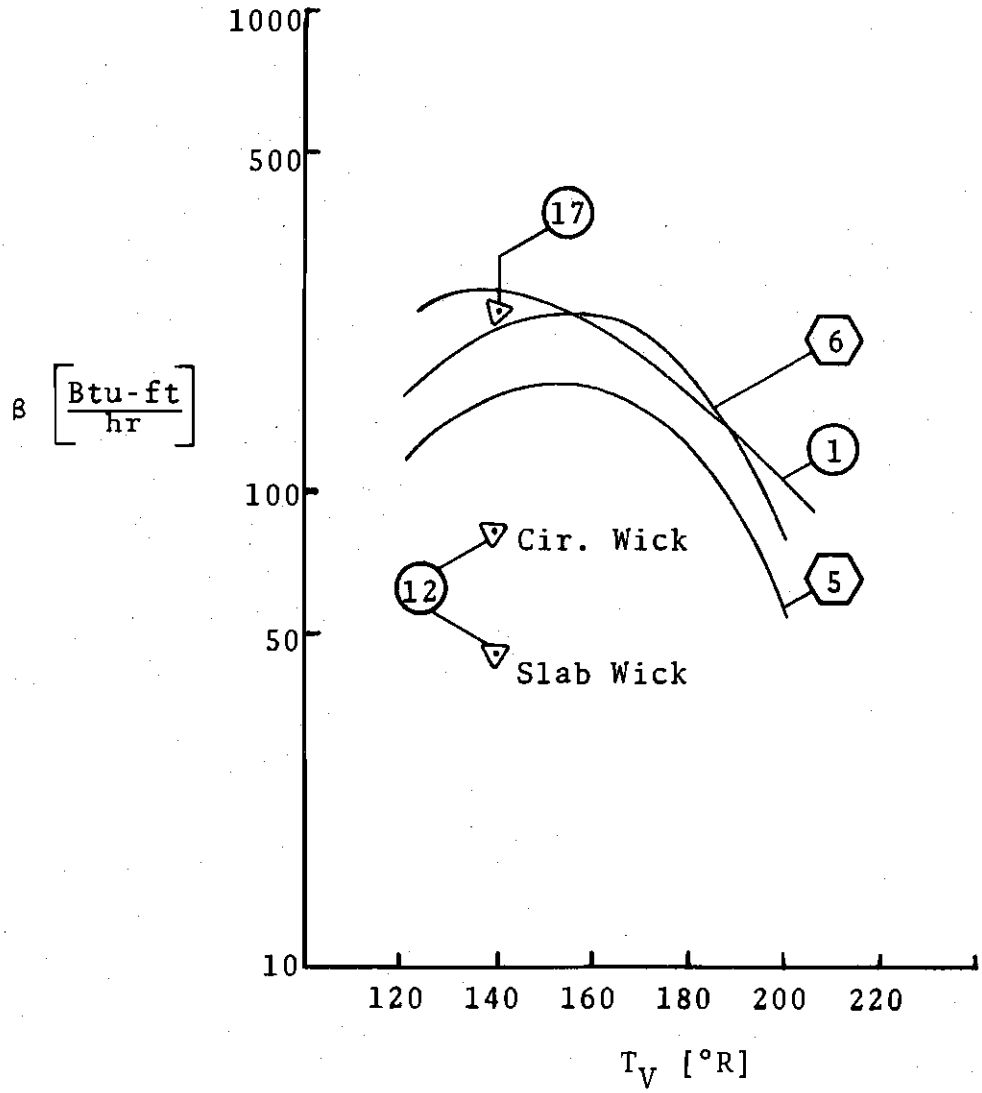

Indicates wick composition, see Table 1

Indicates reference, see Table 2

Figure 34. Comparison of Heat Transfer Capability

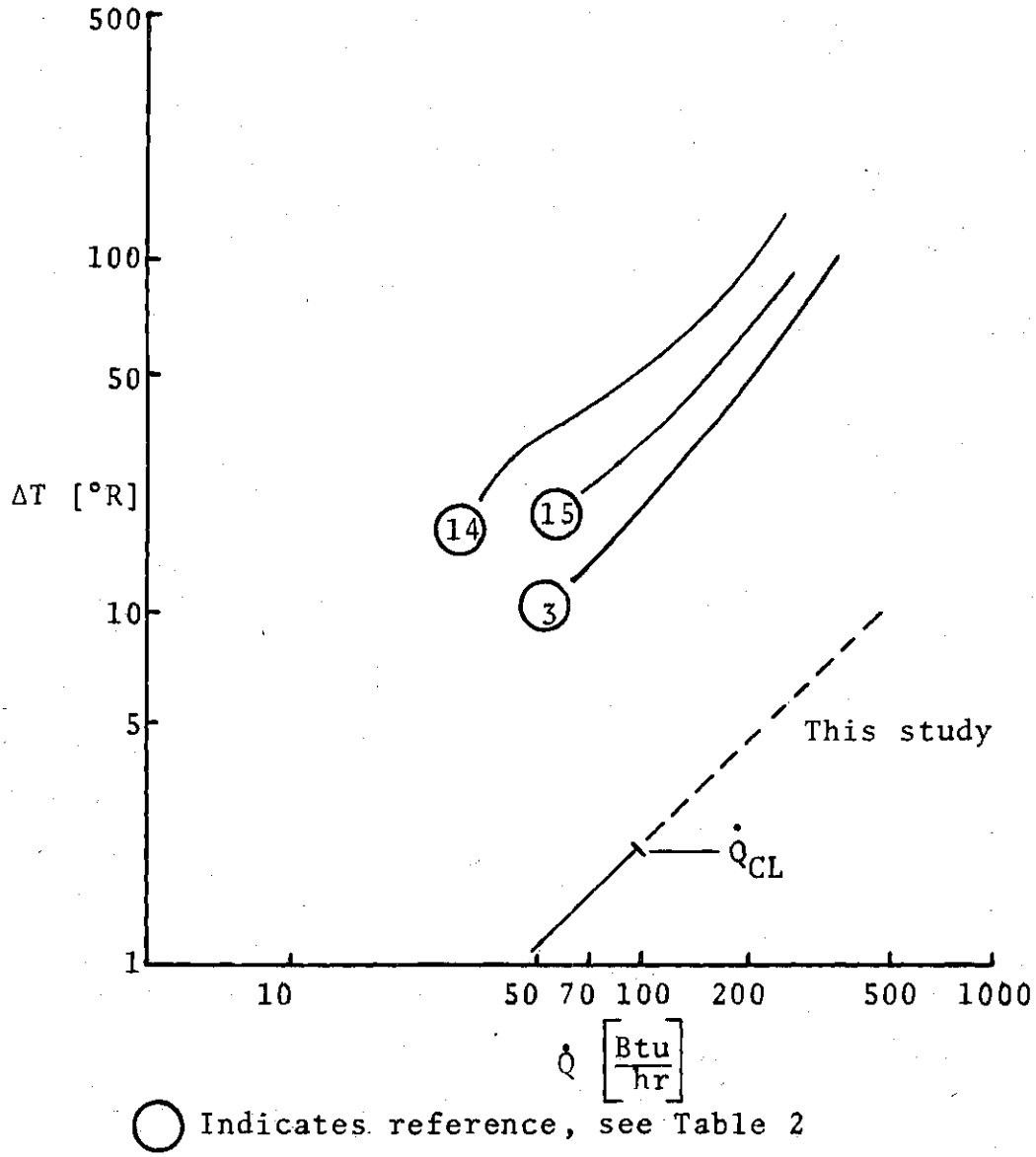

Figure 35. Comparison of Heat Transfer Rate Versus ΔT for Various Studies. Wick Composition 6, T_V = 160°R

packing of the several screen layers in the circumferential wick is another factor which tends to increase the thermal resistance by leaving internal voids in the porous media. In addition to these factors, the conservative theoretical approach taken in this study may have contributed substantially to the discrepancy.

D. Results of Study

The contribution made by this study is the three computer programs which model the composite wick systems (see Appendices C, D, and E). These programs were written to facilitate alterations being made in the composite slab and circumferential wicks. Thus the wick composition corresponding to the optimum heat pipe performance may be determined by a trial and error procedure. Desired wick changes are simply input to the digital computer, which calculates not only the performance limitations, but also the thermal resistance of each heat pipe component. Interpretation of the resulting data leads to design charts and graphs useful for predicting the heat pipe performance.

Table 4 gives a summary of the capillary-limited heat transfer rates obtained for several wick compositions studied at different values of vapor temperature. The data given by Table 4 indicates a capillary-limited heat transfer rate greater than 35 Btu's per hour, a maximum requirement suggested by NASA, for four of the six wick compositions

Table 4. Summary of Heat Pipe Performance Using Different Wick Compositions

Wick Composition Number	Slab				Circumferential				Vapor Temp.°R	$\dot{Q}_{CL}$ $\frac{Btu}{hr}$
	Surface Mesh	Screen n_A	Interior Mesh	Screen n_B	Evap. Mesh	Screen n_C	Cond. Mesh	Screen n_C		
1	250	2	100	8	250	1	250	1	160	2.35
3	400	2	50	5	400	1	400	1	150	37.48
									160	36.17
									170	32.01
4	400	2	30	4	400	1	400	1	150	72.01
									160	70.17
									170	62.52
5	400	2	30	6	400	1	400	1	150	75.2
									160	74.64
									170	67.63
6	400	4	30	5	400	2	400	2	150	103.29
									160	102.53
									170	92.89

considered. Table 4 also points out the strong dependency of the pipe performance on the liquid transport capability of the porous structure.

This work represents the initial step taken at the Georgia Institute of Technology in a program aimed at developing the capability of predicting cryogenic heat pipe performance. Much remains to be done. The next step is to include in the model provisions for accounting for partial capillary structure dry-out and vapor Reynolds number effects. To accomplish this, the work of Williams and Colwell [13] will be incorporated with this study.

It should also be pointed out that concurrent transient cryogenic heat pipe studies are being conducted by Colwell and associates at Georgia Tech. These studies of the non-steady state operation of the heat pipe are being performed with the aid of an analog computer.

CHAPTER V

CONCLUSIONS AND RECOMMENDATIONS

A. Conclusions

The conclusion drawn from this theoretical study is that the use of a composite wick system provides an effective means of improving the liquid transport capability of the capillary structure in heat pipes. Therefore, the heat transfer performance of the heat pipe may be improved by employing such a porous media. In addition, it is concluded that a composite capillary structure capable of meeting the geometric and performance specifications suggested by the sponsoring agency is feasible.

B. Recommendations for Future Study

It is recommended that future studies in this field take into account the following concepts in order to improve theoretical predictions of cryogenic heat pipe performance:

1. Partial dryout of the capillary structure in the circumferential and axial directions. This could be accounted for by incorporating the work of Williams and Colwell [13].

2. Reynolds number effects in the vapor region should be accounted for. Again, the studies conducted by Williams and Colwell may prove valuable in this area.

3. The effects on performance of using grooved evaporator and condenser surfaces in conjunction with the composite slab and circumferential wick system should be investigated.

4. The transient or non-steady state operation. The time-dependent equations governing the heat pipe performance should be modeled using an analog computer.

REFERENCES

1. Kroliczek, E. J. and Brennan, D. J., "Axial Grooved Heat Pipe, Cryogenic through Ambient," ASME Publication 73-ENA-48, 1973.

2. Pauluis, G. and Lang, S. B., "Theoretical Investigations of Hydrogen, Nitrogen, and Oxygen Homogeneous- and Annular-Wick Heat Pipes," ASME Publication 71-WA/HT-13, 1971.

3. Armaly, B. F. and Dudheker, J., "Experimental Study of a Nitrogen Heat Pipe," ASME Publication 71-WA/HT-28, 1971.

4. Santander, Julio A., Study of a Heat Pipe Cooled Microwave Window, MSME Thesis, Georgia Institute of Technology, 1975.

5. Ferrell, J. K. and Johnson, H. R., "The Mechanism of Heat Transfer in the Evaporator Zone of a Heat Pipe," ASME publication 70-HT/SPT-12, 1970.

6. Williams, C. L., Correlation of Heat Pipe Parameter, Ph.D. Dissertation, Georgia Institute of Technology, 1973.

7. Colwell, G. T., Bassett, H. L. and Schuchard, J. M., "Heat Pipe Cooled Microwave Window," Final Report, Georgia Tech Projects E25-635 and A-1532, U. S. Army Contract DAHC60-73-C-0068, February, 1974.

8. Gaugler, R. S., "Heat Transfer Device," U. S. Patent 2,350,348, June, 1944.

9. Grover, G. M., Cotter, T. P., and Erickson, G. F., "Structures of Very High Thermal Conductivity," Journal of Applied Physics, Vol. 35, pp. 1990-1991, 1964.

10. Cotter, T. P., "Theory of Heat Pipes," Los Alamos Scientific Laboratory Report LA-3246-MS, March, 1965.

11. Cosgrove, J. H., Engineering Design of the Heat Pipe, Ph.D. Dissertation, North Carolina State University, 1967.

12. Skarbek, E. A. and Beinert, W. B., Heat Pipe Design Handbook, Part I, NASA-CR-134264, August, 1972.

13. Williams, C. L. and Colwell, G. T., "Heat Pipe Model Accounting for Variable Evaporator and Condenser Lengths," AIAA Journal, Vol. 12, No. 9, pp. 1261-1267, September, 1974.

14. Haskin, W. L., "Cryogenic Heat Pipe," AFFDL-TR-66-228, June, 1967.

15. Chi, S. W. and Cygnarowicz, T. A., "Theoretical Analyses of Cryogenic Heat Pipes," ASME Publication 70-HT/SPT-6, 1970.

16. Sherman, A. and Brennan, P., "Cryogenic and Low Temperature Heat Pipe/Cooler Studies for Spacecraft Application," Presented at the AIAA/ASME 1974 Thermophysics and Heat Transfer Conference, Boston, Massachusetts, July 15-17, 1974.

17. Joy, P., "Optimum Cryogenic Heat Pipe Design," ASME Publication 70-HT/SPT-7, 1970.

18. Kirkpatrick, J. P. and Brennan, P. J., "The Advanced Thermal Control Flight Experiment," Presented at the AIAA 8th Thermophysics Conference, Palm Springs, California, July 16-18, 1973.

19. Ollendorf, S., "Low Temperature Heat Pipes, Applications, Performance, Future Development," Presented at the NSF Heat Pipe Conference, University of Maryland, November 5-6, 1973.

20. Ferrell, J. K., Winton, H. and Davis, R., "Heat Pipe Wick Properties and Performance," Presented at NSF Heat Pipe Conference, University of Maryland, November, 1973.

21. Armour, J. C. and Cannon, J. N., "Fluid Flow Through Woven Screens," AIChE Journal, Vol. 14, Number 3, pp. 415-420, May, 1968.

22. Chun, K. R., "Some Experiments on Screen Wick Dry-Out Limits," ASME Publication 71-WA/HT-6, November, 1971.

23. Corman, J. C. and Walmet, G. E., "Characterization of Parameters for Liquid Flow in Rigid Porous Media," General Electric Corporation Research and Development Report 72CRD115, April, 1972.

24. Corman, J. C., "Engineering Design of Heat Pipes," General Electric Corporation Research and Development Report 71-C-271, December, 1971.

25. Freggens, R. A., "Experimental Determination of Wick Properties for Heat Pipe Application," Fourth Intersociety Energy Conversion Engineering Conference, September, 1969.

26. Phillips, E. C. and Hinderman, J. D., "Determination of Properties of Capillary Media Useful in Heat Pipe Design," ASME Publication 69-HT-18, 1969.

27. Muskat, M., The Flow of Homogeneous Fluids Through Porous Media, McGraw-Hill Book Co., Inc., 1937.

28. Hilsenrath, J., Beckett, C., Benedict, W., Fano, L., Hoge, H., Masi, J., Nuttall, R., Touloukian, Y., and Wooley, H., "Tables of Thermal Properties of Gases," U. S. Department of Commerce, National Bureau of Standards, Circular 564, November, 1955.

29. Esterman, I. and Zimmerman, J. E., "Heat Conduction in Alloys at Low Temperature," Journal of Applied Physics, Vol. 23, pp. 578, 1952.

30. Powell, R. L. and Blanpied, W. A., "Thermal Conductivity of Metals and Alloys at Low Temperatures--A Review of the Literature," National Bureau of Standards, Circular 556, September, 1954.

31. Kreith, F., Principles of Heat Transfer, Second Edition, International Textbook Co., Scranton, Pa., 1966.

32. Chisholm, D., The Heat Pipe, Mills and Boon Limited, London, 1971.

33. Davis, W. R., Evaporative Heat Transfer of Liquid Potassium in Porous Media, Ph.D. Dissertation, Department of Chemical Engineering, North Carolina State University, Raleigh, North Carolina, 1974.

34. Scheidegger, A. E., The Physics of Flow Through Porous Media, The MacMillan Co., New York, N. Y., 1960.

35. Swanson, W. M., Fluid Mechanics, Holt, Rinehart, and Winston, New York, N. Y., 1970.

36. Hansen, A. G., Fluid Mechanics, John Wiley and Sons, Inc., New York, N. Y., 1967.

37. Bird, R. B., Stewart, W. E., Lightfoot, E. N., Transport Phenomena, John Wiley and Sons, Inc., New York, N. Y., 1960.

38. Kunz, H. R., Langston, L. S., Hilton, B. H., Wyde, S. S., and Nasbick, G. H., "Vapor-Chamber Fin Studies," NASA Contractor Report NASA CR-812, June, 1967.

39. Terry, M. J., Lynch, J. T., Burclark, M., Mansell, K. R., and Staveley, L. A., "The Densities of Liquid Argon, Krypton, Xenon, Oxygen, Nitrogen, Carbon Tetrafluoride Along Orthabaric Liquid Curve," Journal of Chemical Thermodynamics, p. 418, 1969.

APPENDICES

APPENDIX A

DISCUSSION OF SCREEN PROPERTIES

Of paramount importance in any attempt to model a composite wick system are the screen properties. Of particular interest is the group of properties which govern flow of liquid through the screen. This group includes porosity, pore radius, wire diameter, and permeability. Considerable variations of these properties are reported in the literature. For this reason, data obtained from several references is presented in tables and graphs included in this appendix. The corresponding number of the reference from which the data was taken is indicated in the title of each table.

The screen property permeability, K', has considerable influence on the mechanism of liquid flow through the screen. Convenience dictates the use of the inverse permeability, sometimes referred to as the friction factor, defined as:

$$K = \frac{1}{K'} \left[ft^{-2} \right] \qquad \text{(A-1)}$$

It should be pointed out that the inverse permeability of a mesh screen may be based on either the liquid pore velocity or on the liquid approach velocity. Converting a value of inverse permeability based on pore velocity to the

corresponding value based on approach velocity is accomplished by dividing the former by the porosity of the screen. Thus:

$$K_{app} = \frac{1/K'_{pore}}{\varepsilon} = \frac{1}{\varepsilon K'_{pore}} \qquad \text{(A-2)}$$

where

K'_{pore} = permeability based on pore velocity

K_{app} = inverse permeability based on approach velocity.

All values of permeability used in this study are based on the liquid approach velocity.

Ferrell [20] gives the following equation for calculating the permeability of a mesh screen:

$$K'_{pore} = \frac{d^2\varepsilon^3}{122\ (1-\varepsilon)^2} \qquad \text{(A-3)}$$

The porosity, ε, may be evaluated from the equation:

$$\varepsilon = 1 - \frac{\pi FMd}{4} \qquad \text{(A-4)}$$

where

d = wire diameter (in)

F = crimping factor (1.05)

M = number of wires per inch (in^{-1}) (mesh number)

Data given by Armour [21] on wire diameter, screen thickness,

and pore radius for various mesh number screens are used in Eqs. (A-3) and (A-4) to yield the screen properties used in this study. A complete listing of these values is shown by Table 5. The values of porosity and inverse permeability used in this study are graphically presented in Fig. 39.

By using the values of porosity given by Armour [21] in Eq. (A-4), the property values shown in Table 6 are obtained. Likewise, Fig. 40 graphically illustrates the porosity and inverse permeability obtained by this procedure. A comparison of Fig. 39 and Fig. 40 points out a considerable difference in these important screen properties calculated by the two procedures described above.

Tables 7 through 11 show values of screen properties for various mesh sizes taken from the literature.

Table 5. Screen Data Used in this Study Based on Information Taken from References [20] and [21]

Mesh Size	Wire Diameter Ftx10^4	Screen Thickness Ftx10^3	Pore Radius Ftx10^4	Porosity	$K'_{pore}(ft^2)x10^9$
30	11.68	2.04	3.419	.6532	25.9123
50	7.32	1.47	3.009	.6378	8.6861
70	7.61	1.368	2.600	.4728	1.80506
100	5.35	1.03	2.143	.4706	.87237
150	3.01	.50	1.625	.5532	.62978
200	2.07	.3705	1.3325	.5903	.43039
250	1.58	.284	1.176	.6091	.30261
325	1.30	.267	1.00	.5820	.15628
400	1.02	.244	.625	.5960	.110616

Mesh Size	$K_{pore}\ (ft^{-2})x10^{-9}$	$K^* = \frac{K_{pore}}{\varepsilon}(ft^{-2})x10^{-9}$
30	.0385917	.059081
50	.115126	.18050
70	.55399	1.1717
100	1.1463	2.4358
150	1.5879	2.8704
200	2.3235	3.9361
250	3.3046	5.4254
325	6.3988	10.995
400	9.0403	15.168

*Based on liquid approach velocity

Table 6. Screen Properties from Reference [21]

Mesh Size	Porosity	$K'_{pore}(ft^2)x10^9$	$K_{pore}(ft^{-2})x10^{-9}$	$K^*=\frac{K_{pore}}{\varepsilon}(ft^{-2})x10^{-9}$
30	.384	1.668	.59952	1.5613
50	.523	2.762	.36206	.69228
70	.564	4.479	.22326	.39585
100	.6566	5.632	.17756	.27042
150	.745	4.723	.21173	.28420
200	.771	3.069	.32584	.42262
250	.757	1.503	.66534	.87892
325	.714	.6164	1.6223	2.2721
400	.712	.3711	2.6947	3.7847

Table 7. Screen Properties from Reference [22]

Mesh Size	Wire Dia. Ft x 10^4	Pore Radius Ft x 10^4	Porosity	K^* $(ft^{-2})x10^{-9}$
200 (brz)	1.833	2.417	.67	4.5179
200 (nickel)	1.833	2.417	.67	2.6716
325	1.00	1.417	.67	7.0493

Table 8. Screen Properties from Reference [24]

Mesh Size	Pore Radius (ft)10^4	K^* $(ft^{-2})x10^{-9}$
200 (nickel)	2.1	1.21
200 (ss)	1.9	1.79

*Based on approach velocity

Table 9. Screen Properties from Reference [23]

Mesh Size	Wire Dia. (Ft) x 10^4	Pore Radius (Ft) x 10^4	Porosity	K* (Ft^{-2})x10^{-9}
125 (ni)	2.08	4.166	.60	1.083

Table 10. Screen Properties from Reference [25]

Mesh Size	Pore Radius Ft x 10^4	Porosity	K* (ft^{-2})x10^{-9}
60		.67	.1649
50	19.029	.67	.1192
120	6.2336	.67	.2293

Table 11. Screen Properties from Reference [38]

Mesh Size	Wire Dia. (Ft x 10^4)	Screen Thickness (Ft x 10^3)	Pore Radius Ft x 10^4	Porosity	K*(ft^{-2})x10^{-9}
50	7.50	8.833	3.0176	.625	.2240
100	3.75		1.4973	.679	.89838
150	2.50	6.6667		.678	1.3274
200	1.833		1.0119	.676	1.7751

*Based on approach velocity

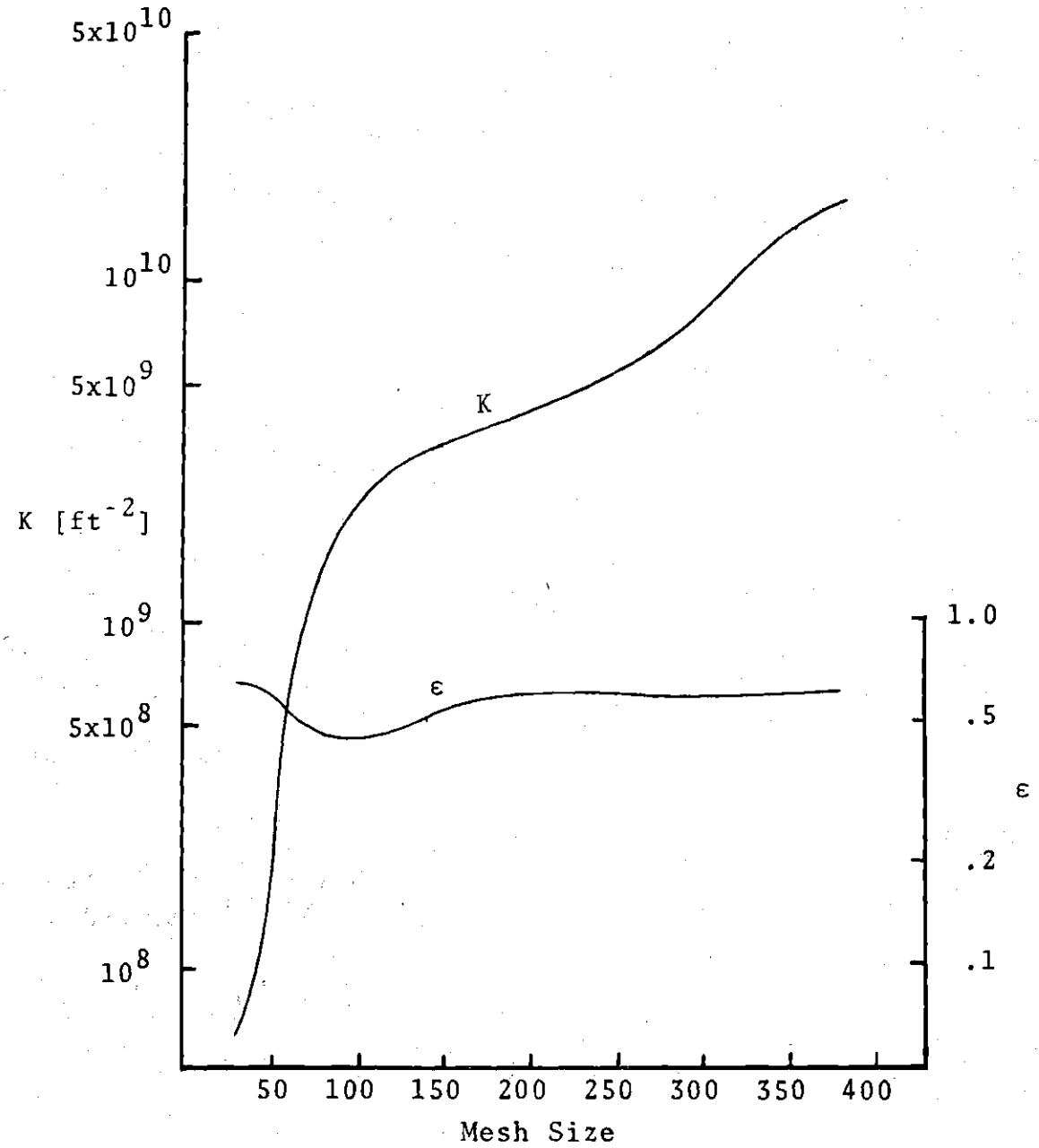

Figure 36. Inverse Permeability and Porosity Versus Screen Mesh Size Used in this Study

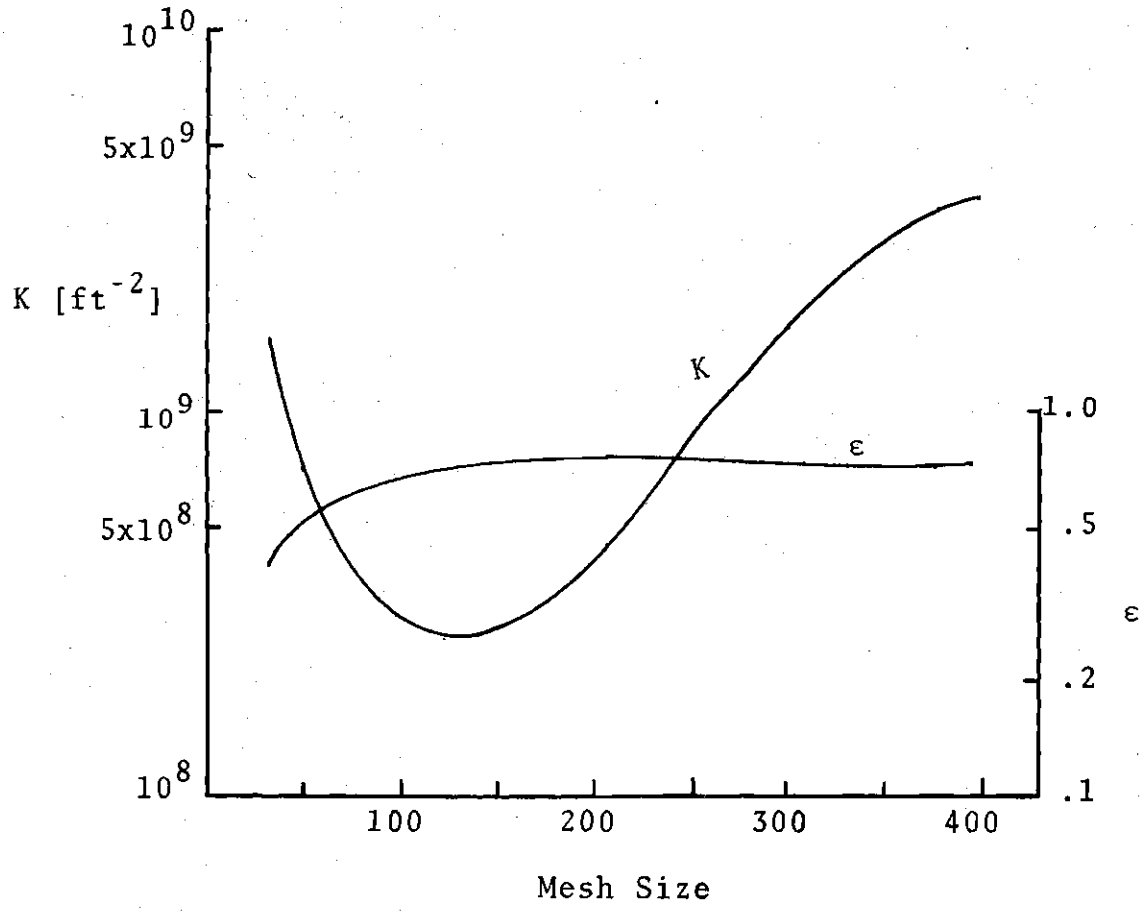

Figure 37. Inverse Permeability and Porosity from Reference [21]

APPENDIX B

THERMODYNAMIC PROPERTY EQUATIONS

1. Nitrogen Property Equations

The following polynomial equations describing the thermodynamic properties of nitrogen, the working fluid, and the thermal conductivity of 304 stainless steel as functions of temperature were generated by using a least squares regression analysis "curve fit" program on the Wang 720 calculating machine. Data used in this program were taken from Refs. [12,30,28, and 39].

T = temperature in degrees Rankine

Vapor Pressure [lb_f/ft^2]

$$P_V = 1.71041\times10^{-6}(T)^5 - 1.20901\times10^{-3}(T)^4 + 3.71275\times10^{-1}(T)^3 - 5.70868\times10(T)^2 + 4.28513\times10^{3}(T) - 1.25125\times10^{5}$$

Density [lb_m/ft^3]

$$\rho_L = - 5.8917\times10^{-13}(T)^7 + 4.50297\times10^{-10}(T)^6 - 1.15298\times10^{-7}(T)^5 + 4.95327\times10^{-6}(T)^4 + 2.9749\times10^{-3}(T)^3 - 5.98552\times10^{-1}(T)^2 + 4.54425\times10(T) - 1.21455\times10^{3}$$

$$\rho_V = 1.39324\times10^{-13}(T)^7 - 1.042325\times10^{-10}(T)^6 + 2.638736\times10^{-8}(T)^5 - 1.14015\times10^{-6}(T)^4 - 6.78395\times10^{-4}(T)^3 + 1.385389\times10^{-1}(T)^2 - 1.07628\times10(T) + 3.10045\times10^{2}$$

Viscosity $[(lb_f\text{-sec})/ft^2]$

$$\mu_V = 8.55910\times10^{-21}(T)^7 - 6.55918\times10^{-18}(T)^6 + 1.70105\times10^{-15}(T)^5 - 8.08553\times10^{-14}(T)^4 - 4.27309\times10^{-11}(T)^3 + 8.90377\times10^{-9}(T)^2 - 6.94007\times10^{-7}(T) + 1.99577\times10^{-5}$$

$$\mu_L = - 4.48282\times10^{-14}(T)^4 + 2.34251\times10^{-11}(T)^3 - 3.55312\times10^{-9}(T)^2 + 3.14221\times10^{-8}(T) + 2.16226\times10^{-5}$$

Thermal Conductivity $[\frac{Btu}{hr\ ft\ ^\circ R}]$ of liquid nitrogen

$$k_L = 1.0970566\times10^{-11}(T)^5 - 9.2427627\times10^{-9}(T)^4 + 3.090593\times10^{-6}(T)^3 - 5.1457532\times10^{-4}(T)^2 + 4.2210737\times10^{-2}(T) - 1.26105$$

Heat of Vaporization $[Btu/lb_m]$

$$h_{fg} = - 4.11334\times10^{-11}(T)^6 + 2.0908\times10^{-8}(T)^5 - 1.43119\times10^{-6}(T)^4 - 1.03235\times10^{-3}(T)^3 + 2.61594\times10^{-1}(T)^2 - 2.40246\times10(T) + 8.89614\times10^{2}$$

Surface Tension $[lb_f/ft]$

$$\sigma = 6.70239\times10^{-12}(T)^4 - 4.60497\times10^{-9}(T)^3 + 1.19096\times10^{-6}(T)^2 - 1.44813\times10^{-4}(T) + 7.58324\times10^{-3}$$

Thermal Conductivity of 304 stainless steel $[\frac{Btu}{hr\text{-}ft^\circ R}]$

Ratio of specific heats of nitrogen

$$k = 1.572403\times10^{-6}(T)^2 - 8.6844907\times10^{-4}(T) + 1.52913275$$

2. Thermal Conductivity of Pipe Material

The following equation for the thermal conductivity of 304 stainless steel was obtained by using data from [24] in the curve fit program described above.

$$k_p = -4.02016\times10^{-5}(T)^2 + 3.20878\times10^{-2}(T) + 1.30266 \left[\frac{Btu}{ft\ hr\ ^\circ R}\right]$$

where T = temperature in degrees Rankine.

APPENDIX C

COMPUTER PROGRAM USED TO CALCULATE THE THERMAL RESISTANCES

The computer program seen in this appendix gives values of the parameters used in calculating the thermal resistances of each heat pipe component. A sample computer output is also given.

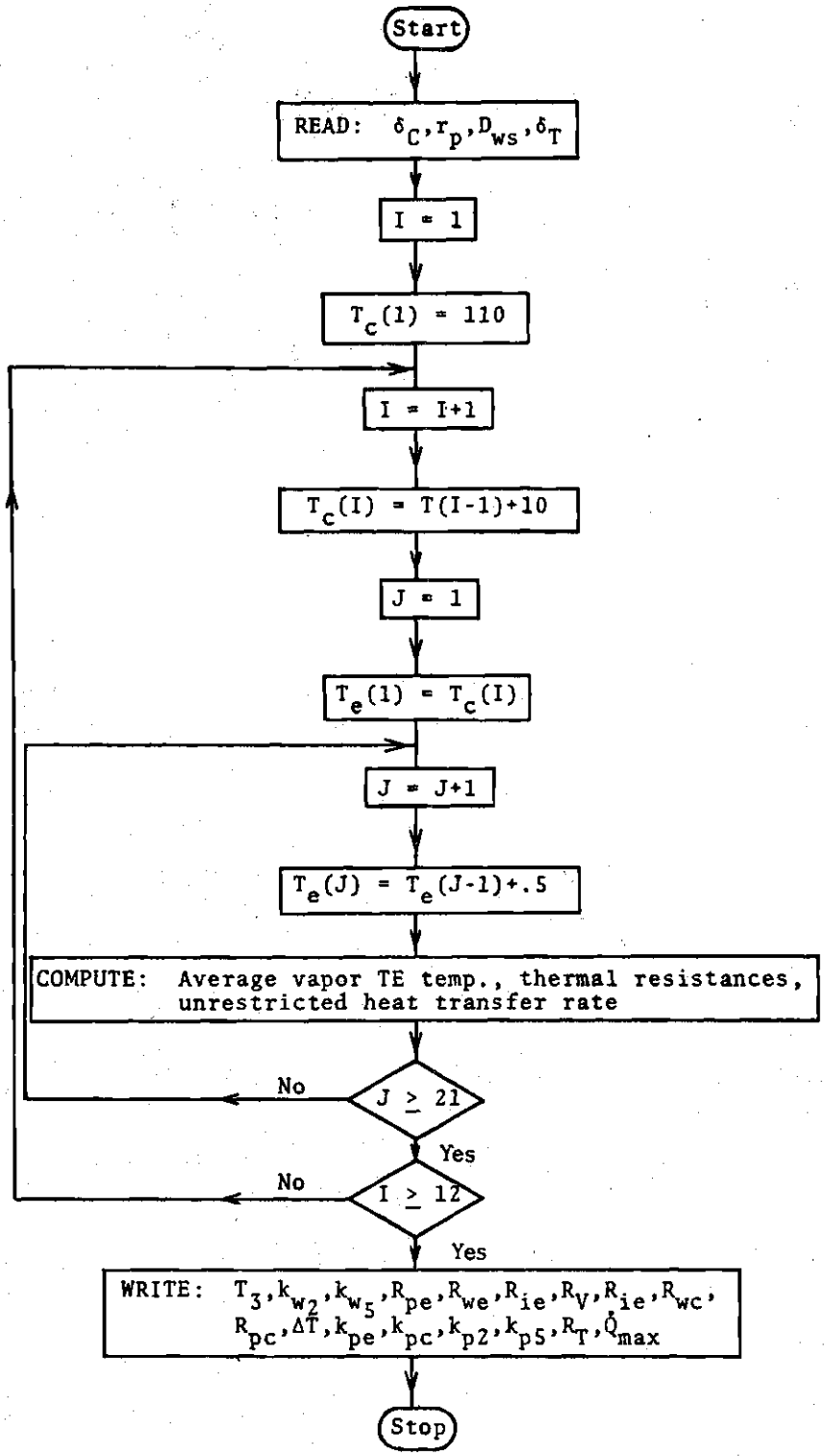

Figure 38. Flow Diagram of Computer Program Used for Calculating the Thermal Resistance

COMPUTER PROGRAM:

```
      DIMENSION TC(20),TE(20),T3(20),XLAMT3(20),XKPTE(20),
     1RHOVT3(20),RHOLT3(20),RPE(20),RV(20),RPC(20),TEMTC(20),
     2SUMR(20),Q2(20),T2(20),T5(20),XKPT2(20),XKPT5(20)
     3XLAMT5(20),XKAYT2(20),XKAYT5(20),VPRET2(20),VPRET5(20),
     4DT5(20),XKWT2(20),XKWT5(20),RWE(20),RIE(20),RIC(20),
     5XMUVT3(20),DT2(20),RWC(20),XLAMT2(20),XKPTC(20)
      WRITE(6,900)
900   FORMAT(1H ,'ENTER:  THICKNESS OF C-LAYER(FT)')
      READ(5,1)DELC
      WRITE(6,901)
901   FORMAT(1H ,9X,'PORE RADIUS(FT)')
      READ(5,1)RPORE
      WRITE(6,902)
902   FORMAT(1H ,9X,'WIRE DIAMETER (FT)')
      READ(5,1)DWIRE
      WRITE(6,903)
903   FORMAT(1H ,9X,'TOTAL THICKNESS OF SLAB (FT)')
      READ(5,1)DELT
1     FORMAT()
      PA=.0208
      RB=.017
      EL=.5
      CL=1.
      P=3.141592654
      TC(1)=110.
      DO 10 I=2,12
      TC(I)=TC(I-1)+10.
      TE(1)=TC(1)
      DO 20 J=2,21
      TE(J)=TE(J-1)+.5
      T3(J)=TC(I)+((TE(J)-TC(I))/(EL+CL))*EL
      T2(J)=T2(J)
      T5(J)=T2(J)
      XKPTE(J)=-4.02016E-5*TE(J)**2+3.20878E-2*TE(J)+1.30266
      XKPTC(J)=-4.02016E-5*TC(I)**2+3.20878E-2*TC(I)+1.30266
      XKPT2(J)=-4.02016E-5*T2(J)**2+3.20878E-2*T2(J)+1.30266
      XKPT5(J)=-4.02016E-5*T5(J)**2+3.20878E-2*T5(J)+1.30266
      XLAMT2(J)=-4.11334E-11*T2(J)**6+2.0908E-8*T2(J)**5
     1-1.43119E-6*T2(J)**4-1.03235E-3*T2(J)**3+2.61594E-1*T2(J)**2
     2-24.0246*T2(J)+8.896142
      XLAMT3(J)=-4.11334E-11*T3(J)**6+2.0908E-8*T3(J)**5
     1-1.43119E-6*T2(J)**4-1.03235E-3*T3(J)**3+2.61        *T3(J)**2
     2-24.0246*T3(J)+8.896142
      XLAMT5(J)=-4.11334E-11*T5(J)**6+2.0908E-8*T5(J)**5
     1-1.43119E-6*T5(J)**4-1.03235E-3*T5(J)**3+2.61594E-1*T5(J)**2
```

```
      2-24.0246*T5(J)+8.89614E2
      RHOVT2(J)=1.39324E-13*T2(J)**7-1.042325E-10*T2(J)**6
     1+2.638736E-8*T2(J)**5-1.14015E-6*T2(J)**4-6.78395E-4*T2(J)**3
     2+1.385389E-1*T2(J)**2-10.7628*T2(J)+3.10045E2
      RHOLT2(J)=-5.89171E-13*T2(J)**7+4.50297E-10*T2(J)**6
     1-1.15298E-7*T2(J)**5+4.95327E-6*T2(J)**4+2.9749E-3*T2(J)**3
     2-5.98552E-1*T2(J)**2+4.54425E1*T2(J)-1.21455E3
      XMUVT2(J)=8.5591E-21*T2(J)**7-6.55918E-18*T2(J)**6
     1+1.70105E-15*T2(J)**5-8.08553E-14*T2(J)**4
     2-4.27309E-11*T2(J)**3+8.90377E-9*T2(J)**2
     3-6.94007E-7*T2(J)+1.99577E-5
      XKAYT2(J)=1.0970566E-11*T2(J)**5-9.2427627E-9*T2(J)**4
     1+3.090593E-6*T2(J)**3-5.1457532E-4*T2(J)**2
     2+4.2210737E-2*T2(J)-1.2615
      XKAYT5(J)=1.0970566E-11*T5(J)**5-9.2427627E-9*T5(J)**4
     1+3.090593E-6*T5(J)**3-5.1457532E-4*T5(J)**2
     2+4.2210737E-2*T5(J)-1.2615
      RWS=DWIRE/2.
      RC=RB-DELC
      VPRETZ(J)=1.7104IE-6*T2(J)**5-1.2090IE-3*T2(J)**4
     1+3.71275E-1*T2(J)**3-5.70868E1*T2(J)**2
     2+4.28513E3*T2(J)-1.25125E5
      VPRET5(J)=1.7104IE-6*T5(J)**5-1.2090IE-3*T5(J)**4
     1+3.71275E-1*T5(J)**3-5.70868E1*T5(J)**2
     2+4.28513E3*T5(J)-1.25125E5
      A=RPCPE/RWS+1.
      B=RWS/RPCRE+1.
      C=RPCRE/RWS-1.
      DT2(J)=XKAYT2(J)/XKPT2(J)
      DT5(J)=XKAYT5(J)/XKPT5(J)
      XKWT2(J)=XKAYT2(J)*(1./(A*(2.*DT2(J)+C))+
     1(2./(A*DT2(J)*B)+B**-2)
      XKWT5(J)=XKAYT5(J)*(1./(A*(2.*DT5(J)+C))+
     1(2./(A*DT5(J)*B)+B**-2)
      P=(P*RB**2-2.*RB*DELT)/(P*2.*RB-2.*DELT+4.*RB)
      RPE(J)=ALOG(RA/RB)/2./P/XKPTE(J)/EL
      RWE(J)=ALOG(RB/RC)/2./P/XKWT2(J)/EL
      RIE(J)=5.13380E-6*T2(J)**2.5/RC/EL/VPRET2(J)/XLAMT2(J)**2
      RV(J)=2.04569E-6*XMUVT2(J)*T2(J)*(1./RHOVT2(J)-1./RHOLT2(J))
     1/RHOVT2(J)/XLAMT2(J)**2/R**4
      RIC(J)=5.13380E-6*T5(J)**2.5/RC/CL/VPRET5(J)/XLAMT5(J)**2
      RWC(J)=ALOG(RB/RC)/2./P/XKWT5(J)/CL
      RPC(J)=ALOG(RA/RB)/2./P/XKPTC(J)/CL
      TEMTC(J)=TE(J)-TC(I)
      SUMR(J)=RPE(J)+RWE(J)+RIE(J)+RV(J)+RIC(J)+RWC(J)+RPC(J)
      Q2(J)=TEMTC(J)/SUMR(J)
92:20 CONTINUE
```

```
      WRITE(6,800)TC(I)
800   FORMAT(1H1,'CONDENSER TEMPERATURE (DEG. RANK.)',1PE12.3,//)
      WRITE(6,801)
801   FORMAT(1H ,5X,'TE',9X,'T3',6X,'XKWT2',5X,'XKWT5',
     15X,'RPE',7X,'RWE',8X,'RIE',/)
      WRITE(6,802)(TE(K),T3(K),XKWT2(K),XKWT5(K),RPE(K),
     1(RWE(K),RIE(K),K=2,21)
802   FORMAT(1H ,1P7E10.3)
      WRITE(6,100)
      FORMAT(1H ,70(1H-),///)
      WRITE(6,803)
803   FORMAT(1H ,5X,'TE',9X,'RV',7X,'RIC',7X,'RWC',6X,'RPC',
     2X,'TEMTC',5X,'XKPTE',/)
      WRITE(6,802)(TE(K),RV(K),RIC(K),RWC(K),RPC(K),
     1TEMTC(K),XKPTE(K),K=2,21)
      WRITE(6,100)
      WRITE(6,804)
804   FORMAT(1H ,5X,'TE',7X,'XKPTC',5X,'XKPT2',5X,'XKPT5',
     15X,'SUMR',4X,'Q-BTU/HR',/)
      WRITE(6,805)(TE(K),XKPTC(K),XKPT2(K),XKPT5(K),
     1SUMR(K),Q2(K),K=2,21)
805   FORMAT(1H ,1P6E10.3)
      WRITE(6,100)
10    CONTINUE
      STOP
      END
```

Wick Composition 6
ENTER: THICKNESS OF C-LAYER(FT)
4.88E-4
PORE RADIUS(FT)
6.25E-5
WIRE DIAMETER (FT)
1.02E-4
TOTAL THICKNESS OF SLAB (FT)
1.176E-3

CONDENSER TEMPERATURE (DEG. RANK.) 1.200+02

TE	T3	XKWT2	XKWT5	RPE	RWE	RIE
1.220+02	1.207+02	2.453+00	2.453+00	1.190-02	3.670-03	2.412-05
1.240+02	1.213+02	2.460+00	2.460+00	1.179-02	3.659-03	2.315-05
1.260+02	1.220+02	2.467+00	2.467+00	1.168-02	3.649-03	2.224-05
1.280+02	1.227+02	2.474+00	2.474+00	1.157-02	3.638-03	2.136-05
1.300+02	1.233+02	2.481+00	2.481+00	1.147-02	3.628-03	2.051-05

TE	RV	PIC	RWC	RPC	TEMTC	XKPTE
1.220+02	3.055-03	1.206-05	1.835-03	6.011-03	2.000+00	4.619+00
1.240+02	2.678-03	1.158-05	1.830-03	6.011-03	4.000+00	4.663+00
1.260+02	2.359-03	1.112-05	1.824-03	6.011-03	6.000+00	4.707+00
1.280+02	2.085-03	1.068-05	1.819-03	6.011-03	8.000+00	4.751+00
1.300+02	1.849-03	1.026-05	1.814-03	6.011-03	1.000+01	4.795+00

TE	XKPTC	XKPT2	XKPT5	SUMR	Q-BTU/HR
1.220+02	4.574+00	4.589+00	4.589+00	2.651-02	7.544+01
1.240+02	4.574+00	4.604+00	4.604+00	2.600-02	1.538+02
1.260+02	4.574+00	4.619+00	4.619+00	2.556-02	2.348+02
1.280+02	4.574+00	4.634+00	4.634+00	2.516-02	3.180+02
1.300+02	4.574+00	4.649+00	4.649+00	2.480-02	4.032+02

CONDENSER TEMPERATURE (DEG. RANK.) 1.300+02

TE	T3	XKWT2	XKWT5	RPE	RWE	RIE
1.320+02	1.307+02	2.556+00	2.556+00	1.137-02	3.522-03	1.349-05
1.340+02	1.313+02	2.563+00	2.563+00	1.127-02	3.513-03	1.302-05
1.360+02	1.320+02	2.569+00	2.569+00	1.117-02	3.504-03	1.258-05
1.380+02	1.327+02	2.576+00	2.576+00	1.107-02	3.495-03	1.216-05
1.400+02	1.333+02	2.582+00	2.582+00	1.098-02	3.486-03	1.175-05

TE	RV	RIC	RWC	RPC	TEMTC	XKPTE
1.320+02	6.467-04	6.746-06	1.761-03	5.734-03	2.000+00	4.838+00
1.340+02	5.990-04	6.512-06	1.756-03	5.734-03	4.000+00	4.861+00
1.360+02	5.563-04	6.289-06	1.752-03	5.734-03	6.000+00	4.923+00
1.380+02	5.177-04	6.078-06	1.747-03	5.734-03	8.000+00	4.965+00
1.400+02	4.827-04	5.876-06	1.743-03	5.734-03	1.000+01	5.007+00

TE	XKPTC	XKPT2	XKPT5	SUMR	Q-BTU/HR
1.320+02	4.795+00	4.809+00	4.809+00	2.305-02	8.677+01
1.340+02	4.795+00	4.823+00	4.823+00	2.289-02	1.748+02
1.360+02	4.795+00	4.838+00	4.838+00	2.273-02	2.639+02
1.380+02	4.795+00	4.852+00	4.852+00	2.259-02	3.542+02
1.400+02	4.795+00	4.866+00	4.866+00	2.245-02	4.455+02

CONDENSER TEMPERATURE (DEG. RANK.) 1.400+02

TE	T3	XKWT2	XKWT5	RPE	RWE	RIE
1.420+02	1.407+02	2.653+00	2.653+00	1.089-02	3.393-03	8.419-06
1.440+02	1.413+02	2.659+00	2.659+00	1.080-02	3.385-03	8.195-06
1.460+02	1.420+02	2.665+00	2.665+00	1.072-02	3.378-03	7.981-06
1.480+02	1.427+02	2.672+00	2.672+00	1.063-02	3.370-03	7.777-06
1.500+02	1.433+02	2.678+00	2.678+00	1.055-02	3.362-03	7.582-06

TE	RV	RIC	RWC	RPC	TEMTC	XKPTE
1.420+02	2.449-04	4.209-06	1.697-03	5.491-03	2.000+00	5.049+00
1.440+02	2.316-04	4.097-06	1.693-03	5.491-03	4.000+00	5.090+00
1.460+02	2.191-04	3.990-06	1.689-03	5.491-03	6.000+00	5.131+00
1.480+02	2.074-04	3.888-06	1.685-03	5.491-03	8.000+00	5.171+00
1.500+02	1.964-04	3.791-06	1.681-03	5.491-03	1.000+01	5.211+00

TE	XKPTC	XKPT2	XKPT5	SUMR	Q-BTU/HR
1.420+02	5.007+00	5.021+00	5.021+00	2.173-02	9.203+01
1.440+02	5.007+00	5.035+00	5.035+00	2.162-02	1.850+02
1.460+02	5.007+00	5.049+00	5.049+00	2.151-02	2.790+02
1.480+02	5.007+00	5.062+00	5.062+00	2.140-02	3.739+02
1.500+02	5.007+00	5.076+00	5.076+00	2.129-02	4.696+02

CONDENSER TEMPERATURE (DEG. RANK.) 1.500+02

TE	T3	XKWT2	XKWT5	RPE	RWE	RIE
1.520+02	1.507+02	2.744+00	2.744+00	1.047-02	3.280-03	5.926-06
1.540+02	1.513+02	2.750+00	2.750+00	1.039-02	3.273-03	5.811-06
1.560+02	1.520+02	2.756+00	2.756+00	1.032-02	3.266-03	5.701-06
1.580+02	1.527+02	2.762+00	2.762+00	1.024-02	3.259-03	5.595-06
1.600+02	1.533+02	2.768+00	2.768+00	1.017-02	3.252-03	5.493-06

TE	RV	RIC	RWC	RPC	TEMTC	XKPTE
1.520+02	1.107-04	2.963-06	1.640-03	5.276-03	2.000+00	5.251+00
1.540+02	1.053-04	2.906-06	1.637-03	5.276-03	4.000+00	5.291+00
1.560+02	1.002-04	2.850-06	1.633-03	5.276-03	6.000+00	5.330+00
1.580+02	9.535-05	2.797-06	1.630-03	5.276-03	8.000+00	5.369+00
1.600+02	9.079-05	2.747-06	1.626-03	5.276-03	1.000+01	5.408+00

TF	XKPTC	XKPT2	XKPT5	SUMR	Q-BTU/HR
1.520+02	5.211+00	5.225+00	5.225+00	2.079-02	9.621+01
1.540+02	5.211+00	5.238+00	5.238+00	2.069-02	1.933+02
1.560+02	5.211+00	5.251+00	5.251+00	2.060-02	2.913+02
1.580+02	5.211+00	5.264+00	5.264+00	2.051-02	3.900+02
1.600+02	5.211+00	5.278+00	5.278+00	2.042-02	4.897+02

CONDENSER TEMPERATURE (DEG. RANK.) 1.600+02

TE	T3	XKWT2	XKWT5	RPE	RWE	RIE
1.620+02	1.607+02	2.831+00	2.831+00	1.010-02	3.180-03	4.603-06
1.640+02	1.613+02	2.837+00	2.837+00	1.003-02	3.174-03	4.539-06
1.660+02	1.620+02	2.842+00	2.842+00	9.959-03	3.167-03	4.477-06
1.680+02	1.627+02	2.848+00	2.848+00	9.892-03	3.161-03	4.417-06
1.700+02	1.633+02	2.853+00	2.853+00	9.827-03	3.155-03	4.360-06

TE	RV	RIC	RWC	RPC	TEMTC	XKPTE
1.620+02	5.423-05	2.301-06	1.590-03	5.084-03	2.000+00	5.446+00
1.640+02	5.188-05	2.269-06	1.587-03	5.084-03	4.000+00	5.484+00
1.660+02	4.965-05	2.238-06	1.584-03	5.084-03	6.000+00	5.521+00
1.680+02	4.754-05	2.209-06	1.581-03	5.084-03	8.000+00	5.559+00
1.700+02	4.553-05	2.180-06	1.578-03	5.084-03	1.000+01	5.596+00

TE	XKPTC	XKPT2	XKPT5	SUMR	Q-BTU/HR
1.620+02	5.408+00	5.420+00	5.420+00	2.001-02	9.994+01
1.640+02	5.408+00	5.433+00	5.433+00	1.993-02	2.007+02
1.660+02	5.408+00	5.446+00	5.446+00	1.985-02	3.023+02
1.680+02	5.408+00	5.459+00	5.459+00	1.977-02	4.046+02
1.700+02	5.408+00	5.471+00	5.471+00	1.970-02	5.077+02

CONDENSER TEMPERATURE (DEG. RANK.) 1.700+02

TE	T3	XKWT2	XKWT5	RPE	RWE	RIE
1.720+02	1.707+02	2.913+00	2.913+00	9.763-03	3.091-03	3.847-06
1.740+02	1.713+02	2.918+00	2.918+00	9.700-03	3.085-03	3.809-06
1.760+02	1.720+02	2.923+00	2.923+00	9.639-03	3.079-03	3.773-06
1.780+02	1.727+02	2.929+00	2.929+00	9.579-03	3.074-03	3.738-06
1.800+02	1.733+02	2.934+00	2.934+00	9.520-03	3.069-03	3.704-06

TE	RV	RIC	RWC	RPC	TEMTC	XKPTE
1.720+02	2.927-05	1.923-06	1.545-03	4.913-03	2.000+00	5.632+00
1.740+02	2.820-05	1.905-06	1.543-03	4.913-03	4.000+00	5.669+00
1.760+02	2.718-05	1.886-06	1.540-03	4.913-03	6.000+00	5.705+00
1.780+02	2.620-05	1.869-06	1.537-03	4.913-03	8.000+00	5.741+00
1.800+02	2.527-05	1.852-06	1.534-03	4.913-03	1.000+01	5.776+00

TE	XKPTC	XKPT2	XKPT5	SUMR	Q-BTU/HR
1.720+02	5.596+00	5.608+00	5.608+00	1.935-02	1.034+02
1.740+02	5.596+00	5.620+00	5.620+00	1.928-02	2.075+02
1.760+02	5.596+00	5.632+00	5.632+00	1.920-02	3.124+02
1.780+02	5.596+00	5.645+00	5.645+00	1.914-02	4.181+02
1.800+02	5.596+00	5.657+00	5.657+00	1.907-02	5.245+02

CONDENSER TEMPERATURE (DEG. RANK.) 1.800+02

TE	T3	XKWT2	XKWT5	RPE	RWE	RIE
1.820+02	1.807+02	2.989+00	2.989+00	9.463-03	3.011-03	3.404-06
1.840+02	1.813+02	2.994+00	2.994+00	9.407-03	3.006-03	3.383-06
1.860+02	1.820+02	2.999+00	2.999+00	9.352-03	3.002-03	3.362-06
1.880+02	1.827+02	3.004+00	3.004+00	9.298-03	2.997-03	3.343-06
1.900+02	1.833+02	3.009+00	3.009+00	9.245-03	2.992-03	3.325-06

TE	RV	RIC	RWC	RPC	TEMTC	XKPTE
1.820+02	1.743-05	1.702-06	1.506-03	4.760-03	2.000+00	5.811+00
1.840+02	1.688-05	1.691-06	1.503-03	4.760-03	4.000+00	5.846+00
1.860+02	1.636-05	1.681-06	1.501-03	4.760-03	6.000+00	5.880+00
1.880+02	1.586-05	1.672-06	1.498-03	4.760-03	8.000+00	5.914+00
1.900+02	1.537-05	1.662-06	1.496-03	4.760-03	1.000+01	5.948+00

TE	XKPTC	XKPT2	XKPT5	SUMR	Q-BTU/HR
1.820+02	5.776+00	5.786+00	5.788+00	1.876-02	1.066+02
1.840+02	5.776+00	5.799+00	5.799+00	1.870-02	2.139+02
1.860+02	5.776+00	5.811+00	5.811+00	1.864-02	3.220+02
1.880+02	5.776+00	5.823+00	5.823+00	1.857-02	4.307+02
1.900+02	5.776+00	5.834+00	5.834+00	1.851-02	5.402+02

CONDENSER TEMPERATURE (DEG. RANK.) 1.900+02

TE	T3	XKWT2	XKWT5	RPE	RWE	RIE
1.920+02	1.907+02	3.061+00	3.061+00	9.193-03	2.941-03	3.189-06
1.940+02	1.913+02	3.065+00	3.065+00	9.142-03	2.937-03	3.183-06
1.960+02	1.920+02	3.070+00	3.070+00	9.093-03	2.933-03	3.178-06
1.980+02	1.927+02	3.074+00	3.074+00	9.044-03	2.928-03	3.175-06
2.000+02	1.933+02	3.079+00	3.079+00	8.997-03	2.924-03	3.173-06

TE	RV	RIC	RWC	RPC	TEMTC	XKPTE
1.920+02	1.110-05	1.594-06	1.471-03	4.622-03	2.000+00	5.982+00
1.940+02	1.079-05	1.592-06	1.468-03	4.622-03	4.000+00	6.015+00
1.960+02	1.049-05	1.589-06	1.466-03	4.622-03	6.000+00	6.047+00
1.980+02	1.020-05	1.588-06	1.464-03	4.622-03	8.000+00	6.080+00
2.000+02	9.914-06	1.587-06	1.462-03	4.622-03	1.000+01	6.112+00

TE	XKPTC	XKPT2	XKPT5	SUMR	Q-BTU/HR
1.920+02	5.948+00	5.959+00	5.959+00	1.824-02	1.096+02
1.940+02	5.948+00	5.970+00	5.970+00	1.819-02	2.200+02
1.960+02	5.948+00	5.982+00	5.982+00	1.813-02	3.310+02
1.980+02	5.948+00	5.993+00	5.993+00	1.807-02	4.426+02
2.000+02	5.948+00	6.004+00	6.004+00	1.802-02	5.550+02

CONDENSER TEMPERATURE (DEG. RANK.) 2.000+02

TE	T3	XKWT2	XKWT5	RPE	RWE	RIE
2.020+02	2.007+02	3.127+00	3.127+00	8.950-03	2.879-03	3.261-06
2.040+02	2.013+02	3.131+00	3.131+00	8.904-03	2.875-03	3.282-06
2.060+02	2.020+02	3.135+00	3.135+00	8.859-03	2.871-03	3.305-06
2.080+02	2.027+02	3.139+00	3.139+00	8.816-03	2.868-03	3.332-06
2.100+02	2.033+02	3.144+00	3.144+00	8.773-03	2.864-03	3.362-06

TE	RV	RIC	RWC	RPC	TEMTC	XKPTE
2.020+02	7.383-06	1.631-06	1.440-03	4.498-03	2.000+00	6.144+00
2.040+02	7.199-06	1.641-06	1.438-03	4.498-03	4.000+00	6.176+00
2.060+02	7.023-06	1.653-06	1.436-03	4.498-03	6.000+00	6.207+00
2.080+02	6.854-06	1.666-06	1.434-03	4.498-03	8.000+00	6.238+00
2.100+02	6.693-06	1.681-06	1.432-03	4.498-03	1.000+01	6.268+00

TE	XKPTC	XKPT2	XKPT5	SUMR	Q-BTU/HR
2.020+02	6.112+00	6.123+00	6.123+00	1.778-02	1.125+02
2.040+02	6.112+00	6.133+00	6.133+00	1.773-02	2.256+02
2.060+02	6.112+00	6.144+00	6.144+00	1.768-02	3.394+02
2.080+02	6.112+00	6.155+00	6.155+00	1.763-02	4.538+02
2.100+02	6.112+00	6.165+00	6.165+00	1.758-02	5.689+02

CONDENSER TEMPERATURE (DEG. RANK.) 2.100+02

TE	T3	XKWT2	XKWT5	RPE	RWE	RIE
2.120+02	2.107+02	3.188+00	3.188+00	8.731-03	2.824-03	4.008-06
2.140+02	2.113+02	3.192+00	3.192+00	8.689-03	2.820-03	4.111-06
2.160+02	2.120+02	3.196+00	3.196+00	8.649-03	2.817-03	4.226-06
2.180+02	2.127+02	3.200+00	3.200+00	8.609-03	2.813-03	4.353-06
2.200+02	2.133+02	3.204+00	3.204+00	8.570-03	2.810-03	4.495-06

TE	RV	RIC	RWC	RPC	TEMTC	XKPTE
2.120+02	5.415-06	2.004-06	1.412-03	4.386-03	2.000+00	6.298+00
2.140+02	5.348-06	2.056-06	1.410-03	4.386-03	4.000+00	6.328+00
2.160+02	5.290-06	2.113-06	1.408-03	4.386-03	6.000+00	6.358+00
2.180+02	5.242-06	2.177-06	1.407-03	4.386-03	8.000+00	6.387+00
2.200+02	5.205-06	2.248-06	1.405-03	4.386-03	1.000+01	6.416+00

TE	XKPTC	XKPT2	XKPT5	SUMR	Q-BTU/HR
2.120+02	6.268+00	6.278+00	6.278+00	1.736-02	1.152+02
2.140+02	6.268+00	6.288+00	6.288+00	1.732-02	2.310+02
2.160+02	6.268+00	6.298+00	6.298+00	1.727-02	3.474+02
2.180+02	6.268+00	6.308+00	6.308+00	1.723-02	4.644+02
2.200+02	6.268+00	6.318+00	6.318+00	1.718-02	5.820+02

CONDENSER TEMPERATURE (DEG. RANK.) 2.200+02

TE	T3	XKWT2	XKWT5	RPE	RWE	RIE
2.220+02	2.207+02	3.247+00	3.247+00	8.532-03	2.773-03	8.129-06
2.240+02	2.213+02	3.251+00	3.251+00	8.495-03	2.769-03	8.872-06
2.260+02	2.220+02	3.255+00	3.255+00	8.458-03	2.766-03	9.770-06
2.280+02	2.227+02	3.258+00	3.258+00	8.422-03	2.763-03	1.087-05
2.300+02	2.233+02	3.262+00	3.262+00	8.387-03	2.760-03	1.224-05

TE	RV	RIC	RWC	RPC	TEMTC	XKPTE
2.220+02	5.831-06	4.065-06	1.386-03	4.285-03	2.000+00	6.445+00
2.240+02	6.048-06	4.436-06	1.385-03	4.285-03	4.000+00	6.473+00
2.260+02	6.315-06	4.885-06	1.383-03	4.285-03	6.000+00	6.501+00
2.280+02	6.644-06	5.435-06	1.381-03	4.285-03	8.000+00	6.529+00
2.300+02	7.052-06	6.120-06	1.380-03	4.285-03	1.000+01	6.556+00

TE	XKPTC	XKPT2	XKPT5	SUMR	Q-BTU/HR
2.220+02	6.416+00	6.426+00	6.426+00	1.699-02	1.177+02
2.240+02	6.416+00	6.435+00	6.435+00	1.695-02	2.359+02
2.260+02	6.416+00	6.445+00	6.445+00	1.691-02	3.547+02
2.280+02	6.416+00	6.454+00	6.454+00	1.687-02	4.741+02
2.300+02	6.416+00	6.464+00	6.464+00	1.684-02	5.939+02

APPENDIX D

COMPUTER PROGRAM USED TO CALCULATE HEAT PIPE NUMBER AND CAPILLARY-LIMITED HEAT TRANSFER RATE

This appendix gives the computer program used to calculate the capillary-limited heat transfer rate and the heat pipe number at each value of temperature over the range $120°R \leq T \leq 227°R$. A sample computer output is also given.

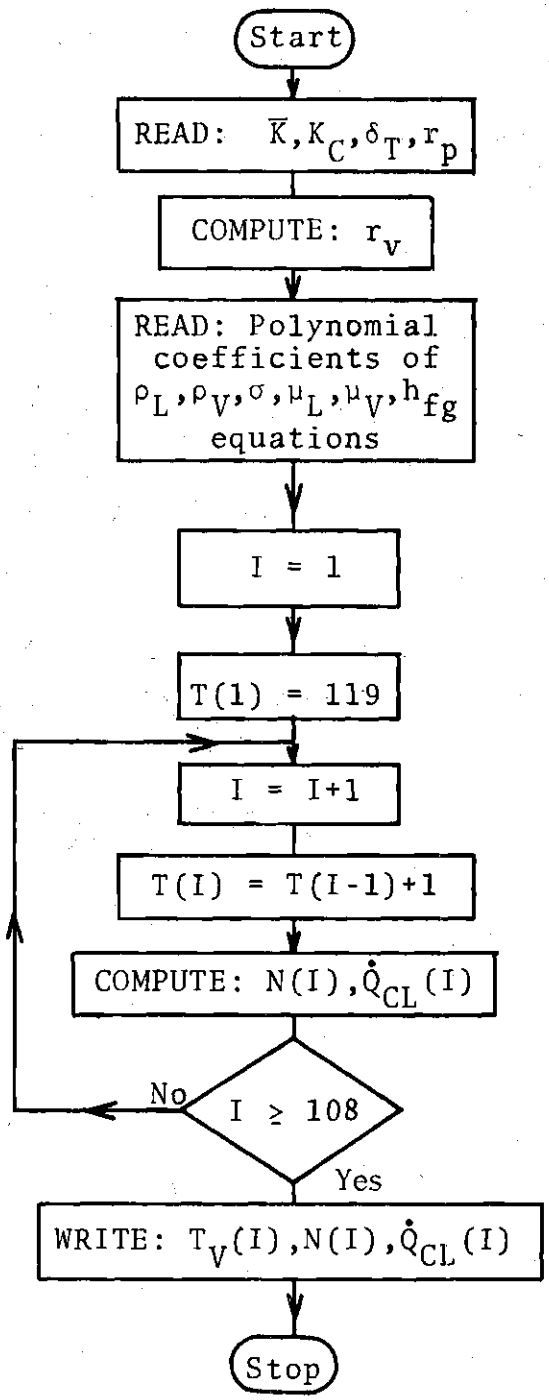

Figure 39. Flow Diagram of Computer Program Used for Calculating the Heat Pipe Number and the Capillary Limited Heat Transfer Rate

COMPUTER PROGRAM:

```
      DIMENSION A(15),TR(125),T(125),RHCL(125),
     1RHCV(125),SIG(125),XMUL(125),XMUV(125),
     2XLAM(125),HPN(125),Q(125),C(15),D(15),E(15),
     3F(15),G(15)
      EL=.5
      CL=1.
      EFFL=2.25
      B=3.5E-2
      RB=1.75E-2
      CEL=1.374E-2
      WRITE(6,800)
800   FORMAT(1H ,'ENTER:  EFFECTIVE PERMEABILITY (FT-2)')
      READ(5,1)XKBAR
      WRITE(6,801)
801   FORMAT(1H ,9X,'PERMEABILITY OF C-LAYER (FT-2)')
      READ(5,1)XKC
      WRITE(6,802)
802   FORMAT(1H ,9X,'THICKNESS OF C-LAYER (FT)')
      READ(5,1)DELC
      WRITE(6,803)
803   FORMAT(1H ,9X,'TOTAL THICKNESS OF SLAB (FT)')
      READ(5,1)DELP
804   FORMAT(1H ,9X,'PORE RADIUS (FT)')
      READ(5,1)RPORE
      P=3.141592654
      D1=XKC*CEL/4./DELC*(1./EL+1./CL)+XKBAR*EFFL/B/DELT
      R=(P*RB**2-2.*RB*DELT)/(P*2.*RB-2.*DELT*4.*RB)
      TR(1)=120.
      DO 10 I=2,108
10    TR(I)=TR(I-1)+1.
      DO 20 I=1,108
20    T(I)=TR(I)/1.8
1     FORMAT()
      KPI=8
      WRITE(6,201)
201   FORMAT(1H ,'ENTER:@ADD BILL.RHCL')
      READ(5,1)(A(I),I=1,KPI)
      DO 110 IJ=1,108
      FUN=A(1)
      DO 100 I=2,KPI
100   FUN=FUN+A(I)*T(IJ)**(I-1)
110   RHCL(IJ)=FUN*6.242977E-2
```

```
      WRITE(6,211)
211   FORMAT(1H ,'ENTER:@ADD BILL.RHCV')
      READ(5,1)(G(I),I=1,KP1)
      DO 120 IJ=1,108
      FUN=G(1)
      DO 121 I=2,KP1
121   FUN=FUN+G(I)*T(IJ)**(I-1)
120   RHCV(IJ)=FUN*6.242977E-2
      KP1=5
      WRITE(6,221)
221   FORMAT(1H ,'ENTER:@ADD BILL.SIG')
      READ(5,1)(C(I),I=1,KP1)
      DO 130 IJ=1,108
      FUN=C(1)
      DO 131 I=2,KP1
131   FUN=FUN+C(I)*T(IJ)**(I-1)
130   SIG(IJ)=FUN*6.85218E-5
      WRITE(6,231)
231   FORMAT(1H ,'ENTER:@ADD BILL.XMUL')
      READ(5,1)(D(I),I=1,KP1)
      DO 140 IJ=1,108
      FUN=D(1)
      DO 141 I=2,KP1
141   FUN=FUN+D(I)*T(IJ)**(I-1)
140   XMUL(IJ)=FUN*2.0885434E-8
      KP1=8
      WRITE(6,240)
240   FORMAT(1H ,'ENTER:@ADD BILL.XMUV')
      READ(5,1)(E(I),I=1,KP1)
      DO 150 IJ=1,108
      FUN=E(1)
      DO 151 I=2,KP1
151   FUN=FUN+E(I)*T(IJ)**(I-1)
150   XMUV(IJ)=FUN*2.0885434E-8
      KP1=7
      WRITE(6,250)
250   FORMAT(1H ,'ENTER:@ADD BILL.XLAM')
      READ(5,1)(F(I),I=1,KP1)
      DO 160 IJ=1,108
      FUN=F(1)
      DO 161 I=2,KP1
161   FUN=FUN+F(I)*T(IJ)**(I-1)
160   XLAM(IJ)=FUN*0.4301724
      DO 500 I=1,108
      HPN(I)=RHCL(I)*SIG(I)*XLAM(I)*3600/XMUL(I)
      DZ=8.*XMUV(I)*RHCL(I)*EFFL/P/RHCV(I)/XMUL(I)/R**4
```

```
 90:500   Q(I)=2.*HPN(I)/(RPCRE*(D1+D2))
 91:      WRITE(6,600)
 92:600   FORMAT(1H1,2X,'DEGREE RANKINE',3X,'HPN(BTU FT-2 HR-1)'
 93:     1,4X,'Q(BTU HR-1)')
 94:      WRITE(6,601)
 95:601   FORMAT(1H ,60(1H-))
 96:      WRITE(6,602)(TR(I),HPN(I),Q(I),I=1,108)
 97:602   FORMAT(1H ,1P1E10.3,1P2E20.4)
 98:      WRITE(6,601)
 99:      STOP
100:      END
```

Wick Composition 6

ENTER: EFFECTIVE PERMEABILITY (FT-2)
>6.4709E7
PERMEABILITY OF C-LAYER (FT-2)
>15.1683E9
THICKNESS OF C-LAYER (FT)
>4.88E-4
TOTAL THICKNESS OF SLAB (FT)
>11.1761-3
PORE RADIUS (FT)
>6.25E-5

DEGREE RANKINE	HPN(BTU FT-2 HR-1)	Q(BTU HR-1)
1.200+02	2.4447+09	6.8325+01
1.210+02	2.4536+09	7.0748+01
1.220+02	2.4629+09	7.3072+01
1.230+02	2.4727+09	7.5243+01
1.240+02	2.4829+09	7.7283+01
1.250+02	2.4934+09	7.9175+01
1.260+02	2.5043+09	8.0933+01
1.270+02	2.5154+09	8.2580+01
1.280+02	2.5268+09	8.4123+01
1.290+02	2.5384+09	8.5568+01
1.300+02	2.5500+09	8.6932+01
1.310+02	2.5619+09	8.8216+01
1.320+02	2.5735+09	8.9436+01
1.330+02	2.5852+09	9.0600+01
1.340+02	2.5967+09	9.1704+01
1.350+02	2.6080+09	9.2762+01
1.360+02	2.6190+09	9.3771+01
1.370+02	2.6297+09	9.4738+01
1.380+02	2.6399+09	9.5663+01
1.390+02	2.6496+09	9.6550+01
1.400+02	2.6587+09	9.7393+01
1.410+02	2.6672+09	9.8199+01
1.420+02	2.6748+09	9.8959+01
1.430+02	2.6816+09	9.9678+01
1.440+02	2.6874+09	1.0035+02
1.450+02	2.6922+09	1.0096+02
1.460+02	2.6959+09	1.0155+02
1.470+02	2.6984+09	1.0207+02
1.480+02	2.6995+09	1.0254+02
1.490+02	2.6993+09	1.0294+02
1.500+02	2.6976+09	1.0329+02
1.510+02	2.6943+09	1.0356+02

1.520+02	2.6894+09	1.0377+02
1.530+02	2.6829+09	1.0390+02
1.540+02	2.6745+09	1.0396+02
1.550+02	2.6644+09	1.0393+02
1.560+02	2.6523+09	1.0383+02
1.570+02	2.6384+09	1.0364+02
1.580+02	2.6224+09	1.0336+02
1.590+02	2.6044+09	1.0299+02
1.600+02	2.5845+09	1.0253+02
1.610+02	2.5624+09	1.0198+02
1.620+02	2.5383+09	1.0134+02
1.630+02	2.5122+09	1.0060+02
1.640+02	2.4840+09	9.9771+01
1.650+02	2.4538+09	9.8848+01
1.660+02	2.4217+09	9.7832+01
1.670+02	2.3875+09	9.6727+01
1.680+02	2.3515+09	9.5532+01
1.690+02	2.3137+09	9.4251+01
1.700+02	2.2741+09	9.2888+01
1.710+02	2.2328+09	9.1442+01
1.720+02	2.1900+09	8.9918+01
1.730+02	2.1456+09	8.8323+01
1.740+02	2.0999+09	8.6657+01
1.750+02	2.0528+09	8.4925+01
1.760+02	2.0046+09	8.3133+01
1.770+02	1.9554+09	8.1285+01
1.780+02	1.9052+09	7.9386+01
1.790+02	1.8541+09	7.7440+01
1.800+02	1.8024+09	7.5454+01
1.810+02	1.7501+09	7.3431+01
1.820+02	1.6974+09	7.1379+01
1.830+02	1.6443+09	6.9299+01
1.840+02	1.5910+09	6.7200+01
1.850+02	1.5377+09	6.5085+01
1.860+02	1.4843+09	6.2956+01
1.870+02	1.4310+09	6.0825+01
1.880+02	1.3780+09	5.8690+01
1.890+02	1.3252+09	5.6556+01
1.900+02	1.2728+09	5.4429+01
1.910+02	1.2210+09	5.2312+01
1.920+02	1.1696+09	5.0208+01
1.930+02	1.1189+09	4.8120+01
1.940+02	1.0689+09	4.6052+01
1.950+02	1.0196+09	4.4006+01
1.960+02	9.7107+08	4.1985+01
1.970+02	9.2341+08	3.9992+01
1.980+02	8.7662+08	3.8027+01

1.990+02	8.3075+08	3.6095+01
2.000+02	7.6583+08	3.4196+01
2.010+02	7.4188+08	3.2331+01
2.020+02	6.9893+08	3.0502+01
2.030+02	6.5701+08	2.8712+01
2.040+02	6.1614+08	2.6961+01
2.050+02	5.7633+08	2.5250+01
2.060+02	5.3762+08	2.3582+01
2.070+02	5.0003+08	2.1957+01
2.080+02	4.6354+08	2.0375+01
2.090+02	4.2820+08	1.8840+01
2.100+02	3.9405+08	1.7352+01
2.110+02	3.6109+08	1.5913+01
2.120+02	3.2934+08	1.4524+01
2.130+02	2.9885+08	1.3187+01
2.140+02	2.6964+08	1.1905+01
2.150+02	2.4175+08	1.0677+01
2.160+02	2.1520+08	9.5077+00
2.170+02	1.9005+08	8.3961+00
2.180+02	1.6631+08	7.3499+00
2.190+02	1.4405+08	6.3688+00
2.200+02	1.2331+08	5.4482+00
2.210+02	1.0410+08	4.5982+00
2.220+02	8.6487+07	3.8182+00
2.230+02	7.0487+07	3.1098+00
2.240+02	5.6127+07	2.4741+00
2.250+02	4.3426+07	1.9121+00
2.260+02	3.2388+07	1.4241+00
2.270+02	2.2992+07	1.0092+00

APPENDIX E

COMPUTER PROGRAM USED TO CALCULATE THE SONIC-LIMITED HEAT TRANSFER RATE

This appendix gives the computer program used to calculate the sonic limitation on heat transfer rate over the temperature range $120°R \leq T \leq 227°R$. A sample computer output is also given.

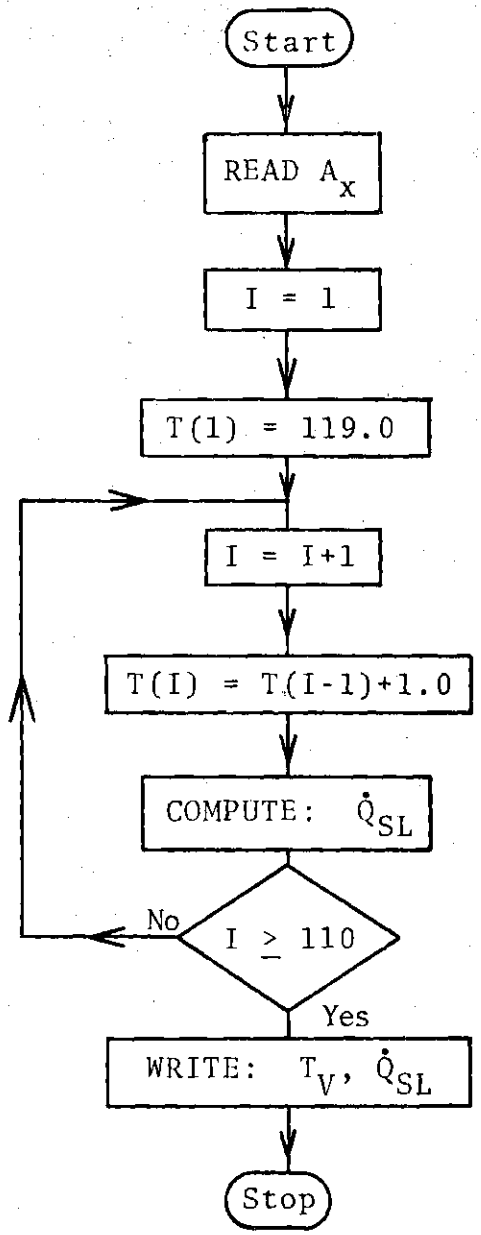

Figure 40. Flow Diagram of Computer Program Used for Calculating the Sonic Limited Heat Transfer Rate

COMPUTER PROGRAM:

```
      DIMENSION OMSL(125),XLAM(125),RHOV(125),XKSHR(125),T3(125)
      WRITE(6,100)
100   FORMAT(1H ,'ENTER:X-SECTIONAL AREA OF VAPOR SPACE (FT2)')
      READ(5,1)XAVS
1     FORMAT()
      T3(1)=119.
      DO 10 I=2,110
      T3(I)=T3(I-1)+1.
      XLAM(I)=-4.11334E-11*T3(I)**6+2.0908E-8*T3(I)**5
     1-1.43119E-6*T3(I)**4-1.03235E-3*T3(I)**3
     2+2.61594E-1*T3(I)**2-24.0246*T3(I)+8.896145
      RHOV(I)=1.39324E-13*T3(I)**7-1.042325E-10*T3(I)**6
     1+2.638736E-8*T3(I)**5-1.14015E-6*T3(I)**4
     2-6.78395E-4*T3(I)**3+1.385369E-1*T3(I)**2
     3-10.7628*T3(I)+3.100456
      XKSHR(I)=1.572403E-6*T3(I)**2-8.6844907E-4*T3(I)
     1+1.52913275
10    OMSL(I)=1.51645*XAVS*XLAM(I)*RHOV(I)*XKSHR(I)**.5
     1*T3(I)**.5
      WRITE(6,200)
200   FORMAT(1H1,2X,'VAPOR TEMP.',4X,'MAX. HEAT TRANSFER')
      WRITE(6,201)
201   FORMAT(1H ,3X,'DEG. RANK.',4X,"SONIC LIM. BTU/HR")
      WRITE(6,202)
202   FORMAT(1H ,40(1H-))
      WRITE(6,300)(T3(I),OMSL(I),I=2,110)
300   FORMAT(1H ,1P2E15.5)
      WRITE(6,202)
      STOP
      END
```

Wick Composition 6

ENTER:X-SECTIONAL AREA OF VAPOR SPACE (FT2)
5.72956-4

VAPOR TEMP. DEG. RANK.	MAX. HEAT TRANSFER SONIC LIM. BTU/HR	VAPOR TEMP. DEG. RANK.	MAX. HEAT TRANSFER SONIC LIM. BTU/HR
1.20000+02	7.09390+03	1.60000+02	8.79177+04
1.21000+02	7.95961+03	1.61000+02	9.18403+04
1.22000+02	8.89269+03	1.62000+02	9.59007+04
1.23000+02	9.89327+03	1.63000+02	1.00090+05
1.24000+02	1.09603+04	1.64000+02	1.04409+05
1.25000+02	1.20544+04	1.65000+02	1.08848+05
1.26000+02	1.32052+04	1.66000+02	1.13422+05
1.27000+02	1.43996+04	1.67000+02	1.18124+05
1.28000+02	1.56308+04	1.68000+02	1.22952+05
1.29000+02	1.69035+04	1.69000+02	1.27903+05
1.30000+02	1.82077+04	1.70000+02	1.32998+05
1.31000+02	1.95510+04	1.71000+02	1.38188+05
1.32000+02	2.09301+04	1.72000+02	1.43509+05
1.33000+02	2.23474+04	1.73000+02	1.48962+05
1.34000+02	2.38060+04	1.74000+02	1.54530+05
1.35000+02	2.53052+04	1.75000+02	1.60224+05
1.36000+02	2.68527+04	1.76000+02	1.66043+05
1.37000+02	2.84414+04	1.77000+02	1.71967+05
1.38000+02	3.00918+04	1.78000+02	1.78015+05
1.39000+02	3.17934+04	1.79000+02	1.84186+05
1.40000+02	3.35554+04	1.80000+02	1.90471+05
1.41000+02	3.53832+04	1.81000+02	1.96873+05
1.42000+02	3.72773+04	1.82000+02	2.03394+05
1.43000+02	3.92469+04	1.83000+02	2.10036+05
1.44000+02	4.12979+04	1.84000+02	2.16791+05
1.45000+02	4.34249+04	1.85000+02	2.23670+05
1.46000+02	4.56396+04	1.86000+02	2.30675+05
1.47000+02	4.79508+04	1.87000+02	2.37792+05
1.48000+02	5.03541+04	1.88000+02	2.45054+05
1.49000+02	5.28592+04	1.89000+0	2.52425+05
1.50000+02	5.54666+04	1.90000+02	2.59947+05
1.51000+02	5.81814+04	1.91000+02	2.67589+05
1.52000+02	6.10061+04	1.92000+02	2.75355+05
1.53000+02	6.39437+04	1.93000+02	2.83270+05
1.54000+02	6.70017+04	1.94000+02	2.91313+05
1.55000+02	7.01762+04	1.95000+02	2.99477+05
1.56000+02	7.34739+04	1.96000+02	3.07787+05
1.57000+02	7.69077+04	1.97000+02	3.16227+05
1.58000+02	8.04461+04	1.98000+02	3.24807+05
1.59000+02	8.41190+04	1.99000+02	3.33501+05

2.00000+02	3.42332+05
2.01000+02	3.51222+05
2.02000+02	3.60233+05
2.03000+02	3.69283+05
2.04000+02	3.78390+05
2.05000+02	3.87559+05
2.06000+02	3.96693+05
2.07000+02	4.05595+05
2.08000+02	4.14443+05
2.09000+02	4.23381+05
2.10000+02	4.31422+05
2.11000+02	4.39340+05
2.12000+02	4.46739+05
2.13000+02	4.53445+05
2.14000+02	4.59290+05
2.15000+02	4.64180+05
2.16000+02	4.67580+05
2.17000+02	4.69491+05
2.18000+02	4.69519+05
2.19000+02	4.67281+05
2.20000+02	4.62350+05
2.21000+02	4.54227+05
2.22000+02	4.42363+05
2.23000+02	4.26087+05
2.24000+02	4.04712+05
2.25000+02	3.77358+05
2.26000+02	3.43085+05
2.27000+02	3.00823+05
2.28000+02	2.49335+05

APPENDIX F

SAMPLE CALCULATION OF THE EFFECTIVE THERMAL CONDUCTIVITY OF THE CIRCUMFERENTIAL WICK/LIQUID COMBINATION

Equation (3.4) gives the effective thermal conductivity of the circumferential wick/liquid combination as:

$$\frac{k_w(t)}{k_L(t)} = \frac{1}{[A][2D+C]} + \frac{2.0}{[A][D][B]} + \frac{1}{[B]^2} \qquad (3.4)$$

where

$$[A] = \frac{r_p}{r_{ws}} + 1.0$$

$$[B] = \frac{r_{ws}}{r_p} + 1.0$$

r_{ws} = radius of screen element

$$[C] = \frac{r_p}{r_{ws}} - 1.0$$

$$[D] = \frac{k_L(t)}{k_p(t)}$$

For wick composition 6, at a temperature of 160°R the following data is given:

$r_p = 6.25 \times 10^{-5}$ [ft] from Table 5

$r_{ws} = (1.02 \times 10^{-4})/2.0 = 5.10 \times 10^{-5}$ [ft] from Table 5

$k_{L(160)} = 7.16075 \times 10^{-2} \left[\frac{Btu}{ft\text{-}hr\text{-}^\circ R}\right]$ from Appendix B

$k_{p(160)} = 5.40755 \left[\frac{Btu}{ft\text{-}hr\text{-}^\circ R}\right]$ from Appendix B

Therefore:

$$[A] = \frac{6.25 \times 10^{-5} ft}{5.10 \times 10^{-5} ft} + 1.0 = 2.225$$

$$[B] = \frac{5.10 \times 10^{-5} ft}{6.25 \times 10^{-5} ft} + 1.0 = 1.816$$

$$[C] = \frac{6.25 \times 10^{-5} ft}{5.10 \times 10^{-5} ft} - 1.0 = 1.225$$

$$[D] = \frac{7.16075 \times 10^{-2}}{5.40755} = 1.324 \times 10^{-2}$$

$$\frac{k_{w(160}}{7.16075 \times 10^{-2}} = \frac{1.0}{(2.225)[2(1.324 \times 10^{-2}) + 1.225]} +$$

$$+ \frac{2.0}{(2.225)(1.324 \times 10^{-2})(1.816)} + \frac{1.0}{(1.816)^2}$$

$$= 3.591 \times 10^{-1} + 3.738 \times 10^{1} + 3.032 \times 10^{-1}$$

$$\frac{k_{w(160)}}{7.16075 \times 10^{-2}} = 3.805 \times 10 \qquad \left[\frac{Btu}{ft\text{-}hr\text{-}^\circ R}\right]$$

$$k_{w_{(160)}} = 2.825 \quad \left[\frac{Btu}{ft\text{-}hr\text{-}^{\circ}R}\right]$$

APPENDIX G

SAMPLE CALCULATION OF THERMAL RESISISTANCES

The following sample calculation of the thermal resistances of the heat pipe components are given for a condenser temperature of 160°R, evaporator temperature of 162°R, and wick composition 6.

1. Thermal Resistance of Pipe Wall

a. Evaporation

Equation (3.2) gives R_{pe} as

$$R_{pe} = \frac{\ln(r_A/r_C)}{2\pi\, k_{pe}\, \ell_e} \qquad (3.2.a)$$

$$= \frac{\ln\left(\frac{2.083\times10^{-2}\text{ft}}{1.75\times10^{-2}\text{ft}}\right)}{(2)(3.14159)\left(5.417\ \frac{\text{Btu}}{\text{ft-hr-°R}}\right)(.5\ \text{ft})}$$

$$R_{pe} = 1.015\times10^{-2} \qquad \left[\frac{\text{hr-°R}}{\text{Btu}}\right]$$

b. Thermal Resistance of Pipe Wall at Condenser

Equation (3.2.b) gives R_{pc} as

$$R_{pc} = \frac{\ln (r_A/r_B)}{2\pi\, k_{p_c}\, \ell_c} \qquad (3.2.b)$$

$$= \frac{\ln\left(\frac{2.083\times10^{-2}\text{ ft}}{1.75\times10^{-2}\text{ ft}}\right)}{(2)(3.14159)\left(5.408\ \frac{\text{Btu}}{\text{ft-hr-°R}}\right)(1.0\text{ ft})}$$

$$R_{pc} = 5.084\times10^{-3} \qquad \left[\frac{\text{hr-°R}}{\text{Btu}}\right]$$

2. Thermal Resistance of the Circumferential Wick at the Evaporator and Condenser

a. Evaporator

Equation (3.3.a) gives R_{we} as

$$R_{we} = \frac{\ln (r_B/r_C)}{2\pi\, k_{w_2}\, \ell_e} \qquad (3.3.a)$$

where:

k_{w_2} is the effective thermal conductivity of the wick-liquid combination evaluated at T_2 (see Appendix F), where T_2 is given by:

$$T_2 = T_c + \frac{(T_e - T_c)\ \ell_e}{(\ell_e + \ell_c)}$$

$$T_2 = 160 + \frac{(2)(.5)}{1.5} = 160.67\ °R$$

($T_2 = T_3 = T_5$ constant internal temperature)

$$k_{w_2} = 2.831 \quad \left[\frac{Btu}{hr\text{-}ft\text{-}^\circ R}\right]$$

therefore:

$$R_{we} = \frac{\ln\left(\frac{1.75\times10^{-2}\,ft}{1.701\times10^{-2}\,ft}\right)}{2(3.14159)\left(2.831\ \frac{Btu}{hr\text{-}ft^\circ R}\right)(.5\ ft)}$$

$$R_{we} = 3.18\times10^{-3} \quad \left[\frac{hr\text{-}^\circ R}{Btu}\right]$$

b. Condenser

Similarly, Eq. (3.3.b) gives R_{wc} as:

$$R_{wc} = \frac{\ln(r_B/r_C)}{2\pi\, k_{w_5}\, \ell_c} \qquad (3.3.b)$$

where k_{w_5} is taken to be equal to k_{w_2} seen above. Therefore,

$$R_{wc} = \frac{\ln\left(\frac{1.75\times10^{-2}\,ft}{1.701\times10^{-3}\,ft}\right)}{(2)(3.14159)\left(2.831\ \frac{Btu}{hr\text{-}ft\text{-}^\circ R}\right)(1.0\ ft)}$$

$$R_{wc} = 1.590\times10^{-3} \quad \left[\frac{hr\text{-}^\circ R}{Btu}\right]$$

3. Thermal Resistance of Wick-Vapor Interface

a. At Evaporator

Equation (3.5.a) gives R_{ie} as

$$R_{ie} = \frac{(2\pi)^{1/2}\ R^{3/2}\ T_2^{5/2}}{4\pi\ r_C\ \ell_e\ P_{V_2}\ h_{fg_2}^2\ g_c^{1/2}} \qquad (3.5.a)$$

A substitution of constant terms and conversion factors yields:

$$R_{ie} = \frac{(6.2832)^{1/2}}{12.566} \times \frac{55.15\frac{\text{ft-lbf}}{\text{lbm°R}}\ \frac{1}{778}\ \frac{\text{Btu}}{\text{ft-lb}_f} \times (55.15\frac{\text{ft-lb}_f}{\text{lbm°R}})^{1/2}}{(32.2\ \frac{\text{lbm}}{\text{lb}_f}\ \frac{\text{ft}}{\text{sec}^2})^{1/2}\ 3600\ \frac{\text{sec}}{\text{hr}}}$$

$$\frac{T_2^{2.5}}{r_C\ \ell_e\ P_{V_2}\ h_{fg_2}^2}$$

or,

$$R_{ie} = 5.1338\text{x}10^{-6}\left[\frac{\text{Btu-hr-lb}_f}{°R^{1.5}\ \text{lb}_m^2}\right]\frac{T_2^{2.5}}{r_C\ \ell_e\ P_{V_2}\ h_{fg_2}^2}$$

$$T_2 = T_3 = T_5 = 160.67 \quad (°R)$$

$$P_{V_2} = P_{V_5} = 7.0265\text{x}10^3 \quad \left[\frac{\text{lb}_f}{\text{ft}^2}\right]$$

$$h_{fg_2} = h_{fg_5} = 7.7913\text{x}10 \quad \left[\frac{\text{Btu}}{\text{lb}_m}\right]$$

Therefore,

$$R_{ie} = 5.1338\text{x}10^{-6} \frac{\text{Btu-hr-lb}_f}{{}^\circ\text{R}^{1.5}\ \text{lb}_m^2}\ \text{x}$$

$$\frac{(160.65^\circ\text{R})^{2.5}}{(1.701\text{x}10^{-2}\text{ft})(.5\ \text{ft})(7.0265\text{x}10^3\ \frac{\text{lb}_f}{\text{ft}^2})(7.7913\text{x}10)^2\ \frac{\text{Btu}}{\text{lbm}^2}}$$

$$R_{ie} = 4.603\text{x}10^{-6} \qquad \left[\frac{^\circ\text{R-hr}}{\text{Btu}}\right]$$

b. Condenser

Similarly, Eq. (3.5.b) may be written as

$$R_{ic} = \frac{5.1338\text{x}10^{-6}(T_5)^{2.5}}{r_C\ P_{V_5}\ (h_{fg_5}^2)\ \ell_c}$$

$$R_{ic} = 5.1338\text{x}10^{-6}\left[\frac{\text{Btu-hr-lb}_f}{{}^\circ\text{R}^{1.5}\text{lbm}^2}\right]\text{x}$$

$$\frac{(160.67)^{2.5}\ {}^\circ\text{R}^{2.5}}{(1.701\text{x}10^{-2}\ \text{ft})(1.0\ \text{ft})(7.0265\text{x}10^3\ \frac{\text{lb}_f}{\text{ft}^2})(7.7913\text{x}10)^2\ \frac{\text{Btu}^2}{\text{lbm}^2}}$$

$$R_{ic} = 2.301\text{x}10^{-6} \qquad \left[\frac{^\circ\text{R-hr}}{\text{Btu}}\right]$$

4. Thermal Resistance of Vapor

The thermal resistance of the vapor "R_V" is given by Eq. (3.12)

$$R_V = \frac{8\mu_V \ell_{eff} T_3 \left(\frac{1}{\rho_V} - \frac{1}{\rho_L}\right)}{\pi \rho_V (h_{fg})^2 r_v^4}$$

By applying proper conversion factors and substituting constant terms, Eq. (3.12) is rewritten as:

$$R_V = \frac{(8)(2.25\ ft)}{(3.14159)(3600\ \frac{sec}{hr})(778\ \frac{ft\text{-}lb_f}{Btu})} \times \frac{\mu_V T_3 \left(\frac{1}{\rho_V} - \frac{1}{\rho_L}\right)}{\rho_V (h_{fg})^2 r_v^4} \quad (3.12.a)$$

$$R_V = 2.0457\times10^{-6}\left[\frac{Btu\text{-}hr}{sec\ lb_f}\right]\frac{\mu_V T_3 \left(\frac{1}{\rho_V} - \frac{1}{\rho_L}\right)}{\rho_V (h_{fg})^2 r_v^4}$$

Where the thermodynamic property terms are evaluated at T_3.

$$R_V = 2.0457\times10^{-6}\left[\frac{Btu\text{-}hr}{sec\ lb_f}\right] \times$$

$$\frac{(1.3783\times10^{-7}\ \frac{lb_f\text{-}sec}{ft^2})(160.67°R)\left[\frac{1}{8.6931\times10^{-1}} - \frac{1}{4.7842\times10}\right]\frac{ft^3}{lbm}}{(8.6931\times10^{-1}\ \frac{lbm}{ft^3})(7.7913\times10)^2\ \frac{Btu^2}{lbm^2}\ (3.753\times10^{-3})^4\ ft^4}$$

$$R_V = 5.423\times10^{-5} \quad \left[\frac{°R\text{-}hr}{Btu}\right]$$

5. Total Thermal Resistance of the Heat Pipe

The total resistance of the heat pipe is simply the sum of the thermal resistance of the components as indicated by Eq. (3.1).

$$R_T = R_{pe} + R_{we} + R_{ie} + R_V + R_{ic} + R_{wc} + R_{pc} \qquad (3.1)$$

or

$$R_T = 1.015\text{x}10^{-2} + 3.18\text{x}10^{-3} + 4.603\text{x}10^{-6} + 5.423\text{x}10^{-5}$$

$$+ 2.301\text{x}10^{-6} + 1.590\text{x}10^{-3} + 5.084\text{x}10^{-3}$$

$$R_T = 2.001\text{x}10^{-2} \qquad \left[\frac{^\circ\text{R-hr}}{\text{Btu}}\right]$$

APPENDIX H

SAMPLE CALCULATION OF THE HYDRAULIC RADIUS

The values for hydraulic radius r_V used in this work were obtained by dividing the cross sectional area of the vapor space by the total "wetted" perimeter exposed to the vapor flow. This is given by the following equation:

$$r_V = \frac{(\pi)(r_C)^2-(2)(r_C)(\delta_T)}{(\pi)(2)(r_C)-(2)(\delta_T)+(4)(r_C)} \quad \text{(ft)} \qquad \text{(H.1)}$$

A sample calculation is given for wick composition 6.

π = 3.1415926

r_C = inside radius of pipe minus the thickness of the circumferential wick.

$r_C = 1.750\times10^{-2}\text{ft} - \delta_C = 1.750\times10^{-2}\text{ft} - 4.88\times10^{-4}\text{ft} = 1.701\times10^{-2}\text{ft}$

$\delta_T = 11.176\times10^{-3}\text{ft}$

$$r_V = \frac{(3.141592)(1.701\times10^{-2}\text{ft})^2-(2)(1.701\times10^{-2})(11.176\times10^{-3}\text{ft})}{(3.141592)(2)(1.701\times10^{-2}\text{ft})-(2)(1.701\times10^{-2}\text{ft})+(4)(1.701\times10^{-2}\text{ft})}$$

$r_V = 3.753\times10^{-3}$ (ft)

APPENDIX I

DERIVATION OF EQUATION (3.19)

Reference [7] gives the relationship between the pressure drop in the liquid phase due to viscosity and the inverse permeability, K, is given by

$$\Delta P_L = K \frac{\mu_L \dot{m}_L \ell_{eff}}{\rho_L A_{w_t}} \qquad \left[\frac{lb_f}{ft^2}\right] \tag{I.1}$$

where the term K is the inverse permeability based on the liquid approach velocity (see Appendix A). The composite slab wick used in this study is composed of several layers of coarse screen (labeled B) "sandwiched" between layers of finer screen (labeled A). The total liquid flow rate in the slab wick is the sum of the liquid flow rates in each portion of the slab. Thus:

$$\dot{m}_L = \dot{m}_{L_A} + \dot{m}_{L_B} \qquad \left[\frac{lb_m}{hr}\right] \tag{I.2}$$

The liquid phase pressure drop in each portion is given by a modification of Eq. (I.1):

$$\Delta P_{L_A} = \frac{K_A \mu_L \dot{m}_{L_A} \ell_{eff}}{\rho_L A_{w_A}} \qquad \left[\frac{lb_f}{ft^2}\right] \tag{I.1.a}$$

and,

$$\Delta P_{L_B} = \frac{K_B \mu_L \dot{m}_{L_B} \ell_{eff}}{\rho_L A_{w_B}} \qquad \left[\frac{lb_f}{ft^2}\right] \qquad (I.1.b)$$

The terms A_{w_A} and A_{w_B}, the cross sections areas of the two slab sections, are given by

$$A_{w_A} = n_A \delta_A b \qquad (ft^2) \qquad (I.3.a)$$

and,

$$A_{w_B} = n_B \delta_B b \qquad (ft^2) \qquad (I.3.b)$$

where

n_A, n_B = number of screen layers in "A" and "B" portion, respectively.

δ_A, δ_B = thickness of screen used in "A" and "B" portion, respectively.

b = width of the slab

By rearranging and substituting Eqs. (I.1.a) and (I.1.b) into Eq. (I.2), the following is obtained:

$$\dot{m}_L = (\Delta P_{L_A}) \frac{\rho_L (n_A \delta_A b)}{K_A \mu_L \ell_{eff}} + (\Delta P_{L_B}) \frac{\rho_L (n_B \delta_B b)}{K_B \mu_L \ell_{eff}} \qquad (I.4)$$

$$\left[\frac{lb_m}{hr}\right]$$

It is assumed that the viscous pressure drops in each portion of the composite slab are equal to the total slab pressure drop. That is:

$$\Delta P_{L_A} = \Delta P_{L_B} = \Delta P_{L_{A+B}} \tag{I.5}$$

A substitution of Eq. (I.5) into Eq. (I.4) gives:

$$\dot{m}_L = \Delta P_{L_{A+B}} \frac{\rho_L \, b}{\mu_L \ell_{eff}} \left[\frac{n_A \delta_A}{K_A} + \frac{n_B \delta_B}{K_B}\right] \quad \left[\frac{lb_m}{hr}\right] \tag{I.6}$$

It is convenient to define an effective inverse permeability, $\overline{K}$, for the composite slab as

$$\frac{\delta_T}{\overline{K}} = \frac{n_A \delta_A}{K_A} + \frac{n_B \delta_B}{K_B}$$

or,

$$\overline{K} = \frac{\delta_T}{\frac{n_A \delta_A}{K_A} + \frac{n_B \delta_B}{K_B}} \qquad (ft^{-2}) \tag{I.7}$$

where

δ_T = the total thickness of the slab wick

By substituting Eq. (I.7) into Eq. (I.6) and rearranging, the following is obtained:

$$\Delta P_{L_{A+B}} = \frac{\dot{m}_L \mu_L \ell_{eff} \overline{K}}{\rho_L b \delta_T} \quad \left[\frac{lb_f}{ft^2}\right] \qquad (I.8)$$

The liquid pressure drop in the circumferential wick due to viscous effects is given by,

$$\Delta P_{L_{C_e}} = K_{C_{APP}} \frac{\mu_L \dot{m}_{L_C} L_e}{\rho_L n_C \delta_C \ell_e} \quad \left[\frac{lb_f}{ft^2}\right] \qquad (I.9.a)$$

for the evaporator section, and

$$\Delta P_{L_{C_c}} = K_{C_{APP}} \frac{\mu_L \dot{m}_{L_C} L_c}{\rho_L n_C \delta_C \ell_c} \quad \left[\frac{lb_f}{ft^2}\right] \qquad (I.9.b)$$

for the condenser section. The terms "L_c" and "L_e" seen in Eqs. (I.9.a) and (I.9.b) above, and illustrated graphically in Fig. 44, represent the average arc length traveled by an element of mass in the circumferential wick at the condenser and the evaporator, respectively. The assumption is made that these two lengths are equal. Thus:

$$L_c = L_e = L \qquad (I.10)$$

The rate of liquid flow through a cross section of either the condenser or evaporator circumferential wick is one-fourth the total liquid flow rate in the composite slab.

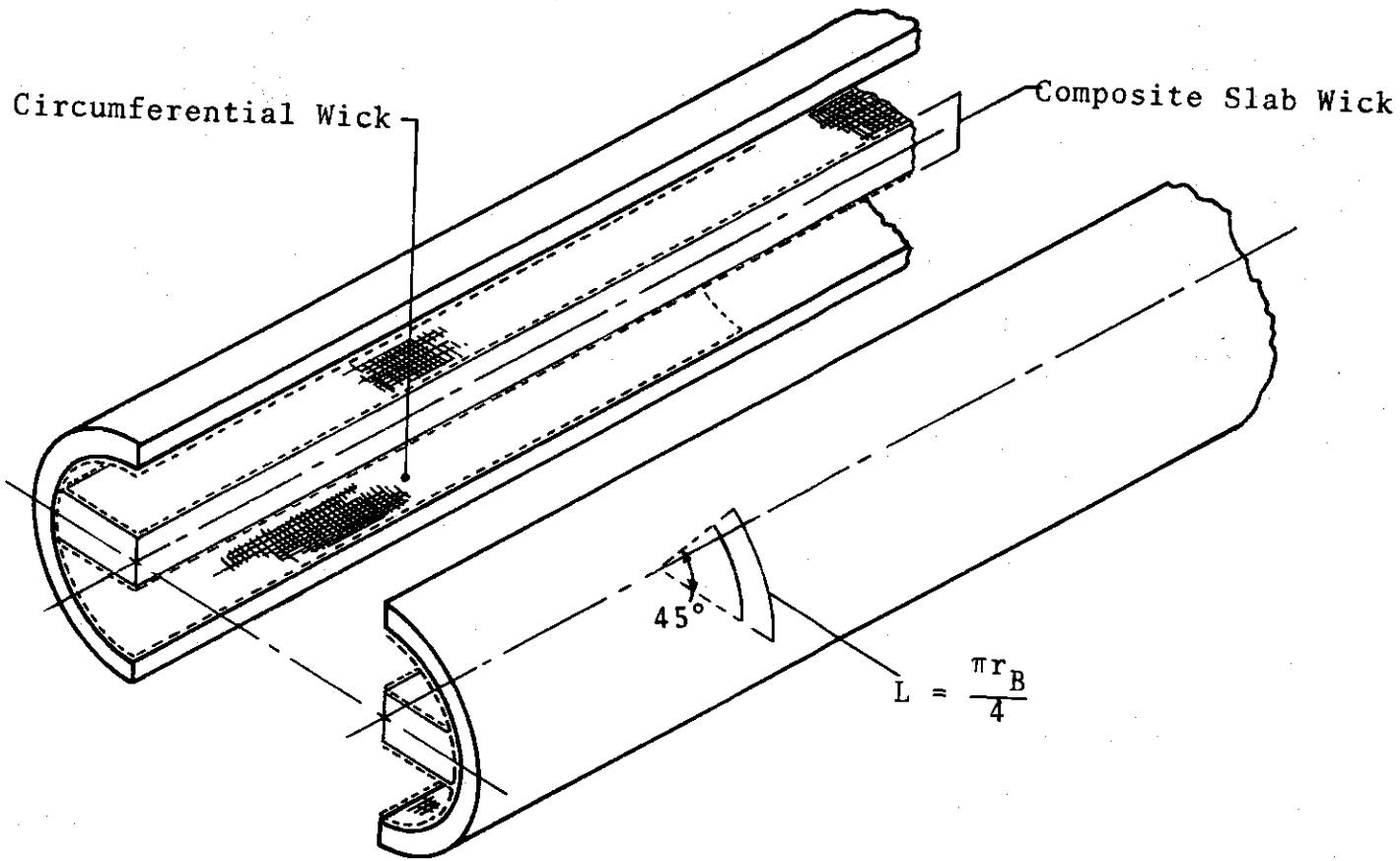

Figure 41. Close-Up of Porous Media Showing Average Distance Traveled by Liquid Mass Element in Circumferential Wick

Thus:

$$\dot{m}_{L_C} = \frac{\dot{m}_L}{4} \qquad \left[\frac{lb_m}{hr}\right] \tag{I.11}$$

The total pressure drop in the circumferential wicks is the sum of the pressure drops of the components:

$$\Delta P_{L_C} = \Delta P_{L_{C_e}} + \Delta P_{L_{C_c}} \tag{I.12}$$

Combining Eqs. (I.9.a), (I.9.b), (I.10), and (I.11) with Eq. (I.12) gives:

$$\Delta P_{L_C} = \frac{\mu_L K_C L \dot{m}_L}{4 n_C \delta_C \rho_L} \left(\frac{1}{\ell_e} + \frac{1}{\ell_c}\right) \qquad \left[\frac{lb_f}{ft^2}\right] \tag{I.13}$$

The total liquid pressure drop due to viscous effects in the composite wick system is given by summing the pressure drops of the slab and circumferential wicks.

$$\Delta P_L = \Delta P_{L_{A+B}} + \Delta P_{L_C} \tag{I.14}$$

By substituting the equations for each term of the right hand side, Eq. (I.14) may be rewritten as

$$\Delta P_L = \frac{\dot{m}_L \mu_L \ell_{eff} \bar{K}}{\rho_L b \delta_T} + \frac{\mu_L K_C L \dot{m}_L}{4 n_C \delta_C \rho_L} \left(\frac{1}{\ell_e} + \frac{1}{\ell_c}\right) \quad \left[\frac{lb_f}{ft^2}\right] \tag{I.15}$$

or,

$$\Delta P_L = \frac{\dot{m}_L \mu_L}{\rho_L} \left[\frac{\bar{K} \ell_{eff}}{b \delta_T} + \frac{K_C L}{4 n_C \delta_C} \left(\frac{1}{\ell_e} + \frac{1}{\ell_c}\right)\right] \quad \left[\frac{lb_f}{ft^2}\right] \tag{3.19}$$

APPENDIX J

ESTIMATION OF THE EFFECTIVE THERMAL CONDUCTIVITY OF THE HEAT PIPE

The effective thermal conductivity of the heat pipe, shown graphically for different wick compositions by Figs. 24, 25, 26, and 27 was calculated by using the following equation:

$$\dot{Q} = k' \frac{\Delta T \, A}{\ell}$$

or, rearranging:

$$k' = \frac{\dot{Q} \, L}{\Delta T \, A}$$

where:

k' = effective thermal conductivity

$\dot{Q}$ = capillary limited heat transfer rate

ℓ = the effective length of the heat pipe in this study (ℓ_{eff})

Δ_T = temperature difference between the evaporator and condenser ends.

A = cross sectional area of the heat pipe.

For wick composition 6, at an evaporator temperature of 162°R, the following sample calculation is offered:

$$A = \frac{\pi D^2}{4} = \frac{\pi(\frac{.5}{12})^2}{4} = 1.3635\text{x}10^{-3} \qquad (ft^2)$$

$$\Delta T = T_e - T_c = 162 - 160 = 2°R$$

$$\ell = \ell_{eff} = 2.25 \quad (ft)$$

$$T_V = T_c + \frac{(\Delta T)(\ell_e)}{(\ell_e + \ell_c)} = 160 + \frac{(2)(.5)}{1.5} = 160.7 \quad (°R)$$

$\dot{Q}_{CL}$ corresponding to above T_V and wick composition = 102.0 $\frac{Btu}{hr}$. Therefore,

$$k' = \frac{(102.0\ \frac{Btu}{hr})(2.25\ ft)}{(2°R)(1.3635\text{x}10^{-3} ft^2)}$$

$$k' = 8.416\text{x}10^4 \qquad \left[\frac{Btu}{hr\text{-}ft\text{-}°R}\right]$$

APPENDIX K

ESTIMATION OF THE HEAT TRANSFER CAPABILITY

The heat transfer capability, "β" for several wick compositions is shown graphically in Figure 28. This parameter is calculated by using the following equation:

$$\beta = (\dot{Q}_{CL})(\ell_{eff}) \qquad \left[\frac{\text{Btu-ft}}{\text{hr}}\right]$$

For wick composite 6, and a vapor temperature of 160.7°R, the following data is obtained

$$\dot{Q}_{CL} = 102.0 \qquad \left[\frac{\text{Btu}}{\text{hr}}\right]$$

$$\ell_{eff} = 2.25 \qquad (\text{ft})$$

Therefore:

$$\beta = (102.0 \ \frac{\text{Btu}}{\text{hr}})(2.25 \text{ ft}) = 229.5 \qquad \left[\frac{\text{Btu-ft}}{\text{hr}}\right]$$

APPENDIX L

SAMPLE CALCULATION OF WICK THICKNESS

The composite slab wick is made up of several interior layers of screen "sandwiched" between surface screens of a different mesh size. The interior layers are screens of small mesh sizes (i.e. large pore radii). The small value of inverse permeability of these layers allows a freer internal flow of liquid. The slab surface layers are screens of large mesh size indicating small pore radii. These layers provide a large pressure differential for capillary pumping.

The total thickness of the slab is the sum of the products obtained by multiplying the number of layers of each type of screen by the thickness of that screen.

$$\delta_T = n_A\delta_A + n_B\delta_B \qquad \text{(L.1)}$$

The values of n_A and n_B are chosen to give a total wick thickness between .1 and .15 inches. The values used for δ_A and δ_B, the thickness of the surface and interior screens, respectively, were taken from Appendix A.

For wick composition 6, the following sample calculation is given:

$n_A = 4$

$n_B = 5$

$\delta_A = 2.44 \times 10^{-4}$ (ft)

$\delta_B = 2.04 \times 10^{-3}$ (ft)

$\delta_T = (4)(2.44 \times 10^{-4} ft) + (5)(2.04 \times 10^{-3} ft) = 11.176 \times 10^{-3}$ (ft)

The thickness of the circumferential wick is found by multiplying the number of layers of screen making up the circumferential wick (n_C) by the thickness of the screen (δ_C).

$$\text{thickness of the "C" layer} = n_C \delta_C \qquad \text{(L.2)}$$

For wick composition 6, this is:

thickness of the "C" layer: $(2)(2.44 \times 10^{-4} ft) = 4.88 \times 10^{-4}$ (ft)

APPENDIX M

SAMPLE CALCULATION OF EFFECTIVE INVERSE PERMEABILITY

The effective inverse permeability of the composite slab wick is given as:

$$\overline{K} = \frac{\delta_T}{\frac{n_A \delta_A}{K_A} + \frac{n_B \delta_B}{K_B}} \qquad (ft^{-2}) \qquad (M.1)$$

The values of δ_A, δ_B, K_A, and K_B are taken from Appendix A. For wick composition 6, the following sample calculation is offered.

$\delta_T = 11.176 \times 10^{-3}$ ft

$\delta_A = 2.44 \times 10^{-3}$ ft

$\delta_B = 2.04 \times 10^{-3}$ ft

$n_A = 4$

$n_B = 5$

$K_A = 15.168 \times 10^{9}$ ft^{-2}

$K_B = 5.908 \times 10^{7}$ ft^{-2}

$$\overline{K} = \frac{11.176 \times 10^{-3} ft}{\frac{(4)(2.44 \times 10^{-3})ft}{15.168 \times 10^{9} ft^{-2}} + \frac{(5)(2.04 \times 10^{-3})ft}{5.908 \times 10^{7} ft^{-2}}}$$

$$\overline{K} = 6.4709 \times 10^{7} \qquad (ft^{-2})$$

APPENDIX N

SAMPLE CALCULATION OF NON-RESTRICTED HEAT TRANSFER RATE

Equation (3.13) gives the theoretical heat transfer rate of the heat pipe disregarding all limitations as:

$$\dot{Q}_{max} = \frac{\Delta T}{R_T} \qquad \left[\frac{Btu}{hr}\right]$$

Sample calculations for $T_c = 160°R$, $T_e = 162°R$, and wick composition 6 are presented as follows

$$\dot{Q}_{max} = \frac{\Delta T}{R_T} = \frac{T_e - T_c}{R_T} \qquad \left[\frac{Btu}{hr}\right]$$

where R_T, the total thermal resistance of the pipe, is taken from Appendix G

$$\dot{Q}_{max} = \frac{162.160°R}{2.001x10^{-2}\ \frac{°R\text{-}hr}{Btu}} = 9.994x10 \quad \left[\frac{Btu}{hr}\right]$$

APPENDIX O

SAMPLE CALCULATION OF THE CAPILLARY-LIMITED HEAT TRANSFER RATE

The capillary limited heat transfer rate, $\dot{Q}_{CL}$, is obtained from Eq. (3.24):

$$\dot{Q}_{CL} = \frac{2N/r_p}{\frac{\overline{K}\,\ell_{eff}}{b\delta_T} + \frac{K_C L}{4n_C\delta_C}\left(\frac{1}{\ell_e} + \frac{1}{\ell_c}\right) + \frac{8\mu_V\,\rho_L\,\ell_{eff}}{\pi\,\mu_L\,\rho_V\,r_v^4}} \qquad \left[\frac{Btu}{hr}\right]$$

A sample calculation of this quantity evaluated at 160°R, using wick composition (6). The following data is given.

$$N = \text{heat pipe number} = \frac{\sigma\, h_{fg}\, \rho_L}{\mu_L} = 2.5845\times10^{9} \qquad \left[\frac{Btu}{ft^2\text{-}hr}\right]$$

r_p = pore radius in the screen of the circumferential wick
$= 6.25\times10^{-5}$ (ft)

$\overline{K}$ = effective inverse permeability = 6.4709×10^{7} (ft^{-2})

K_C = inverse permeability of circumferential wick
$= 15.168\times10^{9}$ (ft^{-2})

b = width of the slab wick = $(2)r_C = 3.402\times10^{-2}$ (ft)

ℓ_{eff} = effective length = $\ell_a + \frac{1}{2}(\ell_e + \ell_c) = 2.25$ (ft)

δ_T = total slab thickness = 11.176×10^{-3} (ft)

L = average arc length traveled by element of liquid mass
$= 1.374 \times 10^{-2}$ (ft)

n_C = number of layers of screen in circumferential wick = 2

δ_C = thickness of screen layer used in circumferential wick
$= 2.44 \times 10^{-4}$ (ft)

ℓ_e = length of evaporator section = .5 (ft)

ℓ_c = length of condenser section = 1.0 (ft)

μ = viscosity of vapor at 160°R = 1.37071×10^{-7} $[lb_f\text{-sec/ft}^2]$

μ_L = viscosity of liquid at 160°R = 2.26061×10^{-6} $[lb_f\text{-sec/ft}^2]$

ρ_V = density of vapor at 160°R = 8.47851×10^{-1} $[lb_m/ft^3]$

ρ_L = density of liquid at 160°R = 4.79546×10 $[lb_m/ft^3]$

r_v = hydraulic radius = 3.753×10^{-3} (ft)

Substitution into Eq. (3.24) gives:

$$\dot{Q}_{CL} = \frac{(2)(2.5845\times10^{9})/6.25\times10^{-5}}{\frac{(6.4709\times10^{7})(2.25)}{(3.402\times10^{-2})(11.176\times10^{-3})} + \frac{(15.168\times10^{9})(1.374\times10^{-2})}{(4)(2)(2.44\times10^{-4})}\left(\frac{1}{.5}+\frac{1}{1.0}\right)}$$

$$\frac{}{\frac{(8)(1.37071\times10^{-7})(4.79546\times10)(2.25)}{(3.1415926)(2.26061\times10^{-6})(8.47851\times10^{-1})(3.753\times10^{-3})^4}}$$

$$\dot{Q}_{CL} = 102.53 \quad \left[\frac{Btu}{hr}\right]$$

APPENDIX P

SAMPLE CALCULATION OF THE SONIC-LIMITED HEAT TRANSFER RATE

Equation (3.28) is used for calculating the sonic limited heat transfer rate:

$$\dot{Q}_{SL} = h_{fg} A_x \rho_V [g_c k R T]^{1/2}$$

A sample calculation for wick composition 5, and vapor temperature of 160°R follows:

$h_{fg} = 78.253$ Btu/lbm

$A_x = 5.1663 \times 10^{-4}$ ft^2 (see Table 11)

$\rho_V = .8478$ lbm/ft^3

$g_c = 32.2 \frac{\text{lbm}}{\text{lb}_f}$ f/sec^2 x $(3600)^2 \frac{\text{sec}^2}{\text{hr}^2} = 4.1731 \times 10^8 \left[\frac{\text{lbm}}{\text{lb}_f} \frac{\text{ft}}{\text{hr}^2}\right]$

$= 55.15 \frac{\text{ft-lb}_f}{\text{lbm °R}}$

$T = 160$°R

$k = 1.429$ (from Figure 10)

Therefore,

$$\dot{Q}_{SL} = (78.253 \frac{\text{Btu}}{\text{lbm}})(5.1663 \times 10^{-4} \text{ft}^2)(.8478 \frac{\text{lbm}}{\text{ft}^3})[(4.1731 \times 10^8 \frac{\text{lbm}}{\text{lb}_f} \frac{\text{ft}}{\text{hr}^2})(1.429)(55.15 \frac{\text{ft-lb}_f}{\text{lbm °R}})(160°\text{R})]^{1/2}$$

$$\dot{Q}_{SL} = 7.9651 \times 10^4 \quad \left[\frac{\text{Btu}}{\text{hr}}\right]$$

Table 12. Cross-Sectional Area of Vapor Space for Various Wick Compositions

Wick Composition	Thickness of Slab-Ft	Cross Sectional Area-Vapor Space-Ft^2
1	8.08×10^{-3}	6.5383×10^{-4}
2	8.754×10^{-3}	6.5572×10^{-4}
3	7.838×10^{-3}	6.8778×10^{-4}
4	8.648×10^{-3}	6.5943×10^{-4}
5	12.728×10^{-3}	5.1663×10^{-4}
6	11.176×10^{-3}	5.7095×10^{-4}

Cross sectional area of vapor space:

$$A = \pi r_B^2 - 2r_B \delta_T$$

where:

$$r_B = 1.75 \times 10^{-2} \text{ feet}$$